March 2019

Design of Shape-Morphing Structures Consisting of Bistable Compliant Mechanisms

Rami Alfattani
University of South Florida, rafattni@gmail.com

Design of Shape-Morphing Structures Consisting of Bistable Compliant Mechanisms

by

Rami Alfattani

A dissertation submitted in partial fulfillment
of the requirements for the degree of
Doctor of Philosophy in Mechanical Engineering
Department of Mechanical Engineering
College of Engineering
University of South Florida

Major Professor: Craig Lusk, Ph.D.
Kyle Reed, Ph.D.
Rasim Guldiken, Ph.D.
Andrés E. Tejada-Martínez, Ph.D.
Jiangfeng Zhou, Ph.D.

Date of Approval:
January 25, 2019

Keywords: Synthesis, Stable Configurations, Kinematics, Kinetics, CAD

DEDICATION

بِسْمِ ٱللهِ ٱلرَّحمنِ ٱلرَّحِيمْ

"In the name of God, the Most Gracious, the Most Merciful"

وَقُل رَّبِّ زِدْنِي عِلْمًا

"O my Lord increase me in knowledge"

اللهم إني أسألك علمًا نافعًا، ورزقاً طيّبًا، وعمَلً متقبَّلً

"O God indeed I ask You for beneficial knowledge,

and Pure Bestowed, and deeds which are accepted"

ACKNOWLEDGMENTS

Graduate studies at the University of South Florida have been both fun and challenging. The classes have broadened my perspective as a mechanical engineering graduate and provided me with the skills and knowledge needed to become an accomplished engineering instructor, and researcher. I also found the research group meetings where we shared updates, carried out small projects, and learned from each other, very beneficial. This interaction has contributed in many ways to the successful completion of this dissertation which represents the most important milestone on my road to graduation. This work would not have been possible without the financial support of the Saudi Arabian Cultural Mission Scholarship (SACM). I would like also to express my appreciation for the Umm Alqura University, Makkah, KSA.

I would like to thank Professor Craig Lusk for his guidance, and also his patience during the extended period that I took to complete this journey. When obstacles came my way, he was always available with solutions to see me through. He has taught me more than I could ever give him credit for here. Many of my friends are of the opinion that I am fortunate to have him as my advisor, and I could not agree more. I am grateful to all of those with whom I have had the pleasure to work during this and other related projects. Each of the members of my Dissertation Committee has provided me extensive personal and professional guidance and taught me a great deal about both scientific research and life in general. I also acknowledge the support of the National Science Foundation, Grant # CMMI-1053956

Nobody has been more important to me in the pursuit of this project than the members of my family. I would like to thank my parents, whose love, guidance, and prayers are with me around

the clock day and night in whatever I pursue. They are the ultimate role models. They are my biggest inspiration and have always push me to superbness. I would like to thank my brothers and my sisters, Hattan, Turki, Rawan, and Bayan whose care and support are always with me all the time. Most importantly, I wish to thank my loving and supportive wife, Ghofran who provides unending inspiration

TABLE OF CONTENTS

LIST OF TABLES

LIST OF FIGURES

ABSTRACT

This dissertation presents a design concept for shape-morphing structures that have two stable configurations. The design concept defines the methodology of transforming a planar structural shape into spatial structural shape using bistable compliant mechanisms. Bistable complaint mechanisms are used to achieve structural stable configurations. The dissertation incorporating geometrical relationships for the mechanisms that form the primary structure described in step-by-step process. This dissertation implements the design layouts for designer to creating shape-morphing structures including origami. The novel contribution of the work is classified in three models. The first model presents a methodology to induce bistability behavior into an origami reverse fold and partially spherical compliant mechanism. The second model presents the design and development of a bistable triangle-shaped compliant mechanism with motion limits and dwell behavior at the two stable configurations. This mechanism can be arrayed to create shape-morphing structures. The third model presents a design and development for a collapsible bistable compliant mechanism used for a shape morphing lamina-emergent frustum. Finally, physical prototypes of all models are presented as proof of concept.

CHAPTER 1

INTRODUCTION

1.1 Objective

The objective of this dissertation is to introduce three new models for shape-morphing structures that transform from planar configurations to various activated configurations. The modeling framework for these structures considers kinematic analysis, kinetic analysis, and the tessellation capability of the systems, as shown in Figure 1.1. Bistable compliant mechanisms are utilized as the morphing elements of the shape-morphing structures. The models are presented in

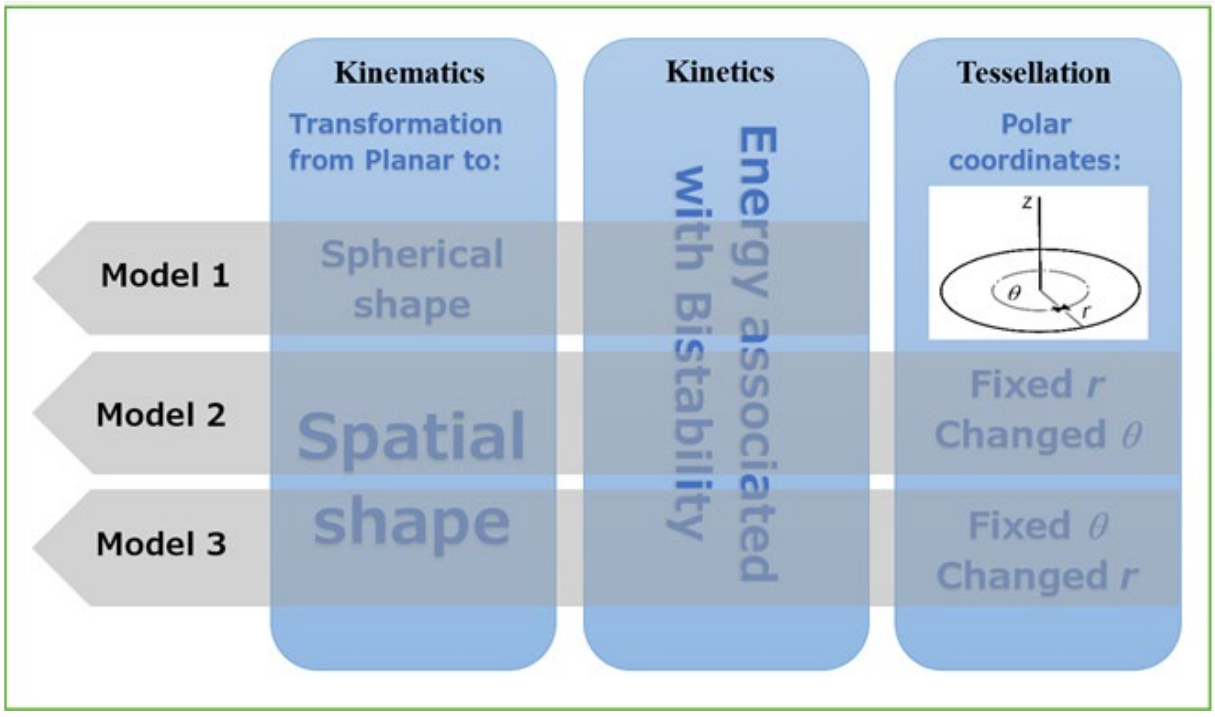

Figure 1.1: The dissertation's objective summary.

detailed design procedures and parametric CAD design strategy guidelines for the shape-morphing structures.

The first model is a spherical bistable mechanism inspired by origami. Examples of the spherical mechanism are modeled and prototyped to demonstrate the design concept.

The second model is a spatial shape-morphing design concept utilizing a bistable triangle-shaped compliant mechanism that when arrayed in three triangles in circular pattern, it morphs to create a cube corner shape. This model focuses on the tessellation in polar coordinates as the angle θ changes and the radius r remain constant. The bistable triangle-shaped compliant mechanisms follow a step by step design process. Examples of this mechanism are modeled and prototyped to demonstrate the design concept.

The third model is a shape-morphing design for a lamina-emergent frustum that morphs from a planar lamina to a frustum shape as an illustration of a general design strategy for shape-morphing structures. This model focuses on the tessellation in polar coordinates as the radius r changes and the angle θ remain constant. An example of the mechanism is modeled and prototyped to demonstrate the design concept.

1.2 Motivation

The motivation for shape-morphing structures occurs in many applications such as wing morphing for enhanced aerodynamic performance, complex deployable structures, and space-saving furniture. [4, 5]. Additionally, if shape-morphing designs have the ability to be manufactured on the micro-scale, they may provide useful functions, such as switches and relays [6]. Currently, shape-morphing structures often consist of a number of parts or mechanisms that may consist of links, springs, and joints, which can have high costs for manufacture, assembly, and maintenance.

The original motivation for the dissertation was a foldable frame that would be stored folded in form of planar shape which provide storage capability and deployed once needed to achieve certain tasks. Possible applications for this study could be a rapidly deployable tent or a collapsible small camping shelters or animal enclosure. Also, the need for such shapes may occur in other applications including aerospace devices, locking devices, and shape-change structures [1, 2, 3]. These applications are to produce shape morphing structures that are fabricated from a flat sheet of material and morph into their desired shape which reduce the assembly processes required.

1.3 Overview

The outline of the rest of the dissertation is arranged as following,

Chapter 2 serves as general background for the dissertation. This includes shape morphing structures and the advantages of using compliant mechanisms and origami over rigid-body mechanisms. Chapter 3 describes a methodology to induce bi-stability behavior into the reverse-fold origami mechanisms and a partially compliant spherical mechanism. The kinematic synthesis was described using an analogy between the synthesis of planar four-bar mechanisms and the synthesis of spherical four-bar mechanisms which are the kinematic model for origami mechanisms and the partially compliant spherical mechanism. Both mechanical prototypes were designed and tested later. Chapter 4 presents the design and development of a bi-stable triangular-shape compliant mechanism with motion limits and dwell behavior at the two stable configurations. The design process, which involves designing of the dead center motion limits using instant center method and kinematic synthesis of the mechanism, is systematically discussed in a step by step process. Two examples which consider an array of three such mechanisms are considered and the two stable configurations of two applications, flat and cube corner and portable

box. Chapter 5 presents a new bistable collapsible compliant mechanism for a Lamina-Emergent Frustum which can transform a polygon spiral into spatial frustum shape. The design process was described in detail, which includes the strategy to morph, the procedure of type synthesis and dimension synthesis, and the way to make it bistable. A prototype was made to verify the design. Chapter 6 concludes this dissertation by summarizing the contribution done to the shape-morphing structures using bistable compliant mechanisms. Recommendations and future work are given to apply and proceed the design concepts.

CHAPTER 2

LITERATURE REVIEW

This chapter serves a general background for the dissertation because chapters 3, 4, and 5 are based on publications, each has background/literature in its own review sections. The general background for this work is in the area of shape-morphing and its sub-disciplines of rigid-body mechanisms, compliant mechanisms and origami.

2.1 Shape-Morphing

Shape-morphing is a phenomenal behavior that exits in nature [7, 8] where it can be beneficial to many applications where their performance can be improved as they adapt to external and environmental conditions. The study of such behavior has been categorized by kinetics, the energy absorbed during motion, and by kinematics, the transforming motion between different states [7]. Th energy absorption can be seen in the stability of the system [9, 10] and the transforming motion can be obtained in common application, such as scissor lift [11], robot manipulators and shape-morphing mechanisms [12, 13, 14]. This suggests a promising route to combine the kinetics and kinematic behaviors into a system of shape-morphing structures. These structures are mechanisms that move internally to alter between different configurations which make them applicable for aircraft wings [15, 16], active antennas [17, 18], engine blades [19], automobile structures, and structural actuators [20, 21, 22, 23]. Alqasimi and Lusk demonstrated a shape-morphing space frame using a linear Bistable Compliant Crank-Slider Mechanism [24] that is arranged in a specific pattern to produce a shape-morphing structure [25]. Bistable shape-shifting surfaces (SSS) can produce morphing structures with line-of-sight integrity, i.e.

effectiveness as a physical barrier [26]. Shape-morphing structures and surfaces can add value to applications as in folding geometries [27, 28, 29, 30].

2.2 Shape Morphing Structures Types

There are many techniques for shape-morphing structures and it can be classified in three main methods: rigid-body mechanisms, compliant mechanisms, and origami.

2.2.1 Rigid-Body Mechanisms

Rigid-body mechanisms are basically systems of moving elements such as linkages and joints, gears, cams and etc. [31]. Rigid-body mechanisms studies and analysis have been used for centuries and are considered very well-established field [32]. The design of rigid-body mechanisms is generally standardized for production and manufacturing [33, 34]. The downsides of using rigid-body mechanisms are summarized in the potential of backlash, assembly time and cost, frequent required maintenance, wear, and weight [35] which raised the need for alternative solutions such as compliant mechanisms, which are discussed in the following section 2.22. As a preliminary to the next section, some rigid-body mechanisms techniques have been adapted in compliant mechanisms design, such as graph theory and spherical mechanisms design.

2.2.1.1 Graph Theory

Graph theory is an approach used to better understand a mechanism by representing the linkages and their connections in mathematics diagrams consisting of vertexes and nodes [36]. Liu and Chou used a graph theoretic approach to generate a creative design for a vehicle suspension [37]. Moreover, graph theory representations were used to evaluate lists of mechanisms by Feng and Liu to design a deployable mechanism used as a reflector antenna [38]. The graph representation allows definition of the structure of a mechanism's connections [39]. Shape-

morphing mechanisms have been successfully studied using topological graph theory to synthesize morphing mechanisms [40, 41].

2.2.1.2 Spherical Mechanisms

Spherical mechanisms are a sub-class of spatial mechanisms that move in the region defining a sphere's surface. A spherical mechanism has links and joints that move at fixed distance from a vertex. Spherical mechanisms have been used in many applications because of their large motion capability, for example as in spherical manipulator [42]. The need of such mechanisms occurs in other application including shape-morphing structures and origami designs. Spherical mechanisms can be used and designed as either rigid-body mechanisms or compliant mechanisms.

2.2.2 Compliant Mechanisms

Unlike rigid-body mechanisms, compliant mechanisms are flexible members that gain their mobility from the deflection of the members rather than at movable joints [32]. The advantages of compliant mechanisms over rigid-link mechanisms are considered in four categories: the reduction of number of elements, the elimination of joint clearances, integrated spring-like energy storage, and potential reductions in cost [2]. Compliant mechanisms enable manufacturing a single layer mechanism that includes compliant joints that function as pin joints. Compliant mechanisms benefit from the deflection of flexible members because a form of strain energy will be stored in the flexible members which can be transformed or released in form of motion. The stored strain energy in the flexible members resembles the strain energy associated in deflected spring [43, 32]. Therefore, the *pseudo-rigid-body* (PRBM) model was developed based on the idea of predicting the deflection of flexible element using integrated spring into rigid-body linkage.

2.2.2.1 Pseudo-Rigid-Body Model

The pseudo-rigid-body method is an approximation technique which is used to model large deflections of a flexural element. It basically converts a compliant element to one or multiple rigid parts connected by torsional spring as shown in Figure 2.1. Howell and Midha first developed the pseudo-rigid-body model concept to model the large deflection of compliant links by using rigid-body component analogies [44]. Pseudo-rigid-body methods reduce the complexity of the design space because rigid-body theory can be used to synthesize the flexible members of the compliant mechanisms [32, 45].For accuracy, it is important for each model to assign the right place for the spring and its stiffness value based on the loading conditions and motion constraints of the flexible member [46].

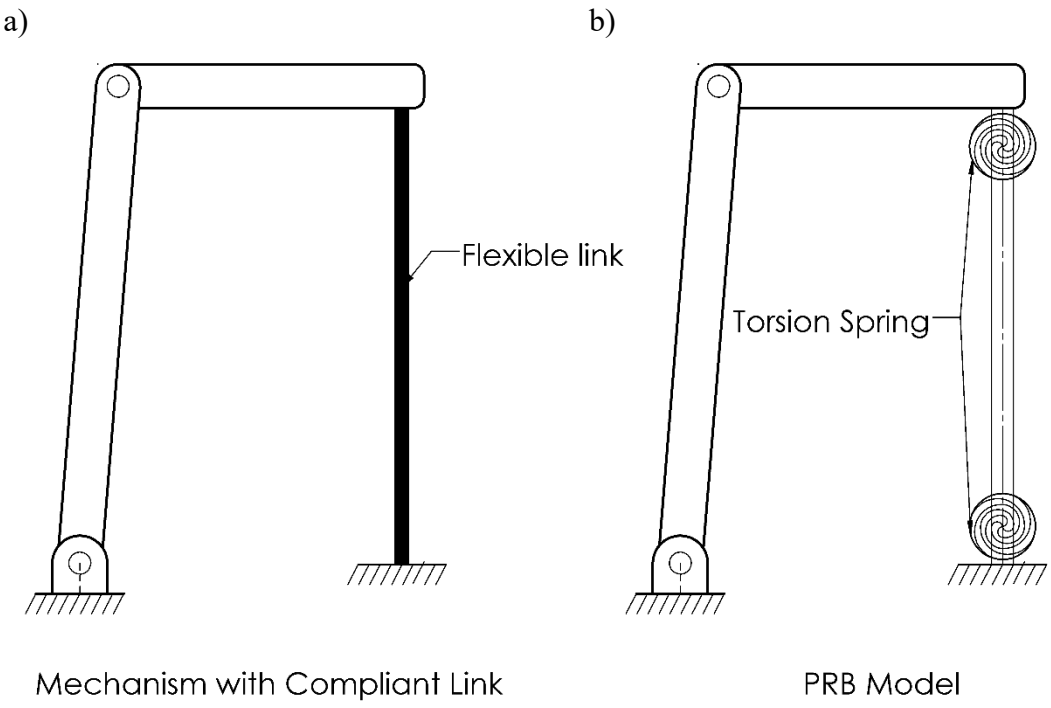

Figure 2.1: a) A four-bar mechanism with one flexible link. b) The pseudo-rigid-body model of the four-bar mechanism. Adapted from [32]**.**

2.2.2.2 Bistability

Bistability of a mechanism means that it can be at a stable equilibrium in two different configurations. [32, 47, 48]. Bistable mechanisms have two distinct stable configurations in which the potential energy of the mechanism is at a minimum. A good way to understand bistability is using the "ball-on-a-hill" analogy [32], which compares the strain energy in a compliant mechanism to the gravitational potential energy of a ball. In Figure 2.2, a ball on an uneven surface is depicted. The ball is at equilibrium at positions A, B, C and D. At position A and C, the ball is at a minimum potential energy and will oscillate about that minimum if it is perturbed slightly from the positions shown. On the other hand, at position B, the ball is at a maximum of potential energy, and if disturbed, it will not return to its original position but will move to one of the stable positions. The equilibrium at D is described as neutral because the potential energy curved is flat in the neighborhood of D, or in other words, unlike positions A,B,C which are isolated equilibrium points, position D one equilibrium point that is part of a compact region of equilibrium points, and is neither a minimum, nor a maximum of potential energy. In mechanisms, potential energy is stored in springs of compliant members as in switches and lock devices.

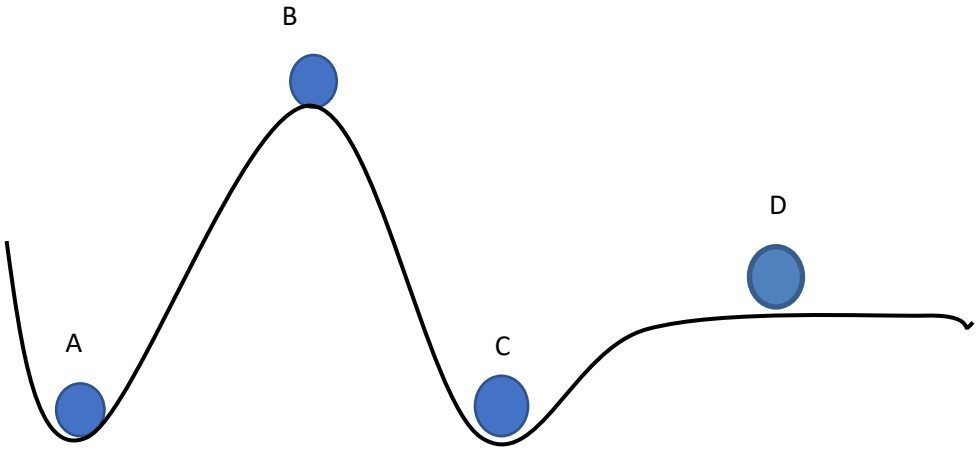

Figure 2.2: The-ball-on-a-hill analogy for bistable mechanisms. Adapted from [32]**.**

2.2.3 Origami

Origami is a technique of folding a sheet of paper into certain shapes. Origami was originally developed in Japan then spread all over the world and recently has been adapted in sciences and mathematics [49, 50, 51]. Many researchers have applied the folding pattern of origami in applications in space [52, 53], packing, storage, and shape morphing structures [54, 55, 56]. It extends more as it exists in nature where it helps scientists understand the folding pattern in animals and bugs to mimic their phenomenal wings and organs movements in practical morphing applications [57]. In this dissertation, we examine a method for making simple origami fold bistable.

2.3 Shape Morphing Structures Methods

The challenging parts of designing shape-morphing structures are synthesis and actuation. An approach called structural optimization has been widely investigated to synthesize shape-morphing structures [58]. However, the structural optimization approach relies heavily on having a large design space which puts limitations in the shape-morphing design [16]. Also, a few researchers have used only the topology of a rigid-body solution to create a design space of the shape-morphing mechanism then searched for a compliant mechanism solution for the same shape-morphing mechanism [59]. Other researchers have studied many solutions for actuating shape-morphing structures and most of them are complicated and are external to the structures [60]. Compliant mechanisms may be a viable solution because of their members' flexibility that allows for appropriate mobility and actuations [61]. In addition, compliant mechanisms provide many advantages for shape-morphing structures as they help overcome actuation problems [58] and have simpler manufacturing processes [32] and joint without torsional springs [32]. Still, the challenge is there to deliver simpler design strategies for fully compliant shape-morphing mechanisms.

CHAPTER 3

DESIGN OF A BISTABLE ORIGAMI REVERSE-FOLD USING SPHERICAL KINEMATICS[1]

3.1 Introduction

This chapter presents a new design concept for bistability that can be implemented as a reverse-fold origami mechanism or as a spherical four-bar mechanism. The design is based on the conceptual overlap between a certain simple class of origami mechanisms (the reverse-fold) and a class of spherical change-point mechanisms. Using both a partially compliant spherical mechanism and a piece of origami made with two sheets of paper, we implement the design concept for bistable behavior. The design concept consists in adapting planar two position synthesis to spherical mechanisms and in using a formal analogy between spherical mechanisms and certain simple origami folds. The dimensional synthesis of these two mechanisms is performed using parametric CAD. The design concept was successfully prototyped both as origami and as a partially compliant spherical mechanism.

The objective of this research was to develop a piece of origami with two stable positions, one of which is the flat sheet, and the other is selected by the designer. We achieved this objective using a synthesis technique based on spherical kinematics. We implemented the design technique not only in origami, but also as a partially compliant spherical mechanism. We believe that the

[1] This chapter is based on a published paper in the proceedings of the ASME 2017 International Design Engineering Technical Conferences & Computers and Information in Engineering Conference, IDETC/CIE 2017, Cleveland, OH, USA. Permission is included in Appendix E.

origami design technique may be an important preliminary to designing and building shape-morphing pieces of origami.

For this chapter, we developed a design concept that can be implemented as a partially compliant bistable spherical change-point mechanism or as a bistable piece of origami. Bistable spherical mechanisms may have applications including aerospace devices, shape-change structures, and deployable structures [62, 63]. Smith and Lusk improved a pseudo-rigid-body model to predict the behaivor of bistable spherical compliant mechansim [64]. Bistable origami has been investigated by several researchers [65, 66, 67]. An origami foldable structure was used to introduce a new vibration isolator that provides bistable folding motion [68]. Also, bistable origami building blocks were integrated in a bioinspired crawling robot that aimed to capture insects as the mechanism snaps due to the bistable behavior [69]. For this work, the background is in the area of spherical mechanisms, origami and bistability. In addition, the kinematic two-position synthesis technique for planar mechanisms [2] was found applicable in synthesis of our design concept. Origami has been studied in many areas, such as mathematics and design [70]. Streinu and Whiteley explained the relationship between a single vertex origami pattern and spherical polygons [71], which is the key concept linking the two different prototypes we produced for this chapter. Bowen *et al,* studied the position analysis of an origami single-vertex mechanism using spherical kinematics [72]. Leal and Dai developed a type of parallel mechanism using a "technomimetics" technique using an origami pattern [73], demonstrating that origami designs can be used as components in mechanism design.

A mechanism is described as "bistable" when it has two distinct configurations which are local minimums of potential energy. A good way to understand bistability is using the "ball-on-a-hill" analogy [32], which compares the strain energy in a compliant mechanism to the gravitational

potential energy of a ball as discussed in chapter 2. Bistable mechanisms have two distinct stable configurations in which the potential energy of the mechanism is at a minimum.

Later in the chapter, we will discuss two position synthesis for a change-point spherical mechanism. As a preliminary to that discussion, we now discuss a two-position synthesis technique for a planar four-bar change-point mechanism. The technique is very similar for a spherical change-point mechanism, but straight lines are replaced with great circle arcs on a sphere. For two position synthesis [2], we use the notion that every point on the perpendicular bisector of a line segment is equidistant to the respective ends of the line segment.

This idea is used as follows: First, we consider the coupler link of a change-point mechanism that moves from configuration *C* to configuration *C'* (as shown in Figure 3.1). To ensure that the mechanism is a change-point four-bar, in configuration *C* we require that the coupler link lie along the *x*-axis of our coordinate system. Second, in configuration *C* we label the

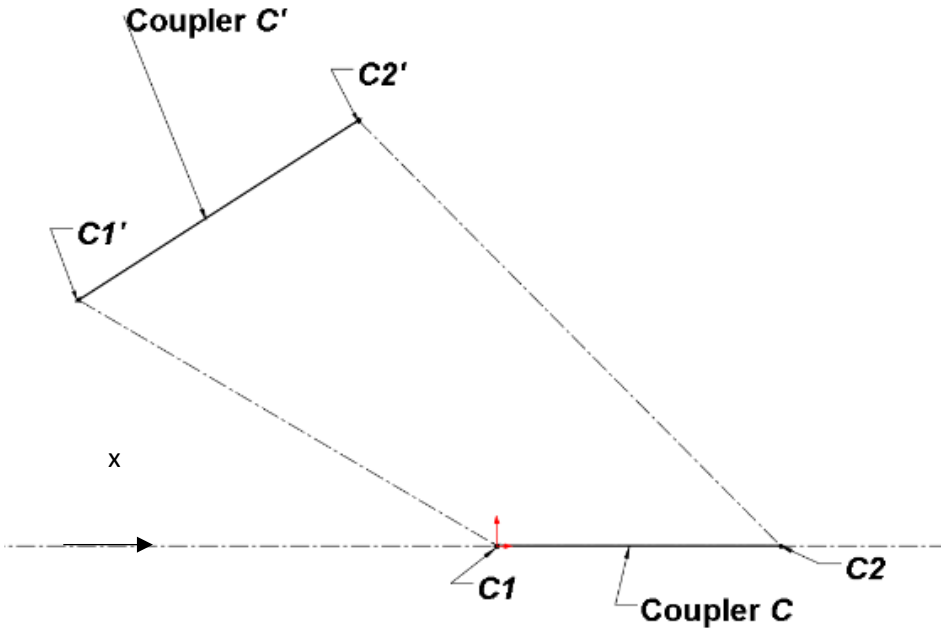

Figure 3.1: *C* and *C'* configurations.

moving pivots of the coupler link C_1 and C_2. Third, in configuration C', these pivots are labeled as C_1' and C_2'. Fourth, we draw line segments connecting the C_1 and C_1', and C_2 and C_2'. Fifth, we draw the perpendicular bisector lines of segment $C_1 - C_1'$ and segment $C_2 - C_2'$, respectively. Finally, the intersections of these bisectors with the x-axis define the locations of the fixed pivots of the change-point mechanism, which are labeled I (for the input pivot on the bisector of segment C_1-C_1') and O (for the output pivot on the bisector of segment C_2-C_2') as shown in Figure 3.2.

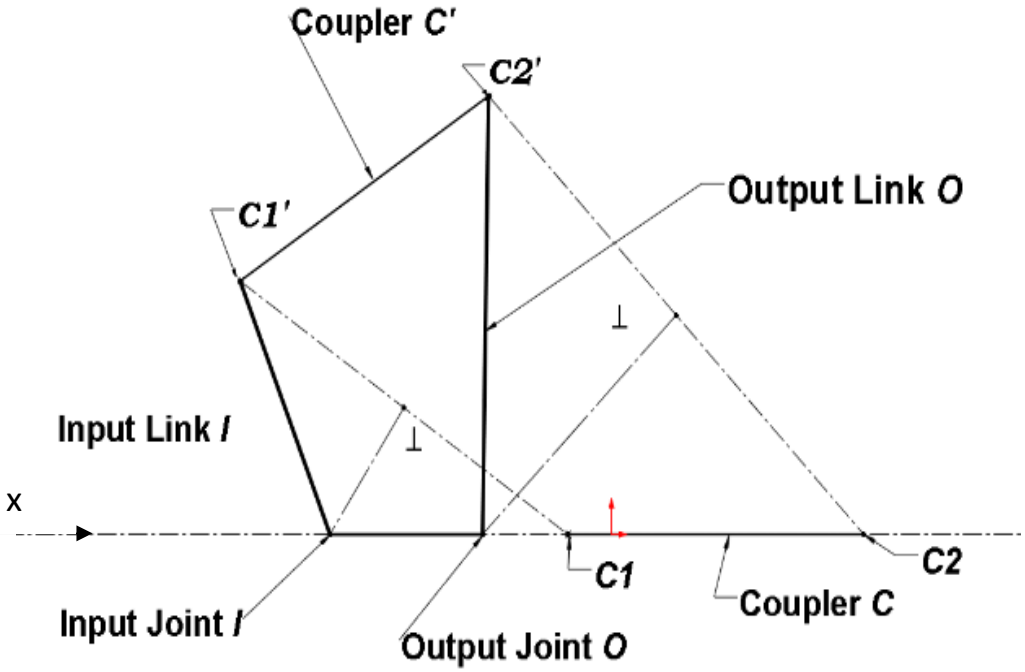

Figure 3.2: The two-position synthesis of the planar mechanism.

Now, the segment I-O is the ground link of change-point mechanism. In configuration C', $C_1' - I$ is the input link and $C_2' - O$ is the output link, and C_1'-C_2' is still the coupler link. In configuration C, the four-bar is in a change-point position in which all four links are collinear, and C_1-I is the input link, C_2-O is the output link, and C_1-C_2 is still the coupler link.

The rest of the chapter is organized as follows: First, we discuss the relationship between simple origami fold patterns and change-point spherical mechanism. Then, we discuss the design

concept for a bistablity, which applies to both spherical mechanisms and simple origami folds. Then, we describe the dimension synthesis procedure for the mechanism. We then show the prototypes for both the bistable spherical mechanism and the bistable origami fold. Finally, we discuss our results and give our conclusions.

3.2 Origami to Spherical Mechanism

Any flat panel can be defined geometrically as an assemblage of triangles. When several triangles are attached together, they can create a piece of origami that can be folded (see Figure 3.3), if the triangles satisfy origami design rules [74].

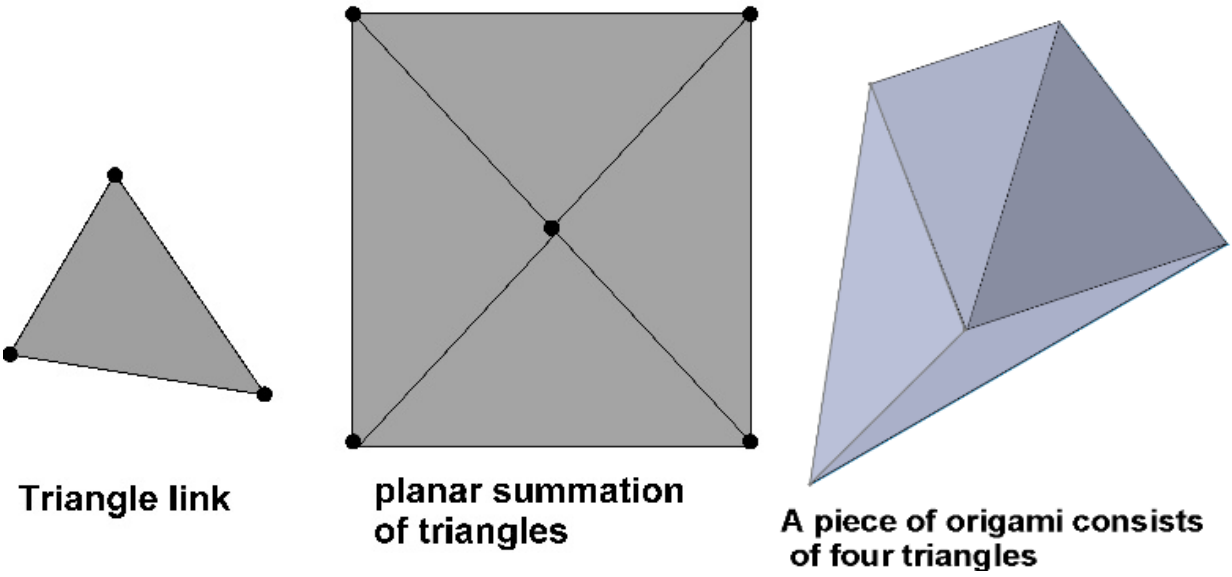

Figure 3.3: Examples of how an origami fold pattern can be assembled from trianglular links.

Each side of the triangle is a crease and it can be either a mountain fold or a valley fold. Each panel of the origami can be considered as a link and every crease is a hinge. Therefore, a folded piece of origami is a mechanism that moves in space. Simple origami mechanisms can be either open-loop or closed-loop mechanisms. Table 3.1 shows examples of the classification of simple origami mechanisms made from connected triangles.

Table 3.1 shows that with four triangles, the simplest closed-loop mechanism is an origami fold pattern known as the *reverse fold*. At the center of all origami closed loops is a single point, called a vertex, as shown in Table 3.1 for four and five link closed-loop mechanisms. Several closed loops can be put together to form more complicated pieces of origami, and the number of interior vertexes is the number of closed loops in the origami mechanism [75, 76].

Table 3.1: Examples of origami's mechanisms. [77].

# of triangles	Open loop	Closed loop
2		Not mechanism possible
3		No mechanism possible
4	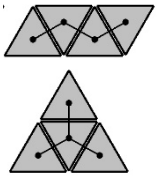	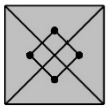
5	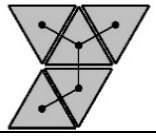	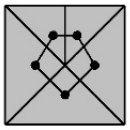

In this chapter, we will focus on how to make the origami reverse-fold bistable. In this process, it is helpful to know that there is an overlap between a certain simple class of origami (the reverse-fold) and a class of spherical mechanisms (see Figure 3.4). If a circle is drawn about the vertex of reverse-fold, the fold lines define link boundaries of a change-point spherical mechanism, one in which the links are circular arcs – defined by the circle's perimeter, and the sum of the four-arcs equals 360°. We can design simultaneously a spherical change-point mechanism and an origami reverse-fold. In the design process, the spherical mechanism version allows us to use

spherical kinematics and synthesis techniques. However, in applications, bistable origami mechanisms may be more useful.

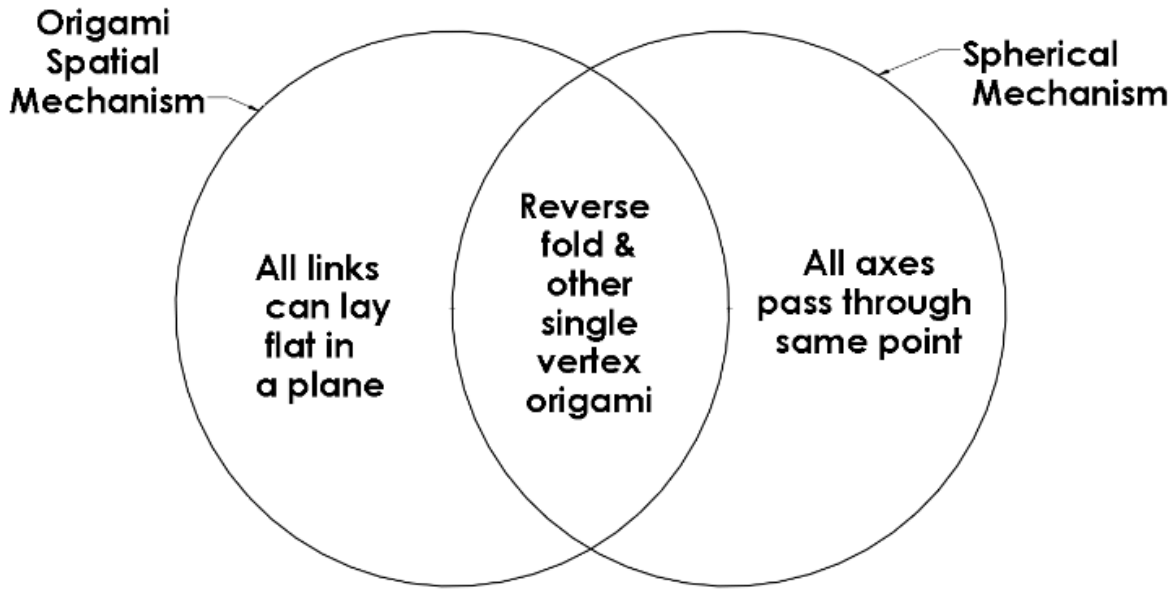

Figure 3.4: Venn diagram showing the overlap between spherical mechanism and origami fold design spaces.

3.3 Bistable Design Concept

This section of the chapter demonstrates a design process for making a reverse-fold (or spherical change-point mechanism) bistable. A bistable mechanism is defined as a mechanism that has two stable configurations which are in equilibrium and which are robust against small perturbations, i.e. a stable configuration is one that a mechanism will return to after it is slightly perturbed away from it [32]. This is achieved when the potential energy of the mechanism is such that there are two local minima of potential energy. The potential energy minimum points are obtained by first choosing the desired stable origami configurations, and then adding a spring element that is designed to be relaxed in the stable configurations. For origami, the first stable configuration is the flat, planar arrangement of the links, i.e. a flat sheet without any folds, which is a configuration when the potential energy is naturally a minimum. This is because a fold always

strains a material. However, by design, the potential energy curve is dominated by an elastic element, such as a spring, a flexure, or gently buckled piece of paper, that stores energy as it bends, stretches, or compresses with mechanism's movement.

The design process is described in next two sections; the first describes the synthesis of the reverse-fold (or spherical mechanism), the second section describes how to place the elastic element so that the desired configurations of the reverse fold origami (or spherical mechanism) are stable. In the discussion that follows, the procedure is equally applicable to origami reverse-folds and spherical change-point mechanisms, and so, for convenience we will refer to "the mechanism" when the discussion is applicable to both reverse-folds and spherical mechanisms.

3.3.1 Kinematic Synthesis of the Mechanism

In this section of the chapter, the mechanism is modeled using parametric CAD software, which provides a clear visualization of the design approach. It makes kinematic chains and their properties, such as displacement, straightforward to analyze. The graphical synthesis technique is adapted from the planar synthesis procedure described in the Introduction.

We consider a sphere with a radius R whose equatorial circle is shown in Figure 3.5. First, we consider a coupler link whose change point configuration C lies in the equatorial plane as shown in Figure 3.5. We define the spherical mechanism with arcs on the sphere, and the origami triangles are easily obtained by connecting the endpoints of the arcs to the center of the sphere. The coupler link will move from configuration C to C', as shown in Figure 3.6. As in the planar case, we label the moving pivots C_1 and C_2 in configuration C, and C_1' and C_2' in configuration C'.

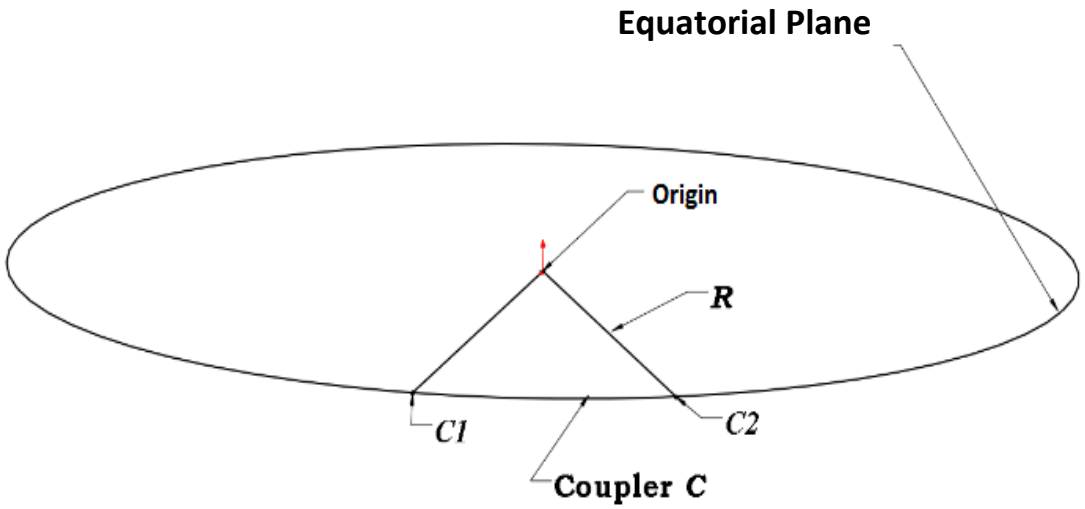

Figure 3.5: Initial planar position of the reverse-fold's coupler link.

Next, we draw the perpendicular bisectors of great circle arcs $C_1 - C_1'$ and $C_2 - C_2'$. These perpendicular bisectors are also great circle arcs. Finally, the intersections of these bisectors with the equatorial circle defines points *I* and *O* as shown in Figure 3.6. In spherical mechanism synthesis, the antipode of a given pivot functions as a kinematically equivalent pivot. This means that there are four different versions of the mechanism, depending on whether we construct the mechanism using ground pivots *I* and *O*, or whether we substitute one or both antipodal points of *I* and *O*.

Although the coupler link is defined, and the construction method defines the planes of the side links, each of the side planes can be attached to the ground plane in two different ways. This leads to four different possible versions of the mechanism, as shown in Figure 3.7.

1. The first version (see Figure 3.7a) uses points *I* and *O*, and both the input and the output sides (spherical link's angles) range from 0° -90°.

2. The second version (see Figure 3.7b) uses *I*'s antipode and *O*, so the input side is over 90° and the output side ranges from 0° -90°.
3. The third version (see Figure 3.7c) uses both *I* and *O*'s antipodes, and both the input and the output sides are over 90°.
4. The fourth version (see Figure 3.7d) use *I* and *O*'s antipode, and the input side between 0° and 90° and the output side is over 90°.

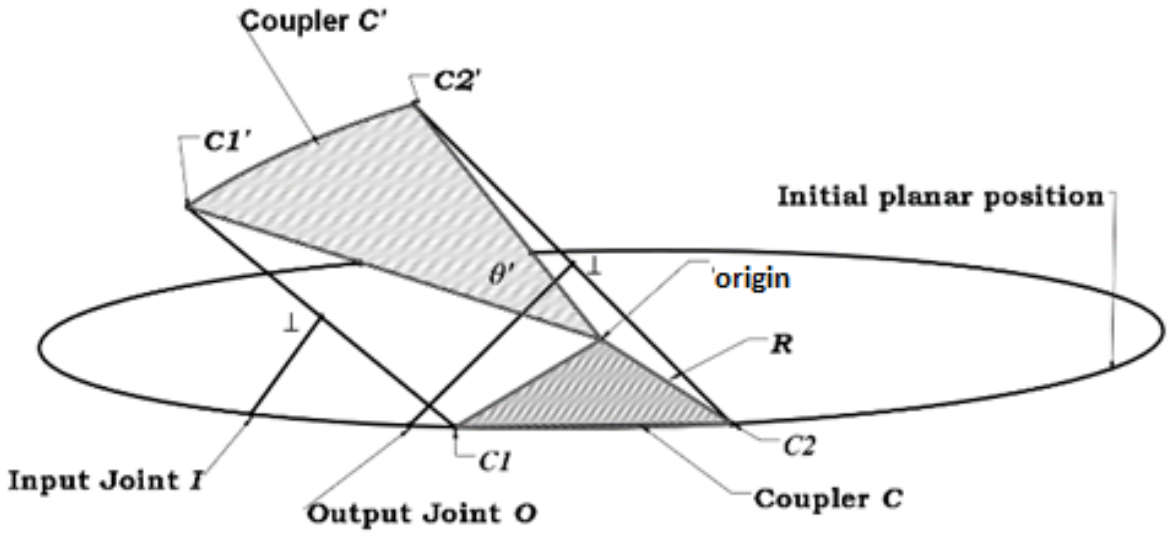

Figure 3.6: Schematic showing two position synthesis for a spherical mechanism. The first stable position of the coupler link *C* is in the equatorial plane of the sphere. The chosen second position can be achieved by any arbitrary rotation about the sphere center point *O*, and is denoted *C'*. The displacement planes for the moving pivots are given by points *O-C1-C1'*, and *O-C2-C2'*, respectively.

The four categories are evaluated using the relationship between angles and sides of a spherical triangle and Napier's rules [78]. In any single vertex piece origami, the summation of sides' angles should add up to 360°. The equations of all sides are calculated as:

$$\delta^\circ + \alpha^\circ + \lambda^\circ + \xi^\circ = 360^\circ. \qquad (3.1)$$

where $\delta°$ is the coupler link's angle, $\alpha°$ is the input link's angle, $\lambda°$ is the output link's angle, and $\xi°$ is the ground link's angle.

$$\cos(A_1) = \cos\left(\frac{b_1}{2}\right)\sin(H_1), \cos(A_2) = \cos\left(\frac{b_2}{2}\right)\sin(H_2), \tag{3.2}$$

$$\cos(J_1) = \cot(H_1)\cot(A), \cos(J_2) = \cot(H_2)\cot(A_2) \tag{3.3}$$

where b_1 and b_2 are the sides of $C_1 - C_1'$ and $C_2 - C_2'$ respectively that define the desired location of the coupler. H_1 and H_2 are the angles between $C_1 - C_1'$ and $C_2 - C_2'$ with the equatorial plane. A's is the angle of the intersections of the bisectors with the equatorial plane. J_1 and J_2 are the sides of C_1–I and C_2–O respectively.

$$\cos(\lambda°) = \cos(b_1)\cos(J_1) + \sin(b_1)\sin(J_1)\cos(H_1). \tag{3.4}$$

$$F = \delta° + J_1 - J_2 \tag{3.5}$$

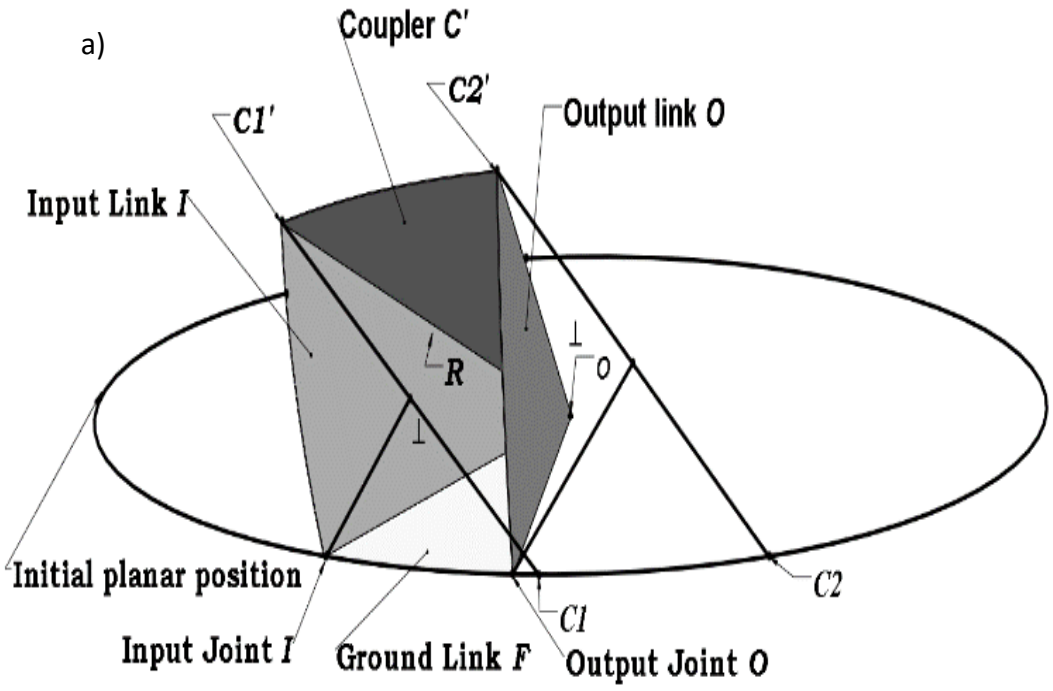

Figure 3.7: Four different reverse-fold mechanisms that satisfy the two position synthesis. As shown in Figure 3.6. Part a) Version 1, Part b) Version 2, Part c) Version 3, and Part d) Version 4.

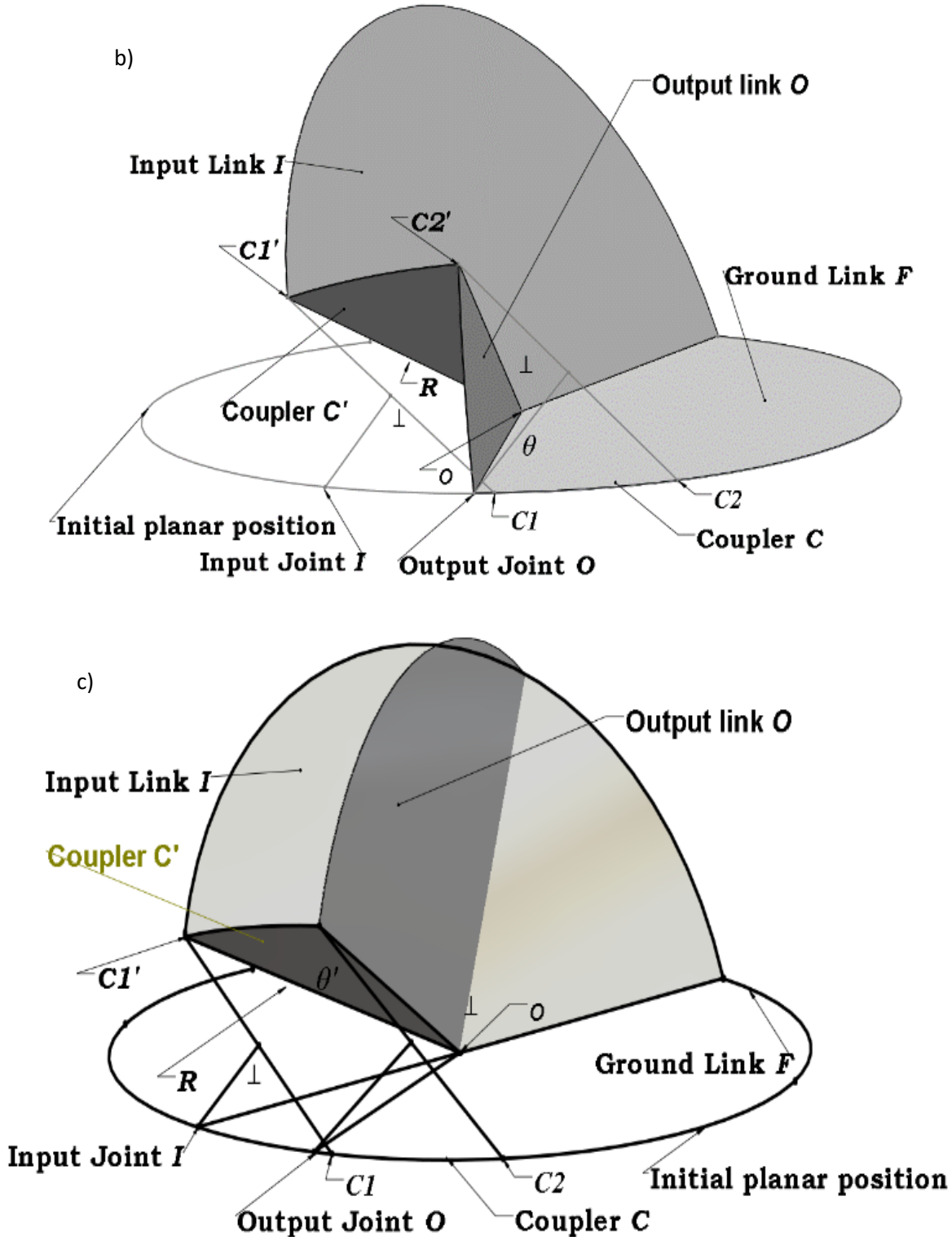

Figure 3.7 (Continued)

d)

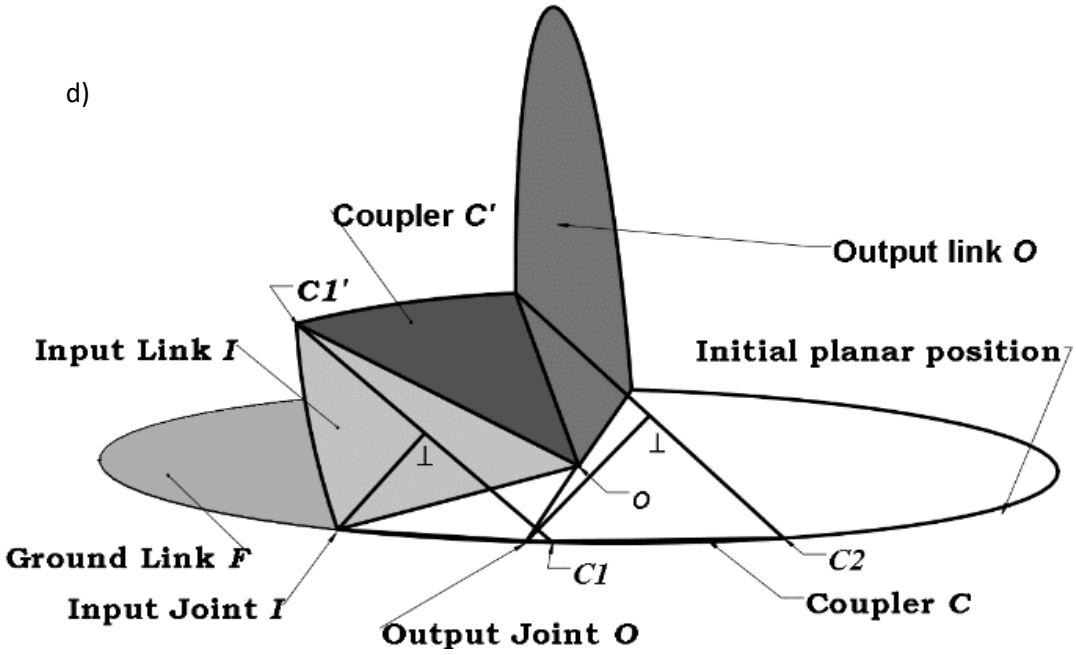

Figure 3.7 (Continued)

Then, Eq. (3.1) can be applied for all four categories to test them as single vertex pieces of origami as detailed in Table 3.2:

Table 3.2: Four versions of the reverse fold origami.

Version 1	$\delta° + \alpha° + \lambda° + \xi° \neq 360°$
Version 2	$\delta° + 180 - \alpha° + \lambda° + 180 - \xi° = 360°$
Version 3	$\delta° + 180 - \alpha° + 180 - \lambda° + \xi° \neq 360°$
Version 4	$\delta° + \alpha° + 180 - \lambda° + 180 - \xi° = 360°$

Table 3.2 shows that version 1 and version 3 cannot be a single vertex origami mechanism as they cannot be folded out of one planar sheet. However, version 2 and version 4 are able to form single vertex origami, where version 4 is the mirror image of version 2. Version 4 is used for the rest of this chapter and for the bistable prototypes.

3.3.2 Bistable Link Position of the Mechanism

The elastic element is designed assuming that it will be attached to the ground link on one end and that it will be attached to the coupler link on the other end. The goal in its design is to pick points on the ground link and coupler link that are equidistant in configuration *C* and *C'*. During the motion of the mechanism, the elastic element experiences compression/tension due the different rigid-body trajectories of the coupler link attachment point and the elastic elements free-end. This difference results in stretching or compressing the elastic element, giving a potential energy curve that can be controlled by adjusting the location of the fixed end at the ground link. A compliant flexure can be used for the elastic element in the spherical mechanism because it is easy to manufacture and provides more control and easier adjustment of its stiffness [32, 79]. In the origami version, the elastic element is made from a second sheet of paper.

The location of the elastic element is chosen using parametric CAD software, and the user can identify the motion limits of the mechanism and where the elastic element might interfere with the mechanism. The design process proceeds as follows:

1. We choose a point *P* on the coupler link, and define its trajectory from configuration *C* to *C'*. In configuration *C*, its location is *P*, and in configuration *C'*, its location is *P'*. In Cartesian coordinates, points *P*, *P'*, and anywhere in between can be found using the following equations (See Figure 3.8) [80, 72]:

$$x_p = R * \left[cos\left(\frac{\delta^\circ}{2}\right) * cos(\alpha^\circ) + sin\left(\frac{\delta^\circ}{2}\right) * cos(\beta) * sin(\alpha^\circ) \right]. \tag{3.6}$$

$$y_p = R * \left[cos\left(\frac{\delta^\circ}{2}\right) * cos(\phi) * sin(I) + sin\left(\frac{\delta^\circ}{2}\right) * sin(\beta) * sin(\phi) - sin\left(\frac{\delta^\circ}{2}\right) * \cos(\beta) * \cos(\alpha^\circ) * \cos(\phi) \right]. \tag{3.7}$$

$$z_p = R * [cos\left(\frac{\delta°}{2}\right) * sin(\phi) * sin(\alpha°) + sin\left(\frac{\delta°}{2}\right) * sin(\beta) * cos(\phi) - sin\left(\frac{\delta°}{2}\right) * \cos(\beta) * \cos(\alpha°) * sin(\phi)] \quad (3.8)$$

where ϕ is the input angle between sides *I* and *F*. β is the angle between the input and the coupler links which calculated as [81]:

$$\beta = arccos\{[sin(\lambda°) * cos(2 * A) * sin(\xi°) + cos(\lambda°) * cos(\xi°) - cos(\alpha°) * cos(\delta°)]/\sin(\alpha°) * \sin(\delta°)\}. \quad (3.9)$$

2. We construct the perpendicular bisector arc to the great circle arc *P-P'*. The fixed end of the elastic element can be chosen to be anywhere on the plane containing this perpendicular bisector arc. This selected point is called *Q*.
3. We draw a great circle arc from *Q* to *P* in configuration *C* and from *Q* to *P'* in configuration *C'*, and verify that these arcs have the same length. (See Figure 3.9).

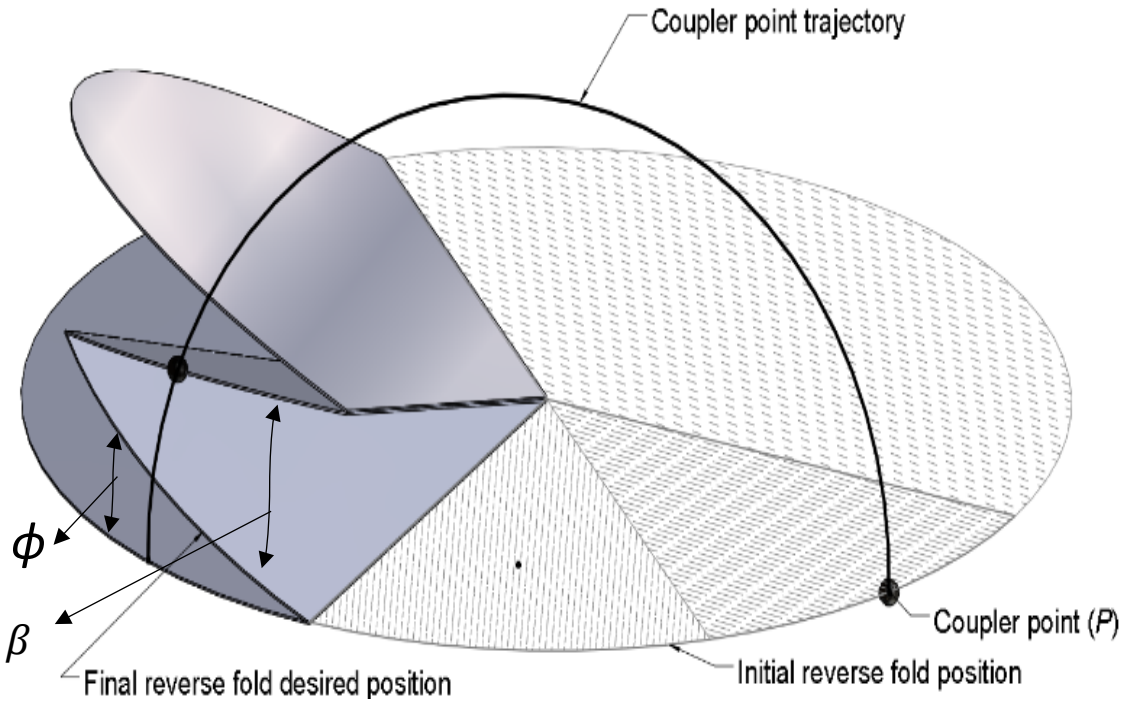

Figure 3.8: The *P* and *P'* configurations of the mechanism and the location of the elastic element.

The length of arc *QP* is equal to the length of the compliant element. The small circle arc centered at *Q* which passes through points *P* and *P'* is the trajectory of the undeflected elastic element, which is different from the coupler trajectory of point *P*. The different paths force the compliant element *QP* to stretch or compress to accommodate the motion of the mechanism from configuration *C* to *C'*, which results in strain energy in the elastic element as the mechanism moves.

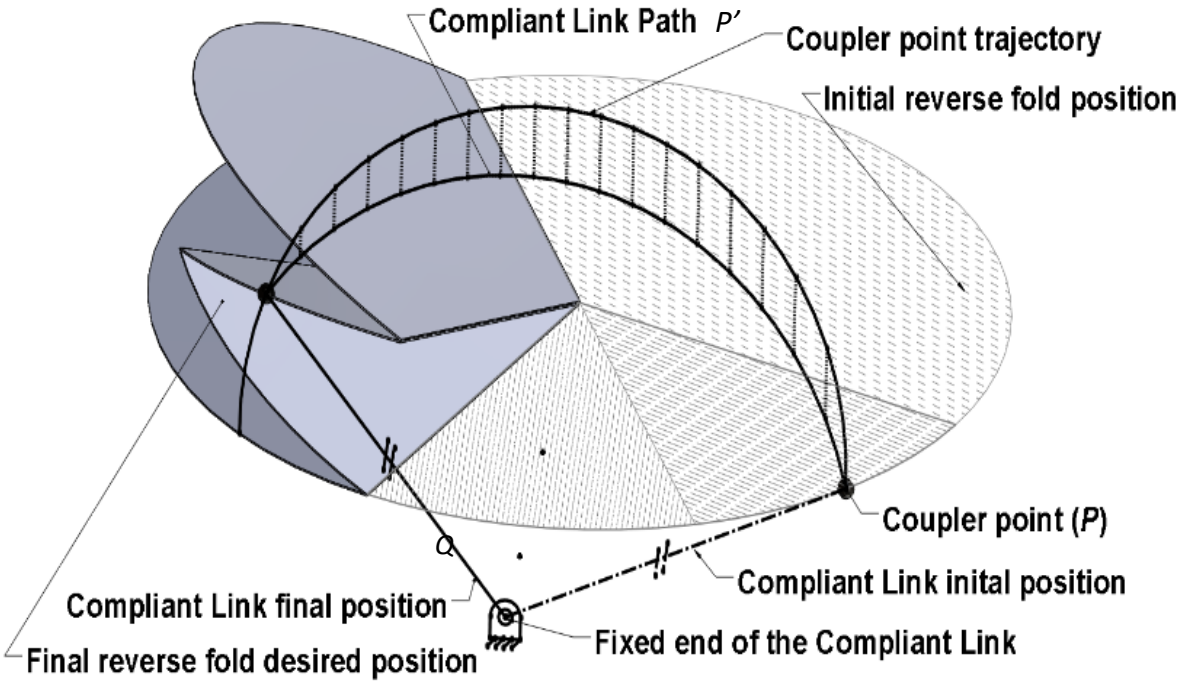

Figure 3.9: The coupler point (*P*) trajectory that goes through the *P* and *P'* locations of the mechanism.

The two paths meet at *P* and *P'* which means an undeflected compliant link and insures their minimum potential energy and equilibrium, provide that other sources of potential energy in the mechanism are negligible in comparison. We can adjust the position of the fixed end of the elastic element to enhance the difference of the two paths which results in greater stability of points *P* and *P'*, provided that we do not exceed the mechanism's stress limitation and ensure that the mechanism links avoid self-interference.

3.4 Spherical Mechanism Prototype

In this section of the chapter, our design was chosen to be a partially compliant spherical change-point mechanism. In the next section, we discuss the origami version of the same design concept. The design was manufactured using a stereo-lithography (STL) 3D printer and a laser cutting machine. Due to the limitations of our STL printer, our design was chosen to have base radius, *R,* of 66 mm (5.2 inches). All parameters of the design are derived from Sec. (3) and parametric CAD and are given in the Table 3.3. These parameters can be used to represent the bistable mechanism in the initial and final positions.

In the fabrication of this mechanism, we chose the fixed end *Q* of the elastic element to be on a parallel plane to the equatorial plane of the spherical mechanism. This allowed us to make the links of the spherical mechanism large enough to support high forces, which were necessary to overcome friction in the joints. This results in a cylindrical topology was easy to implement with screws with providing for the vertical offset. The cylindrical offset position also means that the elastic element, a compliant flexure does not interfere with the spherical mechanism and it gave a reasonable separation between the two planes, allowing a compliant flexure which gave adequate force to change between the stable configurations.

Table 3.3: Design parameters (mm and degrees) for *R*=66mm.

input angle ϕ	Compliant link length	R	$\alpha°$	$\lambda°$
18.6°	50.8	66	45°	135°
X_p	Y_p	Z_p	$\delta°$	$\xi°$
66.04	-4.45	-12.7	45°	135°

The spherical mechanism's links are 3D-printed from a 3/8-inch-thick STL material. The spherical mechanism's links were attached to each other with 3-D printed pins and metal screws. The compliant link was laser cut from a 1/8-inch-thick Polypropylene co-polymer material (Figure 3.10). The links are connected by hinge joints as shown in Figure 3.11.

Figure 3.10: The compliant link that was added to the spherical mechanism to make it bistable.

The compliant link is designed as an initially curved pinned-pinned beam [32]. The compliant link length is initially stretched to compensate the prismatic stresses at the joints that occur due to manufacturing flaws. This compensates somewhat for the joint's tolerances and friction, which affects the stability of the mechanism. Figure 3.12 shows the spherical mechanism in the two stable configurations (*C* and *C'*).

Figure 3.11: The hinge joints used in the mechanism.

Figure 3.12: Stable configuration *C'* (on the left) and stable configuration *C* (on the right) for the partially compliant spherical mechanism.

3.5 Origami Reverse-Fold Prototype

In this section, the same design concept was used to make a bistable reverse-fold using two flat sheets of paper. Figure 3.13 shows the CAD model of the design in the two design configurations. The compliant element here was another sheet of paper that attached to the original reverse-fold origami.

Figure 3.14 shows the prototype of the reverse fold in the two different design configurations. The design was manufactured using black cardboard papers and the elastic element, the second sheet of paper, was attached using staples as shown in Figure 3.15.

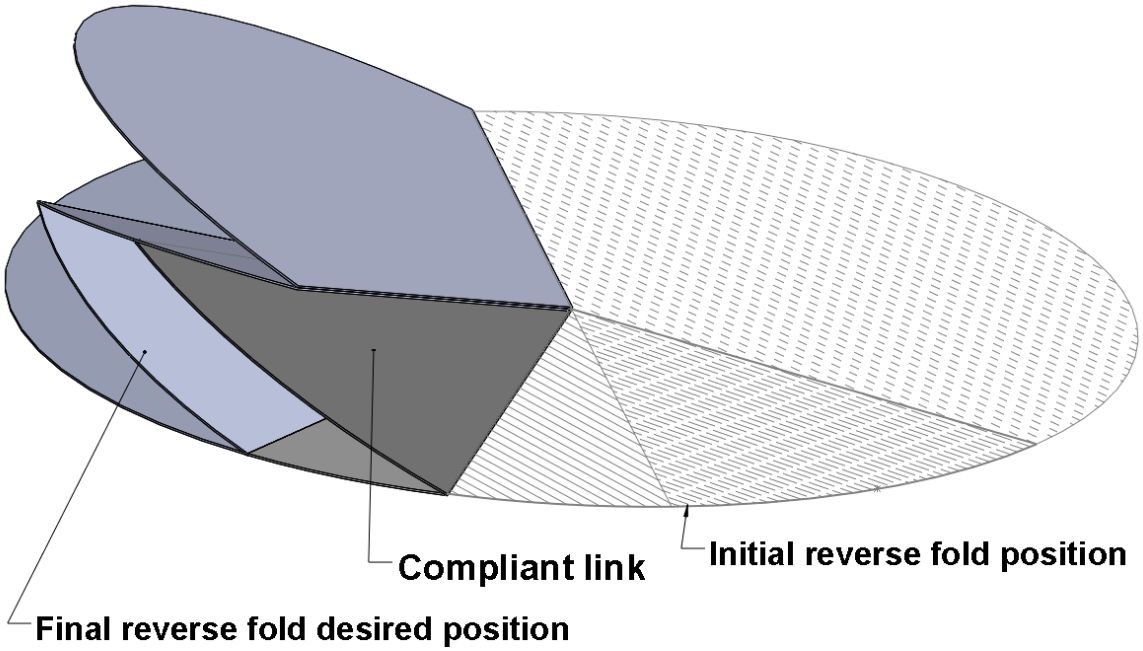

Figure 3.13: The CAD model of the bistable origami reverse-fold.

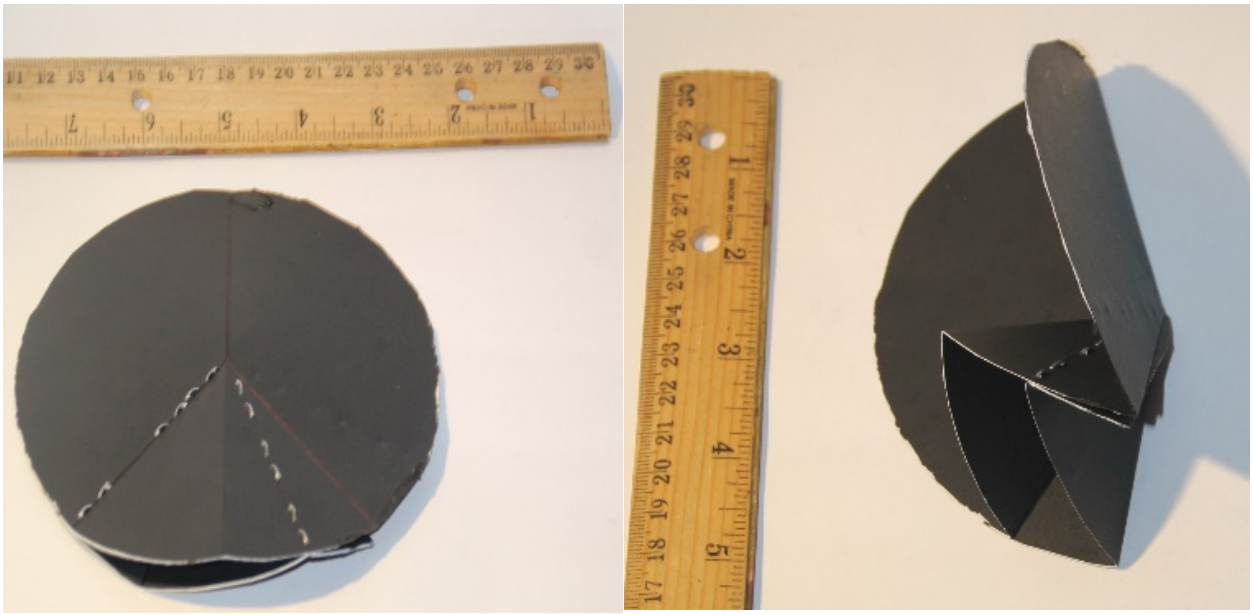

Figure 3.14: Stable configuration *C'* (on the left) and stable configuration *C* (on the right) for the origami reverse-fold.

3.6 Results and Discussion

This section compares the results between the graphical model and the prototypes. The graphical model predicts the stability of the origami reverse-fold mechanism and spherical mechanism at the designed configurations, and the prototypes were tested for their stability at the designed configurations. We verified bistability of the prototypes, verifying that they were robust against small perturbations by shaking them. We found that the spherical mechanism was stable at the designed positions, but that the origami mechanism tended to deform plasticly and to be stable near the designed positions but the actual configurations it assumed changed somewhat depending on how the paper was manipulated as shown in table 3.4. Thus, the stable configurations of the origami could vary by a few degrees of motion of the various links in successive actuations of the prototype.

Table 3.4: Comparison between the mathematical model and the prototype in Angle ϕ.

	Math. Model(mm)	Spherical Mech. Prototype(mm)	Error (%)
Angle (ϕ)	18.6°	20	7.5
	Math. Model(mm)	Origami Prototype(mm)	Error (%)
Angle (ϕ)	18.6°	24.5°	33

3.7 Closure

This chapter has presented new bistable origami reverse fold origami and spherical mechanism. A spherical kinematic synthesis method for a spherical four-bar (or origami reverse-

fold) was described. Spherical kinematics was also used to locate an elastic element to produce bistable behavior. The origami reverse-fold and partially compliant spherical mechanism were modeled geometrically and prototyped as proofs-of-concept for the bistable design technique.

CHAPTER 4

SHAPE-MORPHING USING BISTABLE TRIANGLES WITH DWELL-ENHANCED STABILITY[2]

4.1 Introduction

This chapter presents a new design concept for a morphing triangle-shaped compliant mechanism. The novel design is a bistable mechanism that has one changeable side. These morphing triangles may be arrayed to create shape-morphing structures. The mechanism was based on a six-bar dwell mechanism that can fit in a triangle shape and has stable positions at the motion-limit (dead-center) positions. An example of the triangle-shaped compliant mechanism was designed and prototyped: an isosceles triangle with a vertex that changes from 120 degrees to 90 degrees and vice versa. Three of these in the 120-degree configuration lie flat and when actuated to the 90-degree configuration become a cube corner. This design may be of use for folding and packaging assistance. The force analysis and the potential energy analysis were completed to verify the stability of the triangle-shaped compliant mechanism. Because of its dead-center motion limits the vertex angle cannot be extended past the range of 90 degrees to 120 degrees in spite of the mechanism's compliant joints. Furthermore, because it is a dwell mechanism, the vertex angle is almost immobile near its stable configurations, although other links in the mechanism move. This makes the stable positions of the vertex angle robust against stress relaxation and

[2] This chapter is based on a published paper in proceedings of the ASME 2018 International Design Engineering Technical Conferences & Computers and Information in Engineering Conference IDETC/CIE 2018, Quebec City, Canada

manufacturing errors. We believe this is the first demonstration of this kind of robustness in bistable mechanisms.

The objective of this research was to design a morphing triangle-shaped bistable compliant mechanism with hard motion limits. A triangular morphing element is useful because any polygon shape can be built from a combination of triangles and one polygon may be morphed into another by morphing its constituent triangles. One application of this is to produce polygon designs that are fabricated from a flat sheet of material and morph into their desired shape. Morphing triangle mechanisms may have applications in folding and packaging processes as they can be attached to a cardboard box while in its in flat position and then deployed to change into the closed box shape. Another application is portable boxes that can be deployed as cages for small animals and stored efficiently while flat. The need for morphing triangles may occur in other applications including aerospace devices, locking devices, and shape-change structures [1-3].

For this chapter, we developed a design concept for a bistable triangle compliant mechanism that when arrayed in three triangles in circular pattern, it morphs to create a cube corner shape.

For this work, the background is in the areas of shape-morphing structures, dead-center motion limits, dwell mechanisms, and bistability. Shape-morphing structures have been investigated as morphing wings, automobile structures, and structural actuators [4-8]. The challenging part of shape-morphing structure is actuation. Researchers have studied many solutions for actuating shape-morphing structures and most of them are complicated and are external to the structures [60]. Compliant mechanisms may be a viable solution because of their members' flexibility that allows for appropriate mobility and actuations [61]. Compliant mechanisms provide many advantages for shape-morphing structures as they help overcome

actuation problems [82] and have simpler manufacturing processes [32]. In addition, compliant mechanisms enable the ability of manufacturing a single layer mechanism that include compliant joints that function as pin joints. One way of simulating pin joints in compliant mechanisms is to use a small-length flexural pivot (living hinge). Living hinges are used in many commercial products. Living hinges are very short, very thin flexures that have a negligible resistance to bending so that they can be modeled as a pin joint without torsional spring [4].

Motion limits are useful in compliant mechanisms because they prevent overstress and premature fatigue failure. Dead-center motion limits are positions where mechanisms lose their mobility. They are positions in which the mechanism cannot continue moving in the same direction. Kinematically, it means that the kinematic coefficients (the instantaneous ratios of output velocity to input velocity) become infinity which only occurs when the output is non-zero, and the input is zero. This means the input must stop at the dead position and no further motion in the same direction can be applied. A dead-center example is the crank-slider mechanism when the slider is the input, as shown in Figure 4.1.

This behavior is considered an obstacle in some industrial and machine designs. However, it is useful for other designs, such as in lock devices and motion-limit mechanisms [20].

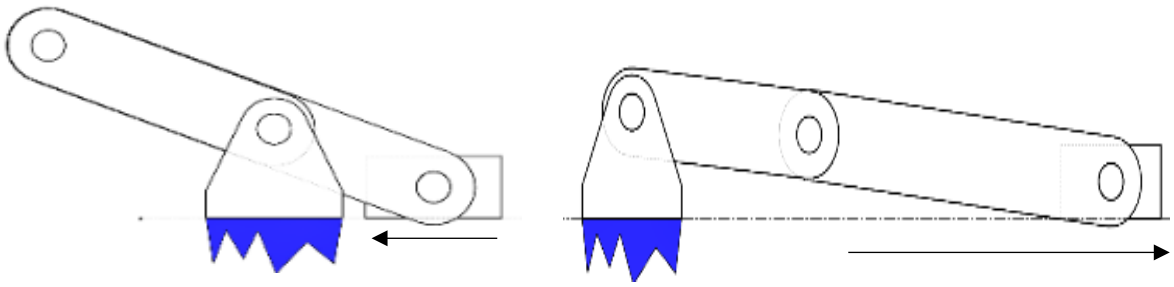

Figure 4.1: A crank-slider mechanism at dead-center positions when the slider link is the input and the transmission angle is 0^o and 180^o.

Another common approach that has similar advantages as dead-center motion limits is having a hard-stop. The hard-stop technique has been used in many applications as it can prevent excessive motion in moving parts [21]. Dead-centers and hard-stops lead to similar results, but dead-centers may have advantages over the hard-stop. A hard-stop is usually external to the linkages which may cause creep with compliant linkages while dead-center is an internal to existing links resulting in less creep issues. A hard-stop required an *ad hoc* placement of the stop which causes contact-based stresses on linkages and may not be appropriate for thin layer linkages. On the other hand, the dead-center position does not require link stresses for its motion-limiting function. It is also applicable for thin laminates like cardboard because the motion limits are due the kinematic of linkages and not stresses, which might result in creep or other deformations.

There are many ways to find the dead-center positions of mechanism [22]. When the determinant of the mechanism's Jacobian matrix goes to zero, the mechanism is at dead-center position [23]. In addition, the graphical instant centers method (IC) has been used to define the dead-center positions of planar linkage mechanisms. It makes kinematic chains and their properties, such as displacement, straightforward to analyze [83]. The instant center, $I(\alpha,\beta)$, is a location at which there is no relative velocity between the two links α and β. The kinematic coefficients for rotating links can be computed based on the locations of their instant centers as:

$$\frac{d\theta_o}{d\theta_i} = h_{oi} = \frac{|I(i,o) - I(g,i)|}{|I(i,o) - I(g,o)|} \tag{4.1}$$

where i is the input link, o is the output link, and g is the ground link and $|I_1 - I_2|$ is the distance between instant centers 1 and 2.

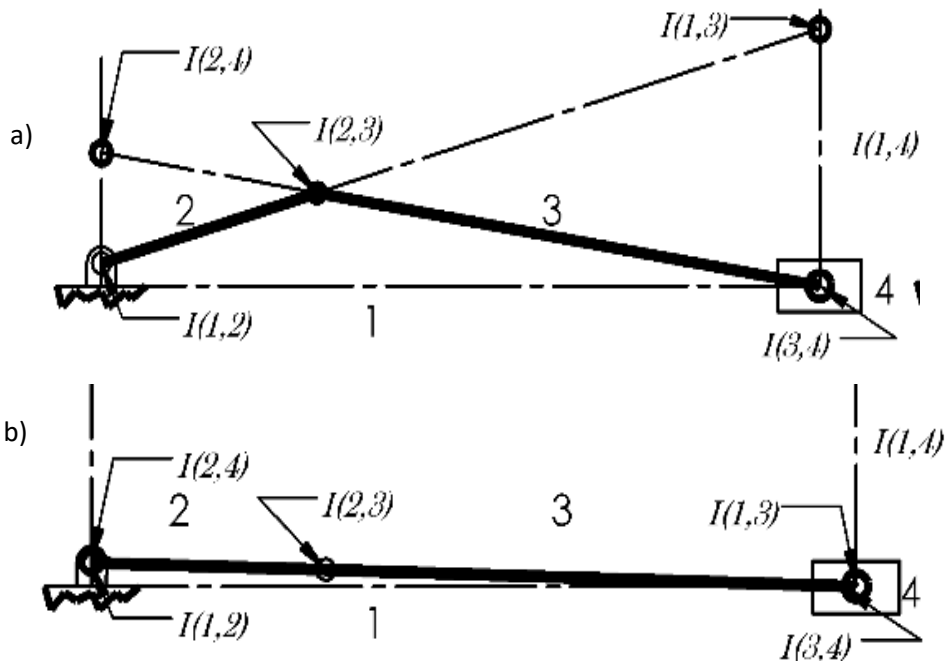

Figure 4.2: a) All ICs on a crank-slider mechanism. b) the crank-slider mechanism at a dead-center position where $\frac{d\theta_4}{d\theta_2} = \frac{|I(2,4)-I(1,4)|}{|I(2,4)-I(1,2)|}$ becomes infinity because $I(2,4)$ and $I(1,2)$ are coincident.

The procedure for finding ICs based on the kinematic pairs in a mechanism and the Aronhold-Kennedy theorem is given in several texts of mechanism design [1]. In Figure 4.2, we illustrate an example of a dead-center position occurring in a crank-slider when the instant centers in the denominator of equation (4.1) become coincident [23] resulting in a motion limit. In addition to the dead-center approach, a complimentary technique for motion limits is to use a dwell mechanism (which may have a dead center).

Dwell mechanisms have an interesting behavior that allows the output of a mechanism to became momentarily stationary at continuous range of input [1]. Figure 4.3 shows a coupler curve path of a four-bar mechanism. The coupler link is attached to link 6 by a pin and slider. When the input is applied, the coupler point goes through colinear motion with link 6 for two different ranges of motion. In these regions, link 6 does not rotate i.e. it dwells at a certain angle.

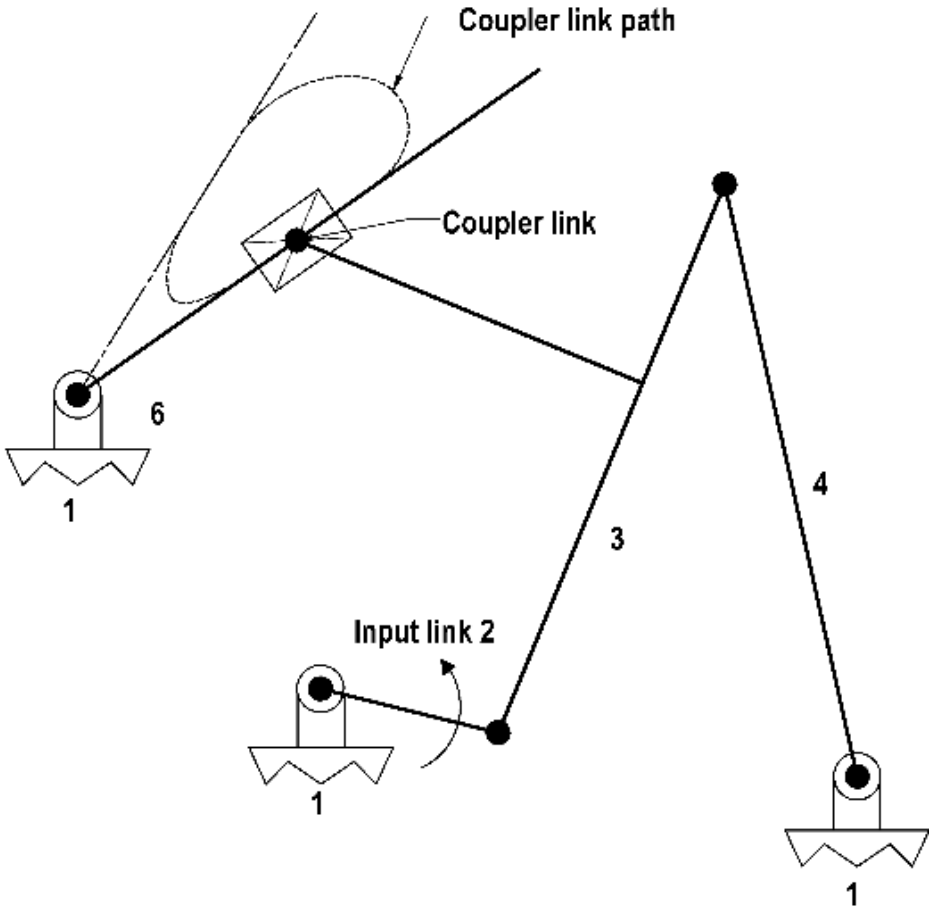

Figure 4.3: Straight-line dwell mechanism. Adapted from [1]**.**

In addition to dead-center motion limits and dwell mechansims, shape-morphing arrays are benefitted by bistability because the distinct array configurations may be stable, i.e. the distinct shapes may be held without actuation. A mechanism is called "bistable", when the mechansim has two distinct configurations which are local minimums of potential energy. One of the best way to describe bistability is using the "ball-on-a-hill" analogy [32], that shows the analogy between the potential energy (strain energy) of a compliant mechanism.

4.2 Polyhedral Surfaces with Triangle-Shaped Mechanisms

Any polyhedral surface can be defined geometrically as an assemblage of triangles. For example, when three triangles of a configuration of (90-45-45 angles) are joined to each other by

the sides adjacent to the right angle, they form a corner of a cube. If the triangles have one changeable side, the assembly of the three triangles can be designed to lay flat (120-30-30 angles) using a shape-morphing triangle as shown in Figure 4.4.

A triangle-shaped mechanism can be designed using a one D.O.F. mechanism (i.e. a single-loop four-bar, a two-loop six-bar, etc.). Four-bar one D.O.F. mechanisms have limits in the number of dead-centers that can be used for stability (discussed in Section 3); moreover, the definition of dead-center in the four-bar mechanisms is when the transmission angle (the angle between the two-unactuated links) becomes either zero or 180 degrees [84]. These limitations make four-bar designs behave somewhat like a hard stop. [85]. Additionally, a 180-degree rotation of the transmission angle is required between the two dead-center positions, which would tend to overstress a compliant joint. Thus, we chose to investigate six-bar one D.O.F. mechanisms. Six-bar mechanisms can have multiple dead-center positions [83] which allows flexibility in satisfying our design objectives. We chose Stephenson's chain for the six-bar triangle mechanism with two ternary links, two binary links, and one slider link as shown in Figure 4.5a. Stephenson's chain has two loops mechanism that allows dead-center to occur with less motion of compliant links. Figure 4.5b shows a symmetry of the mechanism where the slider link turns to a joint that moves linearly to resemble the slider motion. This creates a triangular mechanism where link 2 is the constant sides of the triangle and the changeable side is the virtual distance between the end of link 2 with its symmetry.

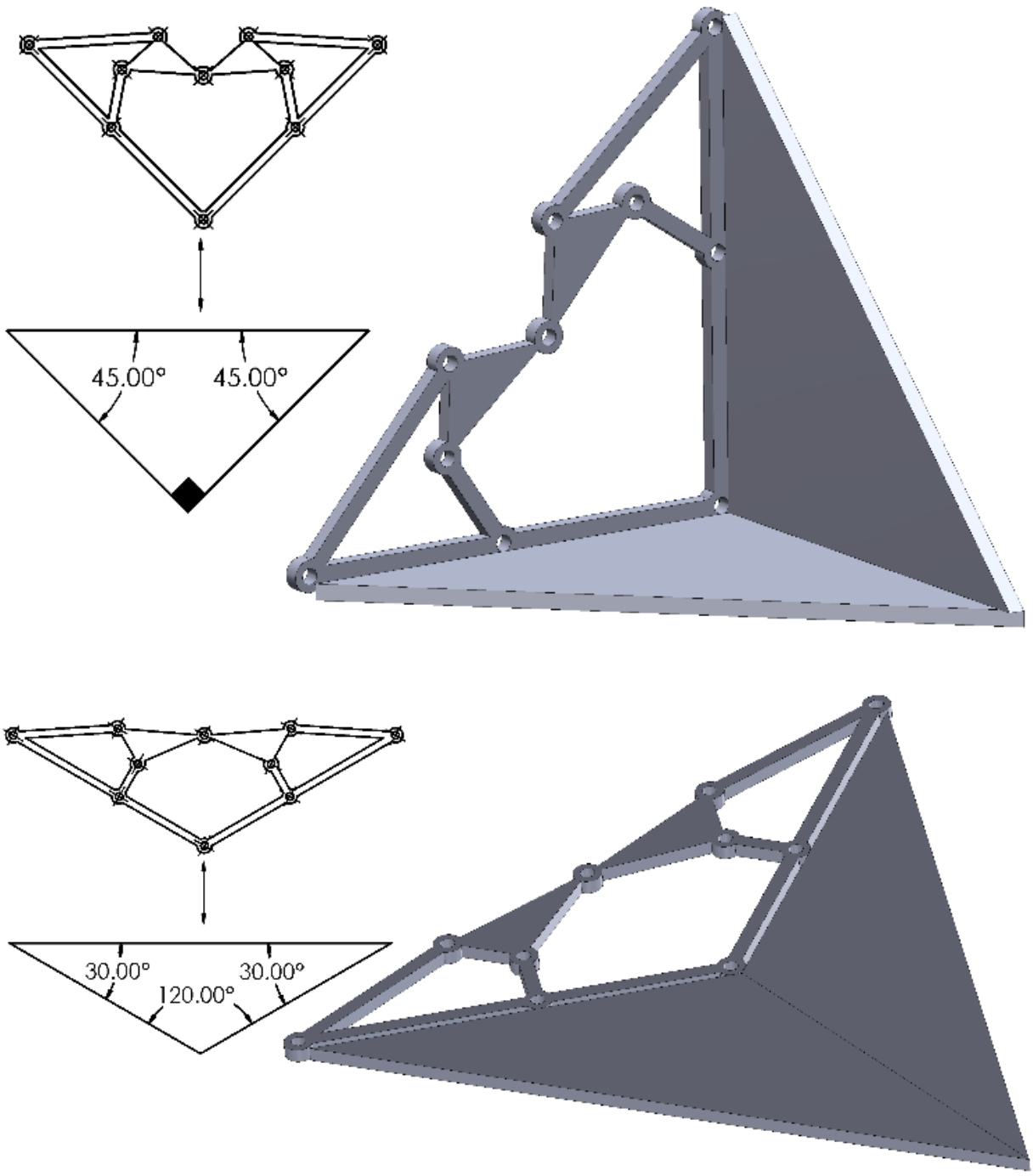

Figure 4.4: A shape-morphing polygon formed of three triangles.

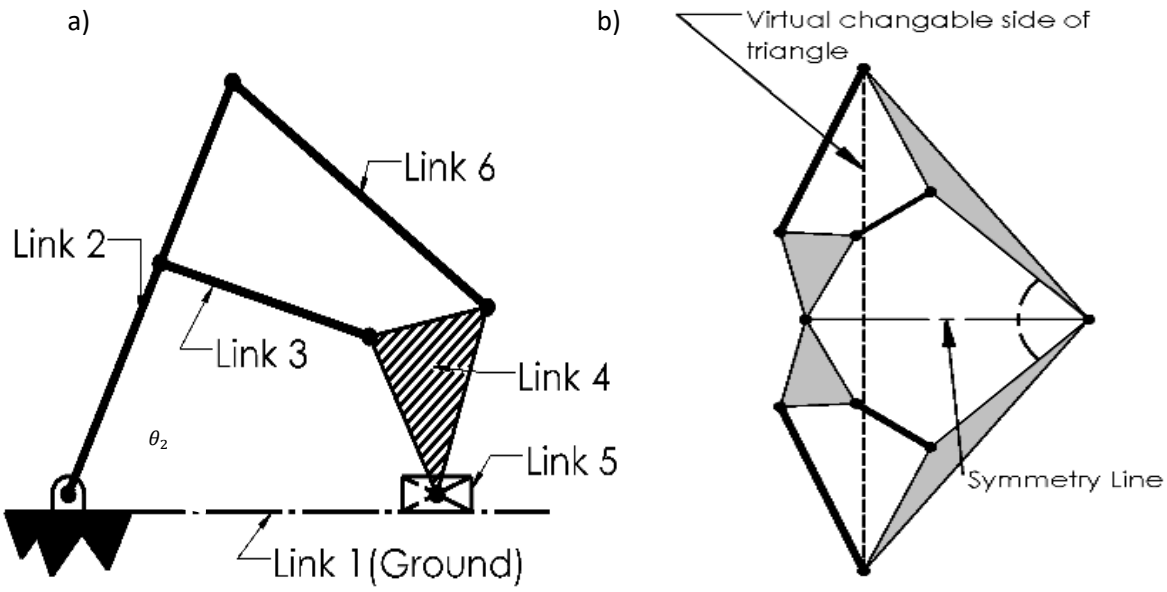

Figure 4.5: a) Stephenson's chain II with slider. b) the symmetry of the mechanism.

The shape-morphing triangle shown in Figure 4.4 may be adapted to a variety of shape morphing tasks. Because the triangle's angles can change by a specified amount, different curved surfaces may be approximated. B plane may be tessellated with triangles, and when the triangles morph, the change in angles can result in a curved surface. If a point in a tessellation is the meeting point of *n* triangles, a measure of curvature at that point is given by [86, 87, 81]:

$$Curvature\ measure(C) = \left[360^o - \sum_{i=1}^{n}(\theta_i)\right] \qquad (4.2)$$

where θ_i refers to the included angles, where the *n* triangles join. The result of the equation can be either $C = 0$ (planar), $C > 0$ (spherical), or $C < 0$ (hyperbolic).

In this work, we focused on the spherical curvature category and designed a structure that lays flat and turns into cube corner, consisting of three triangle-shaped mechanisms. In order to have three triangles that lay flat, the angle between the constant-length sides should be 120° and should morph to 90° to form the cube corner as shown in Figure 4.4. Because the triangle

mechanism uses symmetry, the first and second configurations of the mechanism are θ_2=60° and θ_2=45°.

4.3 Dead-Centers Utility in Compliant Mechanisms

In this section, we show the benefit of the dead-centers in producing stability with motion limits when used in compliant mechanism designs. We present a new technique of designing bistable compliant mechanisms that are stable at the dead-center positions.

A compliant mechanism reaches its target motion position when a load is applied by the deformation of its links and joints, but the motion can be limited if the mechanism encounters a dead-center position. When the compliant mechanism is bounded between dead-centers positions, the mechanism only moves between these positions and cannot exceed them which suggests that the stationary behavior on the dead-centers positions can enhance the stability at these positions. The bistability of the mechanism is a result of the energy storage in compliant links and the kinematic (mechanical advantage) effects of the dead-center positions. This behavior combines the stationary position of the dead-centers with the equilibrium due the storage of strain energy (resistance to deflection) of compliant links to provide precision positions at the desired configurations.

To analytically study this behavior, we apply the principle of virtual work [32, 2] to the triangle-shaped six-bar mechanism. The force is applied vertically on the joint between link 3 and link 4 and a small-length flexural pivot at the joint between link 2 and 6 as shown in Figure 4.6. We assume the energy associated with all other joints (living hinges) to be negligible. The force equation is found to be (see Appendix B for the derivation):

$$F = \frac{-k_6\left[\left(\theta_2 - \theta_{2_0}\right) - \left(\theta_6 - \theta_{6_0}\right)\right]h_{62}}{r_2\cos(\theta_2) - r_3\cos(\theta_3)\,h_{32}} \qquad (4.3)$$

where $h_{32} = \frac{d\theta_3}{d\theta_2}$, is the kinematic coefficients and k_6 is the torsional spring constant. All the angles and link lengths are shown in Figure 4.6.

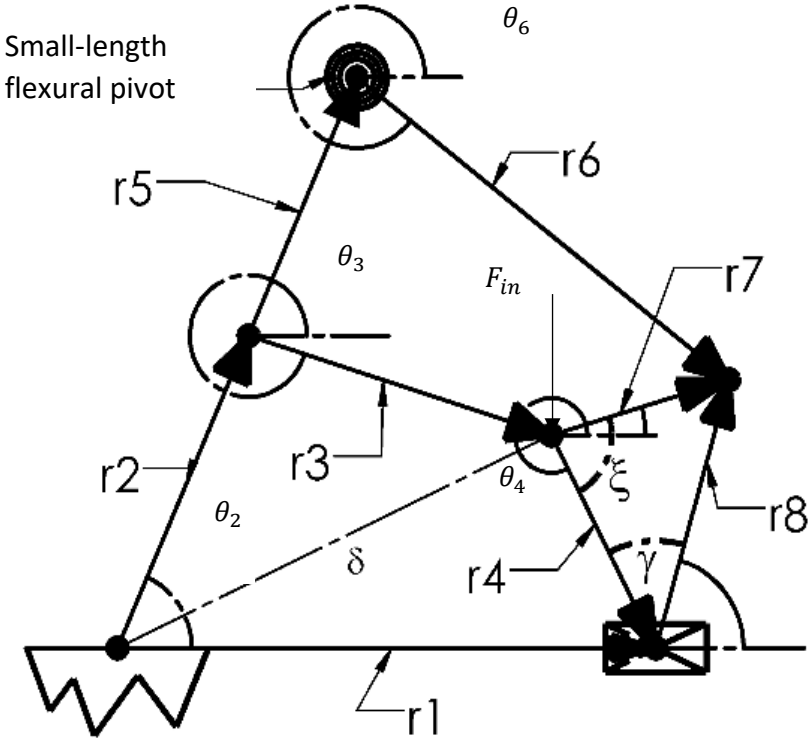

Figure 4.6: The vector loops of the 6-bar mechanism.

We notice that if the h_{32}, at the denominator of the force equation goes to infinity (dead-center), the force will go to zero which means the mechanism is at an equilibrium state.

4.4 Designing Dead-Center Motion Limits Using IC Method

In this section of the chapter, the dead-center position for first and second configurations are found by using instant center method and the dimension synthesis of the six-bar mechanism is described. For the six-bar mechanism, the number of ICs, *N*, is calculated based on the equation $N = \frac{n(n-1)}{2}$, where *n* is the number of links, yielding 15 ICs as shown in Figure 4.7.

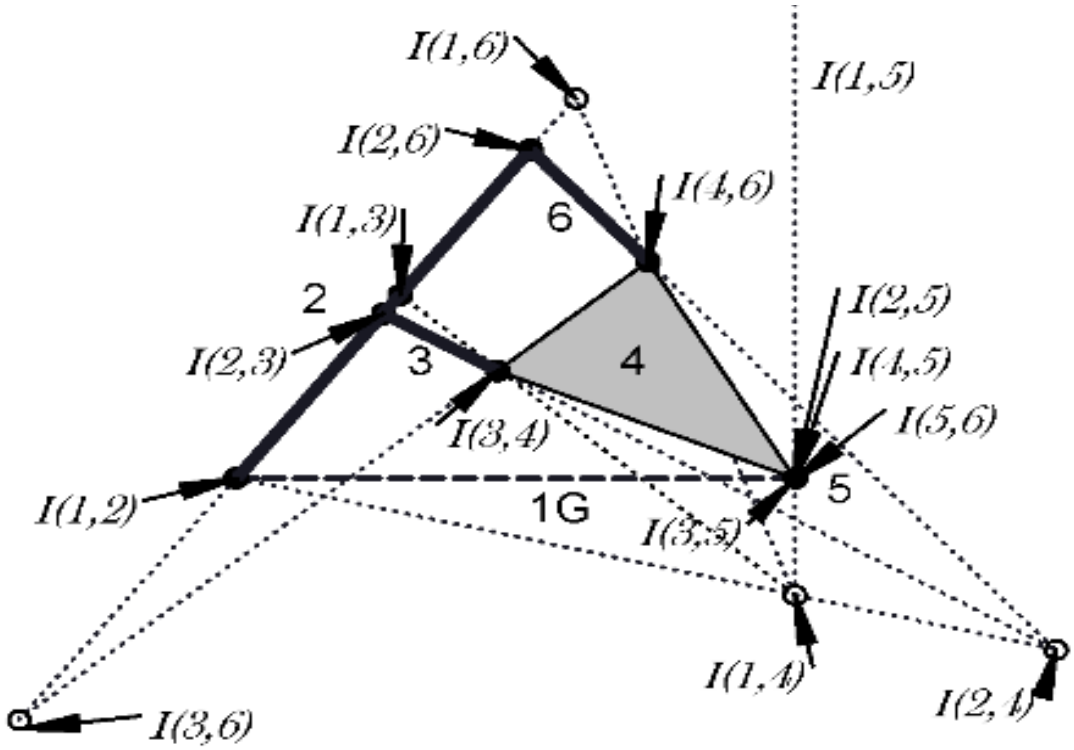

Figure 4.7: Kennedy theorem to locate all ICs.

Because the IC of any two bodies in a planar mechanism is the point where those two bodies have the same velocity at a given instant in time, we can obtain the kinematic coefficients based on ICs considering θ_2 as the input using equation (4.1):

$$\frac{d\theta_3}{d\theta_2} = h_{32} = \frac{|I(2,3) - I(1,2)|}{|I(2,3) - I(1,3)|} \tag{4.4}$$

$$\frac{d\theta_4}{d\theta_2} = h_{42} = \frac{|I(2,4) - I(1,2)|}{|I(2,4) - I(1,4)|} \tag{4.5}$$

$$\frac{d\theta_6}{d\theta_2} = h_{62} = \frac{|I(2,6) - I(1,2)|}{|I(2,6) - I(1,6)|} \tag{4.6}$$

$$\frac{dr_1}{d\theta_2} = h_{12} = |I(2,5) - I(1,2)| \tag{4.7}$$

When the denominator in h_{32}, h_{42},and h_{62} goes to zero (the two ICs are coincident), the kinematic coefficients become infinity which indicates a dead-center configuration.

To apply this process on the mechanism, we used parametric CAD software that allowed us to visualize the movement of the mechanism in and out the dead-center positions. The two desired configurations are constrained to have equal link lengths. The input angle, θ_2, in the first configuration is 45° and 60° for the second configuration. Then, the ICs $I(2,3), I(1,3)$ and $I(2,4), I(1,4)$ are constrained to be coincident for both configurations as shown in Figure 4.8, which shows the six-bar mechanism at the different dead-center configurations 45° and 60°. These constraints are necessary for the desired dead-center positions of link 2, but are not sufficient to specify the entire mechanism design. There is some leeway in the lengths of r_3, and r_4, but these are limited to a small range of lengths or the links may interfere which makes the mechanism not a single-layer-monolithic. We chose to constrain the mechanism so that no interference occurs by letting $r_2 = r_5$ which allows more room inside the vector loops for the links to move. All the chosen design parameters are shown in Table 4.1.

Table 4.1: The six-bar mechanism's parameters. (mm) Where ξ and γ are constant angles as shown in Figure 4.7.

r_2	r_3	r_4	r_5
6.4	4.5	8.6	6.4
r_6	r_7	r_8	γ
6.6	4.4	5.3	25.66°
ξ	I	E	l
31.14°	0.454 mm^4	999.7 Mpa	41.9

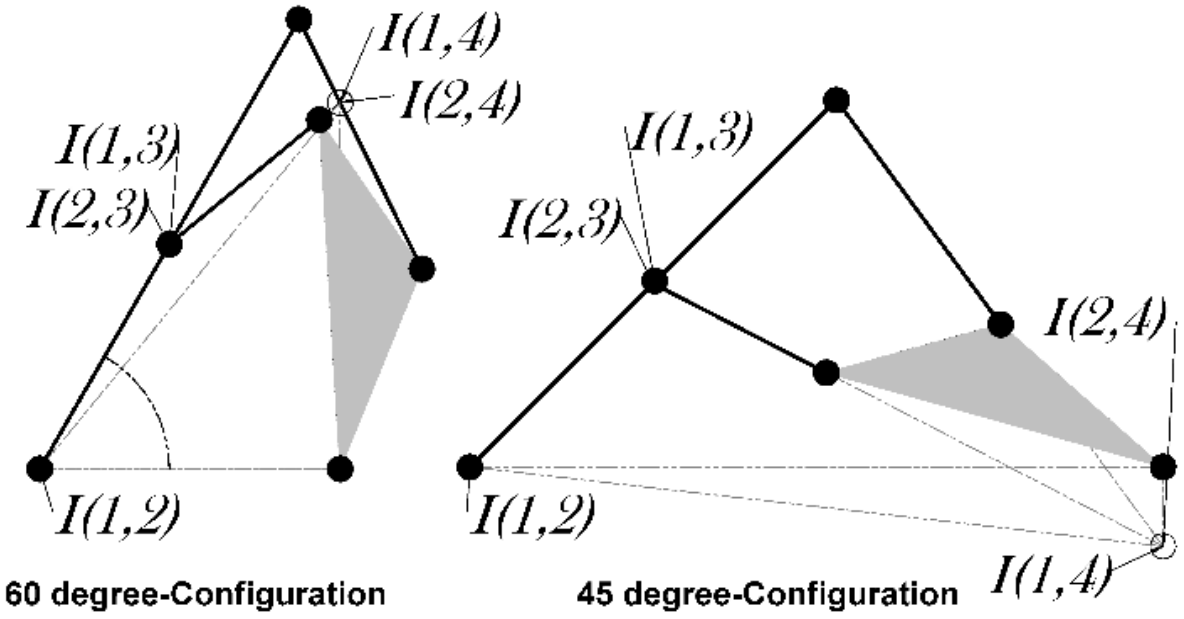

Figure 4.8: Dead-center positions at the first and second configurations.

4.5 Kinematic Synthesis of the Mechanism

This section of the chapter gives the numerical analysis of the six-bar mechanism and verifies the dead-center positions that are found from the IC's method. The parameters that are used for the position analysis and the kinematic coefficients calculations are shown in Table 4.1 Figure 4.7 shows all the parameters and angles required for the calculations. δ is virtual parameter that we set as the input to simplify the position analysis and ranges from 9 mm to 10.7 mm, which is the movement between the two dead-centers. See Appendix C for all the loop closure position equations. The kinematic coefficients are calculated based on the vector loop in Appendix D as:

$$\frac{d\theta_4}{d\theta_2} = h_{42} = \frac{r_5 \sin(\theta_2 - \theta_3) - (r_5 + r_2)(\tan\theta_6 \cos\theta_3 - \sin\theta_3)\sin\theta_2}{r_7 \sin(\theta_7 - \theta_3) + r_8 (\tan\theta_6 * \cos\theta_3 - \sin\theta_3)\cos\theta_8} \tag{4.8}$$

$$\frac{d\theta_3}{d\theta_2} = h_{32} = -\frac{r_2 \cos\theta_2 + r_4 h_{42} \cos\theta_2}{r_3 \cos\theta_6} \tag{4.9}$$

Because the kinematic coefficients are expected to be infinite values, and this would be inconvenient to plot, the inverse of the kinematic coefficients (except h_{62} and h_{12}) are shown and are expected to have zero value at the dead-centers as shown in Figure 4.9 and 4.10.

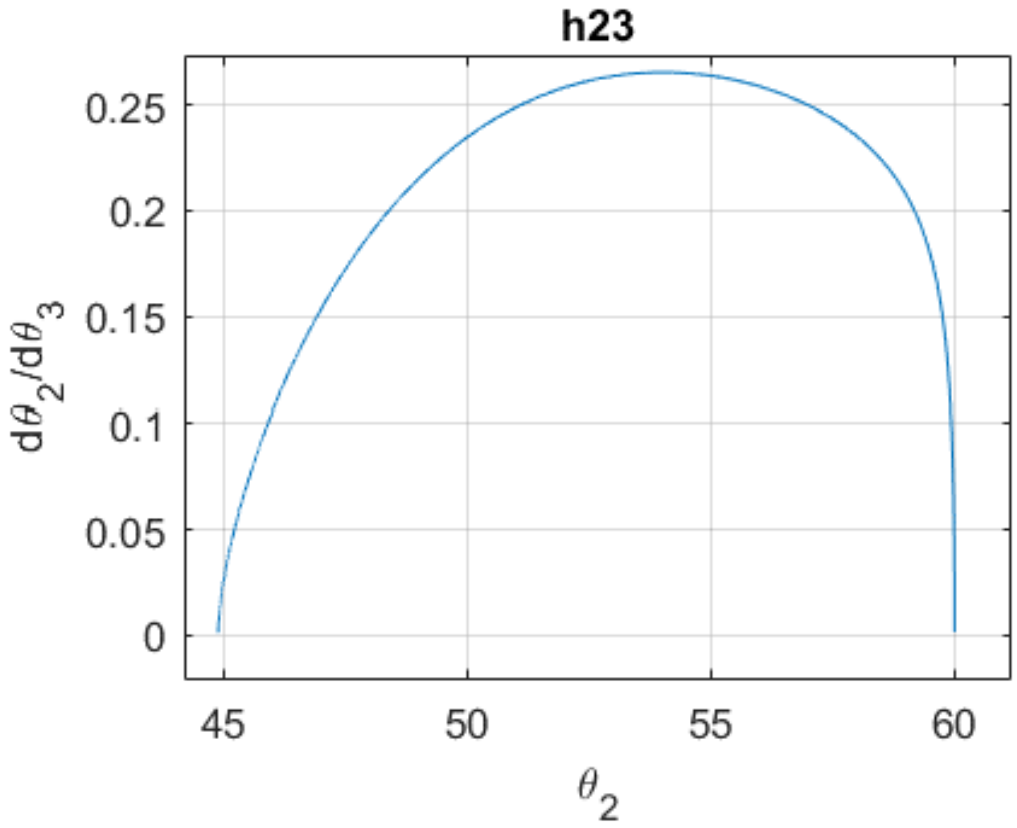

Figure 4.9: The kinematic coefficient with input θ_2 and output θ_3.

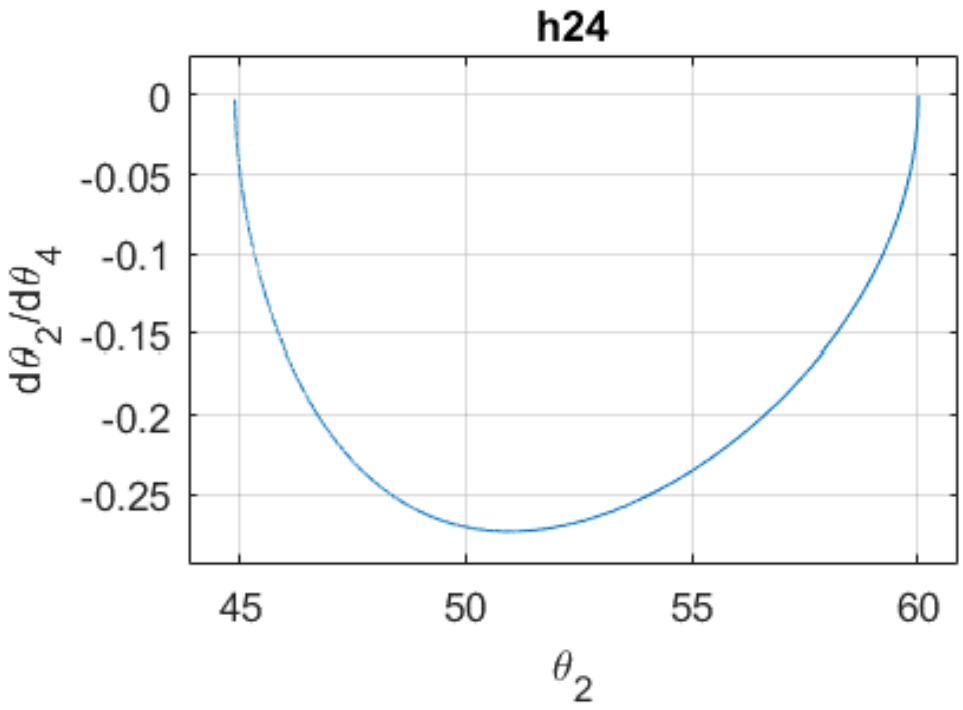

Figure 4.10: The kinematic coefficient with input θ_2 and output θ_4.

The kinematic coefficients h24 and h23 are equal to zero when θ2 at 45o and 60o; in other word, the mechanical advantage (the ability of link 4 and link 3 to affect link 2) of the mechanism when θ2 is 45o or 60o is equal to zero.

4.6 Force Analysis and Potential Energy

The force analysis is modeled using the principle of virtual work as described in Eq. (4.3). The analysis was performed on a six-bar compliant mechanism with the parameters mentioned in Table 4.1. All the mechanism's joints (except joint 6 at k_6) are designed to be thin enough (living hinge) that they do not have a significant impact on the mechanism's stiffness. The characteristic stiffness of the k_6, is given by:

$$k_6 = \frac{EI}{l} \tag{4.12}$$

where E is the modulus of elasticity, I is the cross-sectional moment of inertia, and l is the joint's length. The force-input angle diagram is shown in Figure 4.11. It can be seen that the force goes to zero at the first position and at the second position which indicates the equilibrium states at these positions. The force becomes zero at 48° which an unstable equilibrium position.

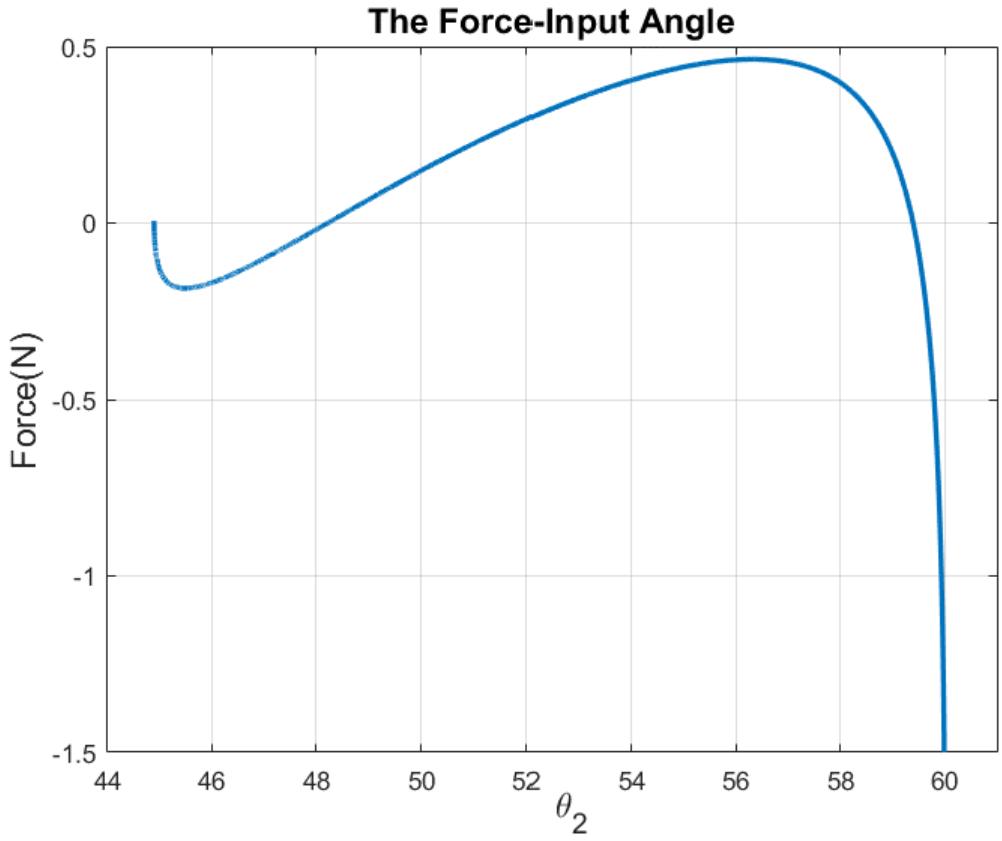

Figure 4.11: The force analysis diagram of input θ_2.

The potential energy associated with the mechanism is calculated and plotted the potential energy curve that has two distinct local minimums positions at the 60° and 45° configurations as shown in Figure 4.12. The compliant mechanisms is bistable at these two distinct stable configurations in because the potential energy of the mechanism is at a minimum.

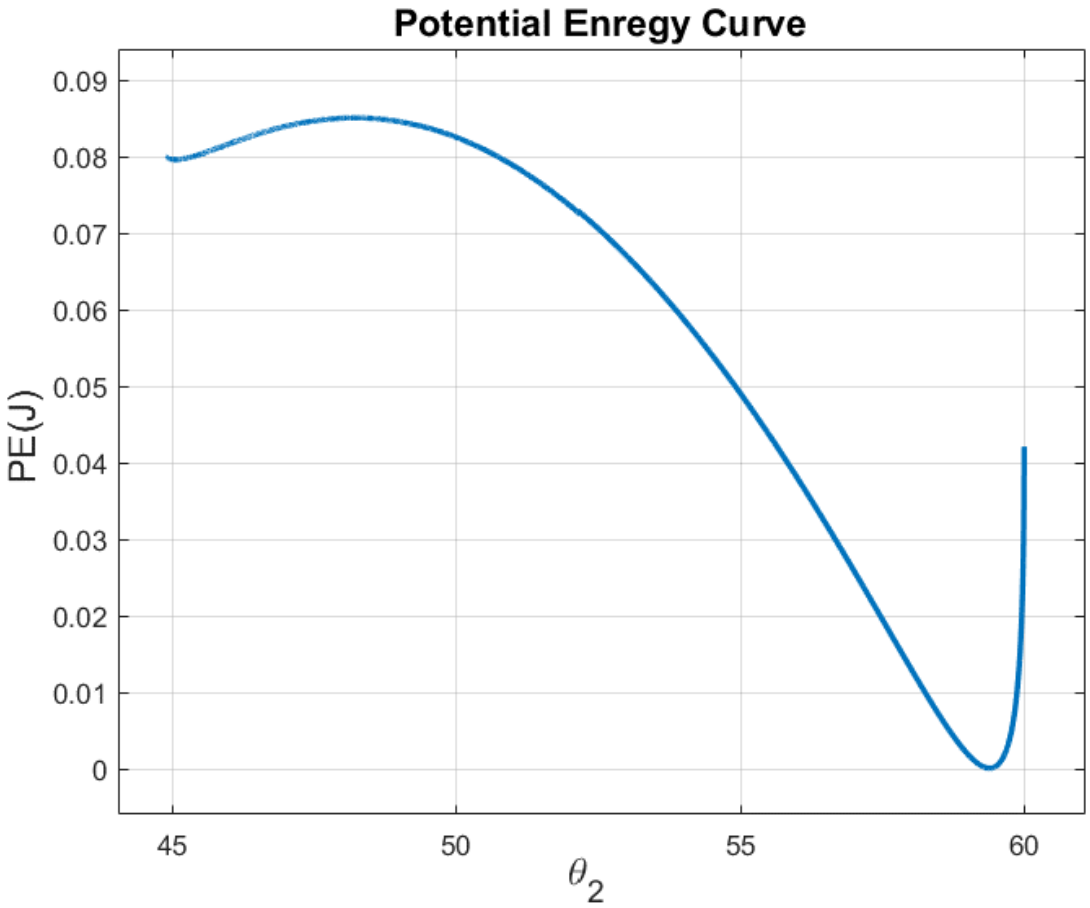

Figure 4.12: The potential energy curve of the six-bar mechanism.

The curve shows the maximum position at 48 degrees which the mechanism is at a maximum of potential energy, and if disturbed, it will move to one of the local minimums positions (stable postions).

4.7 Design Robustness at Bistable Positions

In this section of the chapter, we will discuss the robustness behavior of the motion limits of the bistable triangle-shaped compliant mechanism. A bistable compliant mechanism gains energy when actuated and release it in form of motion until the mechanism reaches a stable position. If the mechanism is disturbed again it may move beyond the stable position and return to

its stable position which means the stability of the compliant mechanism is controlled only be the potential energy curve.

This can be an obstacle in shape-morphing structures as they require the structures to avoid any movement beyond the designed configurations.

The bistable triangle-shaped compliant mechanism is designed, using dead-center motion limits, so that it does not allow significant motion beyond its designed stable configurations. The 45 º dead-center motion limit occurs when link 4 becomes parallel with link 1 (the mirror symmetry line), and the 60º motion limit occurs when links 4 and 6 are parallel. In the fully compliant prototype, these are positions of self-contact in the mechanisms that prevent the mechanism from moving beyond these limits.

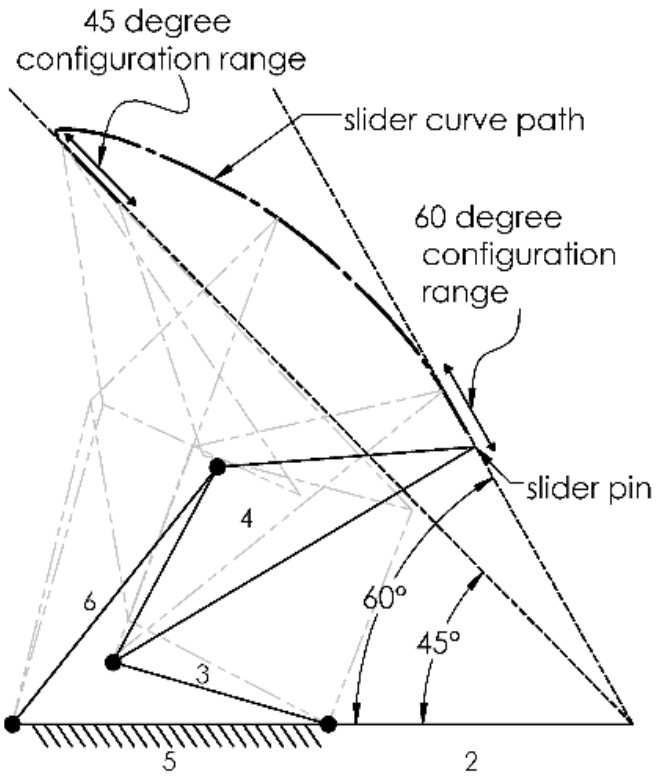

Figure 4.13: Dwell behavior of the triangle-shaped compliant mechanism.

Furthermore, the bistable triangle-shaped compliant mechanism has dwell behavior of the vertex angle θ_2 near the bistable configurations. Near the bistable configurations, the vertex angle θ_2 does not change even when the rest of the mechanism moves due to the dwell-based design. This allows compliant mechanism prototypes made from visco-eleastic materials such polypropylene exhibit creep and plastic deformation in their links and joints (that may result from large stresses in compliant mechanism) and maintain the designed stable configurations. To better show how the dwell mechanism works, we show (in Figure 4.13) the inversion in which r_5 is the ground link and r_1 is the moving link. In this inversion, the pin on the slider link 5 moves as the coupler point in a four-bar mechanism (links 3, 4 5 and 6). Near the stable configurations, the slider pin moves radially (changing the length of r_1) but not tangentially (changing θ_2).

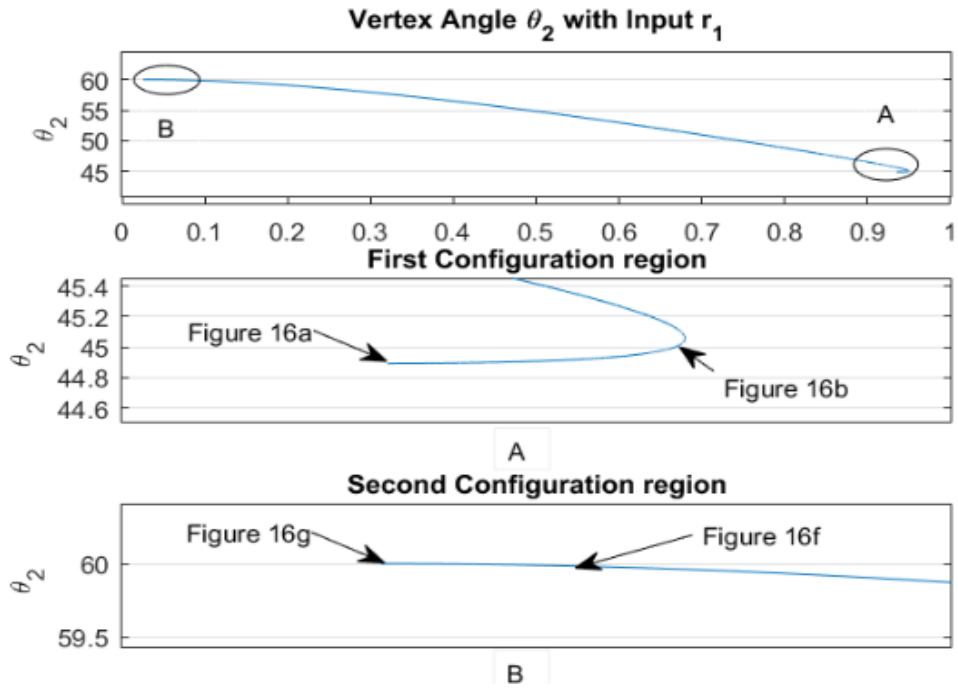

Figure 4.14: The robust design of θ_2 plotted with r_1. The graph is divided to three plots. The first plot shows overall motion, the second plot shows first configuration region, and the third plot shows the second configuration region. The plots in the first and second configurations are related to the mechanism's movement in Figure 4.13.

This produces dwell behavior in θ_2 (the vertex of the triangle) and means that even if the stable configurations change a little due to creep or plastic deformation, it is unlikely to significantly alter to values of θ_2 at the stable configurations.

The dwell mechanism enhances the stability of the design because the stable configurations do not have to be at a particular mechanism configuration, they can fall within a range of configurations that have the same vertex angle.

To further illustrate this behavior, we ran the position analysis of the mechanism with θ_2 is the output and input r_1 as shown in Figure 4.14. In addition, the mechanism is bistable at 45- and 60-degrees positions, but its compliance allows movement if any parameter is actuated yet the vertex angle θ_2 remain very close to the stable position of vertex angle as shown in Figure 4.14. Figure 4.15 shows that the vertex angle θ_2 is limited between 45 degrees and 60 degrees with the various inputs meaning that the mechanism's vertex angle θ_2 is locked between these limits. Figure 4.15 a and b, and f and g show that the portions of the mechanism can move while the vertex angle is nearly constant.

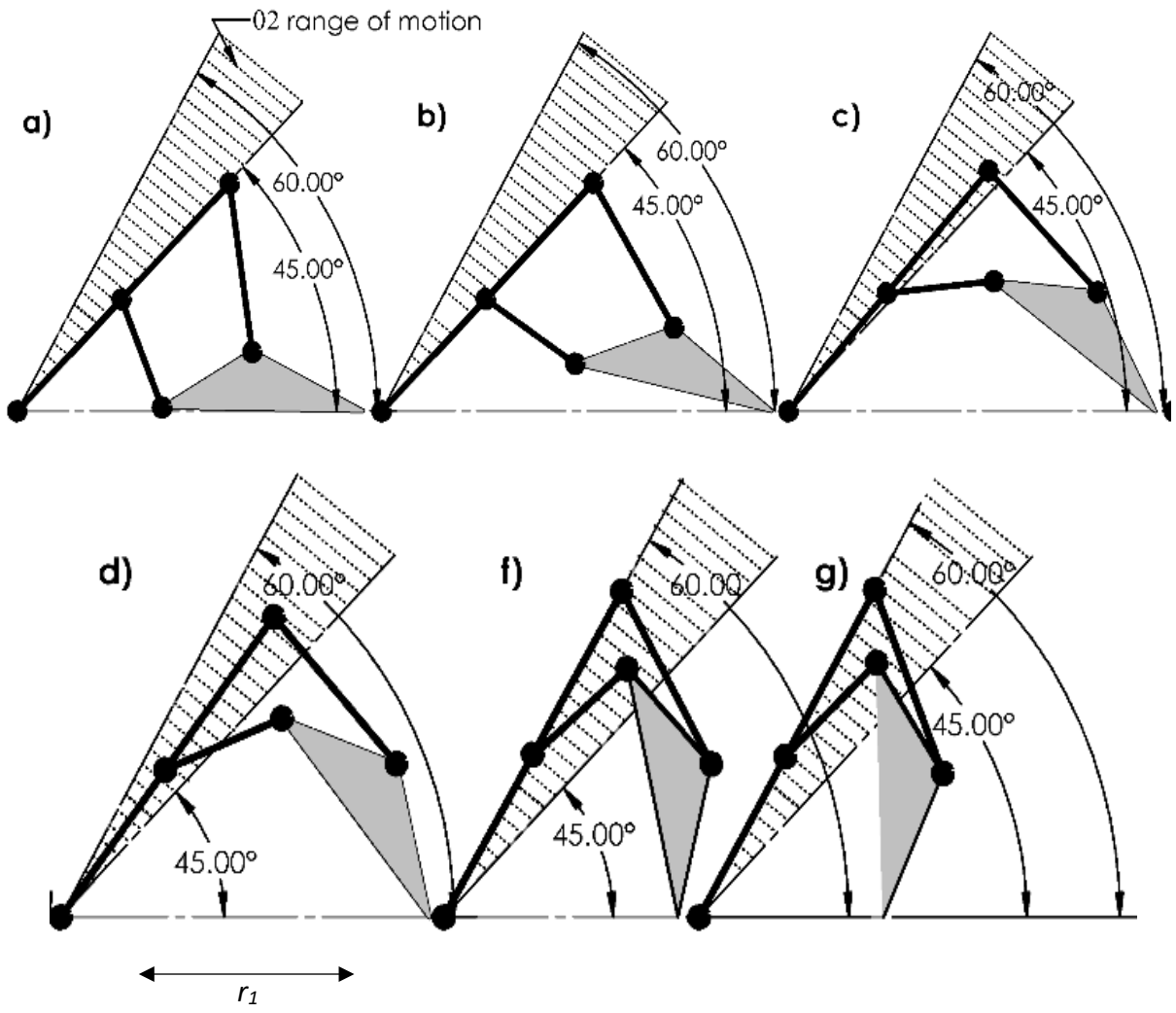

Figure 4.15: The vertex angle's range with the motion of the mechanism. The slider of the mechanism is actuated to show that the vertex angle does not extend beyond its designed limits.

4.8 Design Prototype

In this section of the chapter, two examples will be prototyped to illustrate the use of the bistable triangle-shaped compliant mechanism in shape-morphing mechanisms. The first design is a cube corner that used for packaging assistance. As mentioned in section 4.2, the cube corner is consisted of three units of configuration (120-30-30) that transform to cube corner configuration (90-45-45). Our design was chosen to have $r_2 = r_5 = 76$mm. All parameters of the design were

derived from Section (4.2) and parametric CAD and are given in Table 4.2. Figure 4.16 shows the prototype of the bistable triangle-shaped compliant mechanism in both configurations. The prototype was laser cut from a 1/8-inch-thick Polypropylene co-polymer material as shown in Figure 4.16. Because the prototype was designed to be processed from flat sheet, the initial configuration was (120-30-30). The three units were connected using groove joints [88] that represent a constrained tight fold as shown in Figure 4.17. Figure 4.18 shows the cube corner glued to wood sheets in a flat position and folded to the package shape.

Figure 4.16: The bistable triangle-shaped compliant mechanism in both configurations.

Figure 4.17: Cube corner consisting of three units in flat and corner configurations.

Table 4.2: Prototype mechanism's parameters. (mm)

r_2	r_3	r_4	r_5
38	28.5	50	38
r_6	r_7	r_8	γ
40.5	28	33	25.66°
ξ	I	E	l
31.14°	1.14μm^4	999.7Mpa	3

The second example is a portable box that can be flattened for east storage and deployed to a closed box as needed. The box consisted of six bistable triangle-shaped compliant mechanisms as shown in Figure 4.19. Figure 4.20 shows the deployment process of the portable box. All parameters of the design were derived from Section (4.2) and parametric CAD in the following Table 4.2. The prototype was designed to process from flat sheet.

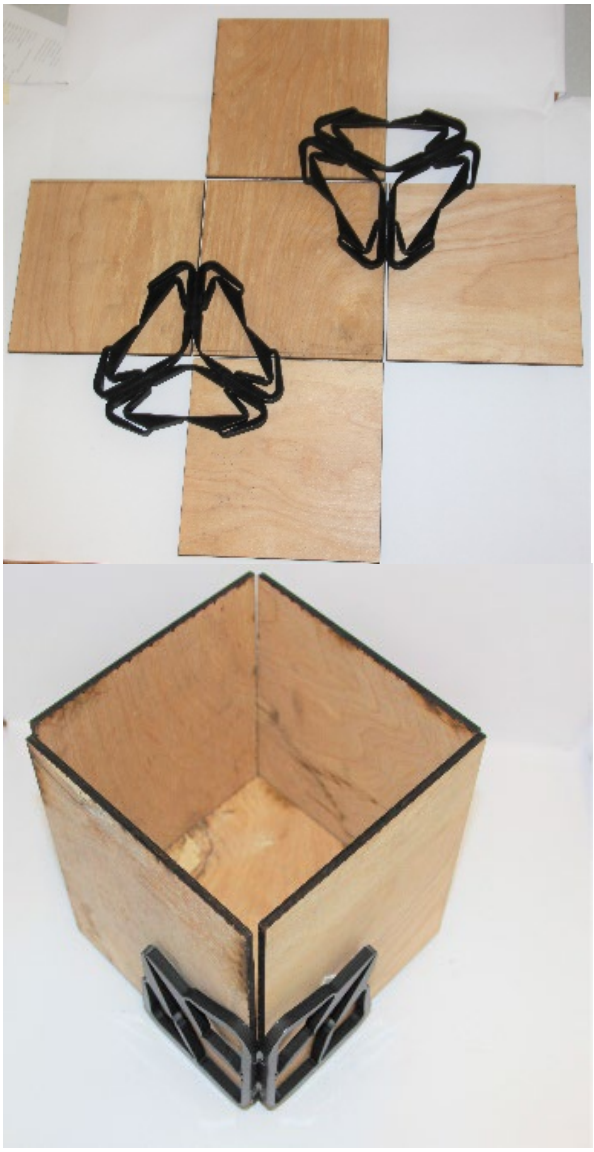

Figure 4.18: Cube corner attached to wood sheets to form a wooden box.

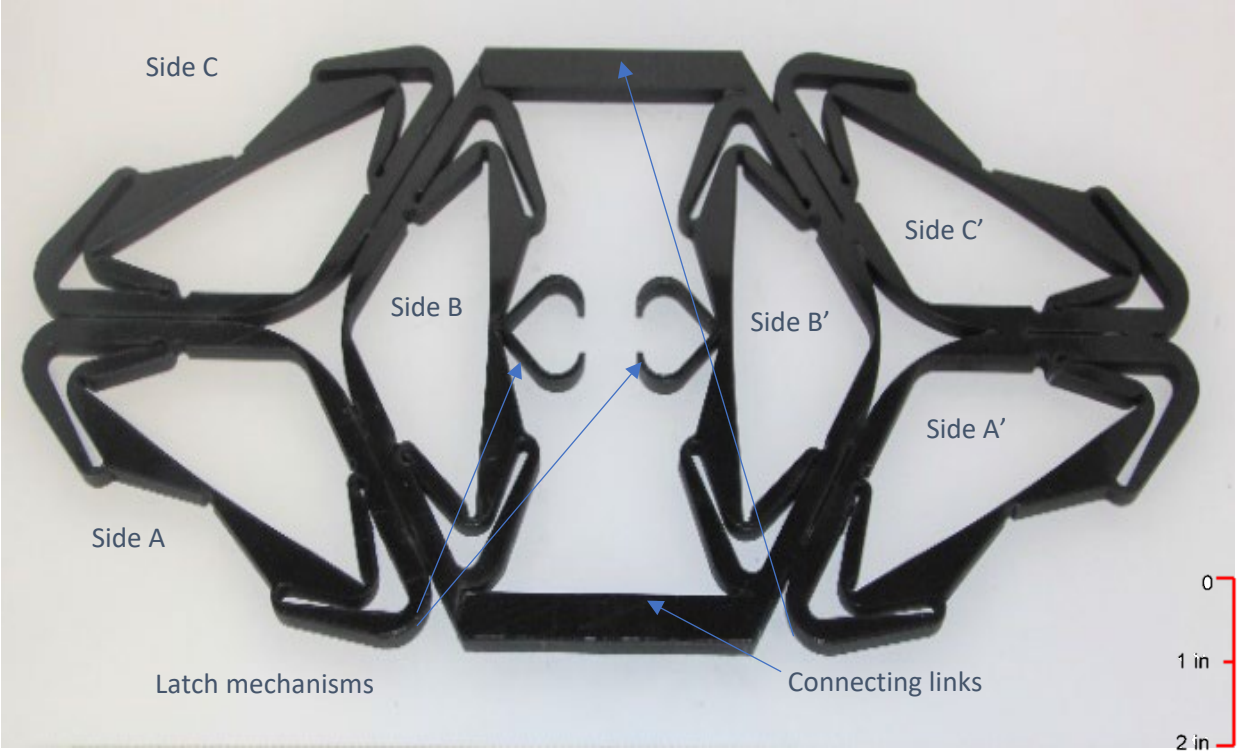

Figure 4.19: Flat configuration of the portable box.

The prototype was laser cut from a 1/8-inch-thick Polypropylene co-polymer material as shown in Figure 4.19. The box was designed of two corner units that were connected of two links and fold opposite to each other as shown in Figure 4.20. Each corner unit is actuated independently, and a latch mechanism is used to lock the two stable corners into the box shape. Groove joints were used to help guide the folding pattern. Figure 4.21 shows the portable box in flat position and folded to the closed box as in Figure 4.19.

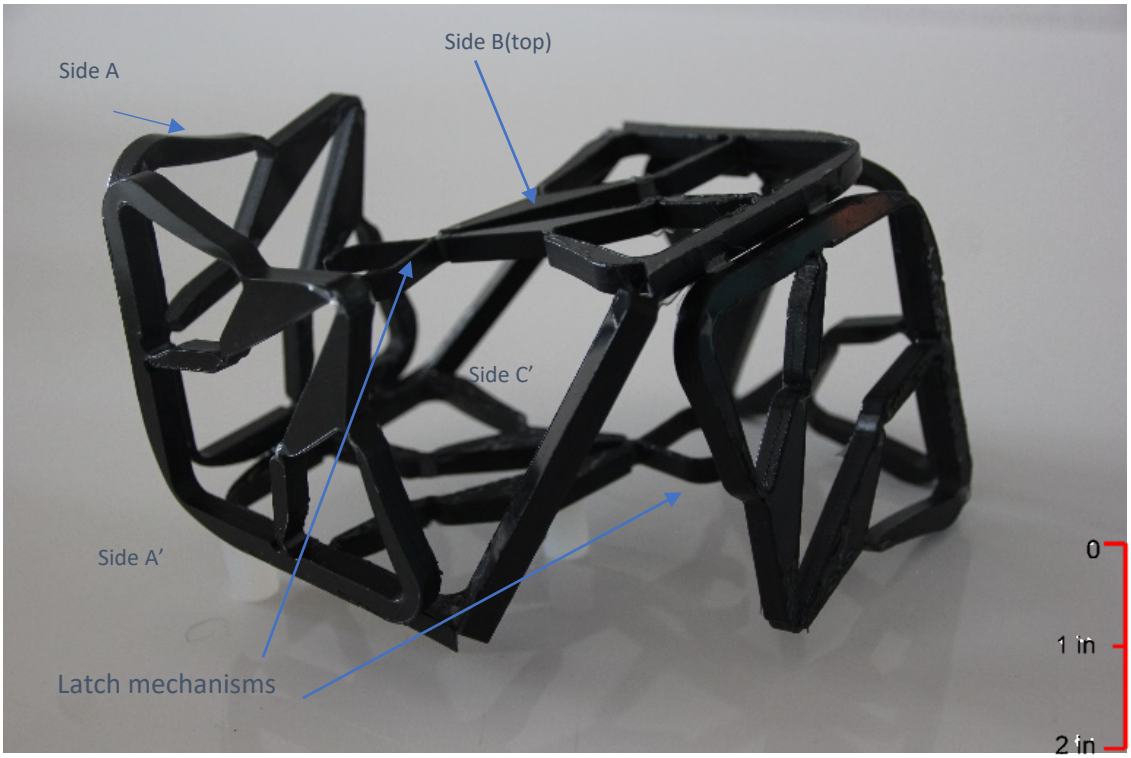

Figure 4.20: The deployment scheme of the portable box.

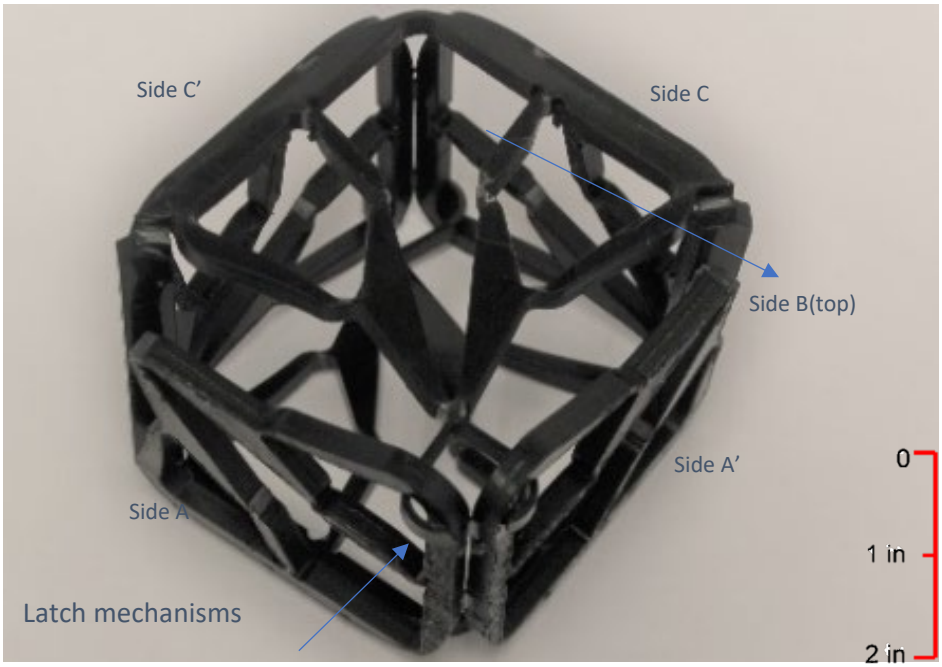

Figure 4.21: Portable box prototype.

4.9 Conclusion

This chapter introduces a new type of bistable mechanism that utilizes dead-center motion limits and dwell mechanism stability enhancement. The mechanism is designed in a triangle-shape with one-side changeable. It can be tessellated for shape-morphing compliant mechanisms. The mechanism has dwell behavior at the bistable configurations that enhances its stability. Both the force analysis and potential energy were calculated to verify the stability at the designed configurations. The bistable triangle-shaped compliant mechanism was prototyped for two tasks; a cube corner and portable box to demonstrate the concept.

CHAPTER 5

A LAMINA-EMERGENT FRUSTUM USING A BISTABLE COLLAPSIBLE COMPLIANT MECHANISM (BCCM)[3]

5.1 Introduction

This paper presents a new Bistable Collapsible Compliant Mechanism (BCCM) that is utilized in a Lamina- Emergent Frustum. The mechanism is based on transforming a polygon spiral into spatial frustum shape using a mechanism composed of compliant links and joints that exhibits bistable behavior. A number of mechanism types (graphs) were considered to implement the shape-morphing spiral, including 4-bar, 6-bar, and 8-bar chains. Our design requirements permitted the selection of a particular 8-bar chain as the basis for the BCCM. Bistable behavior was added to the mechanism by introducing snap-through bistability as the mechanism morphs. Parametric CAD was used to perform the dimensional synthesis. The design was successfully prototyped. We anticipate that the mechanism may be useful in commercial small animal enclosures or as a frame for a solar still.

The objective of this study is to develop a design procedure for a shape-changing structure that morphs from a planar lamina to a frustum shape as an illustration of a general design strategy for shape-changing structures. The motivation for shape-changing structures occurs in many applications such as wing morphing for enhanced aerodynamic performance, complex deployable structures, and space-saving furniture. [4, 5]. Additionally, if shape-morphing designs have the ability to be manufactured on the micro-scale, they may provide useful functions, such as switches

[3] This chapter is based on a published paper in the 2018 ASME Journal of the Mechanical Design, Vol. 140, doi: 10.1115/1.4037621

and relays [6]. Currently, shape-morphing structures often consist of a number of parts or mechanisms that may consist of links, springs, and joints, which can have high costs for manufacture, assembly, and maintenance. Compliant mechanisms offer advantages in these areas and can also be bistable [32, 89]. Bistable compliant mechanisms have been used in many applications including a bistable mechanism for the rear trunk lid of a car, double toggle switching mechanisms, and multistable compliant Sarrus mechanisms. [90, 91, 92].

In this paper, we describe the design of a Bistable Collapsible Compliant Mechanism (BCCM) that, when arrayed transforms from a planar lamina shape to a frustum shape and requires a small wrench, i.e. a torque with a parallel pulling or compressing force to switch between the frustum and lamina states. Compliant structures fabricated from a lamina (planar) sheet which have motion out of the planar sheet are known as Lamina Emergent Mechanisms (LEMs). [93, 94]. We are unaware of any other deployable mechanism with comparable motion to the Lamina-Emergent Frustum described in this work. The original motivation for the design was a collapsible solar still. The solar still would be stored collapsed in a vehicle and assembled to purify water in an emergency. Other possible applications for this design could be a rapidly deployable tent or a collapsible animal enclosure or bird cage.

5.1.1 Background

The majority of the background for this work is in the area of compliant mechanisms and its sub-disciplines of bistability and shape-morphing. The advantages of compliant mechanisms over rigid-link mechanisms are considered in four important areas: the reduction of number of parts, the elimination of joint clearances, integrated spring-like energy storage, and potential reductions in cost [2]. Howell and Midha developed the pseudo-rigid-body model concept to model the large deflection of compliant links by using rigid-body component analogies [44].

Therefore, a compliant mechanism can be analyzed using rigid-link mechanism theory especially when the joints and pivots of the compliant mechanism are short and thin so that its bending stiffness is negligible [32]. Additionally, we found work on the type synthesis of mechanisms using graph theory to be helpful. Shape-changing mechanisms have been successfully studied using topological graph theory to synthesize morphing mechanisms [40, 41]. A Graph theoretic approach was used to generate a creative design for a vehicle suspension by Liu and Chou [37]. Moreover, Feng and Liu used graph theory representations to evaluate lists of mechanisms for a deployable mechanism used as a reflector antenna [38]. The structure of the mechanism's connections can be defined by the graph representation [39].

Bistability of a mechanism means that it can be at a stable equilibrium in two different configurations. [32, 47, 48]. These two configurations are local minimums of potential energy. The best way to understand bistability is using the "ball-on-a-hill" analogy [32], which compares the strain energy in a compliant mechanism to the gravitational potential energy of a ball.

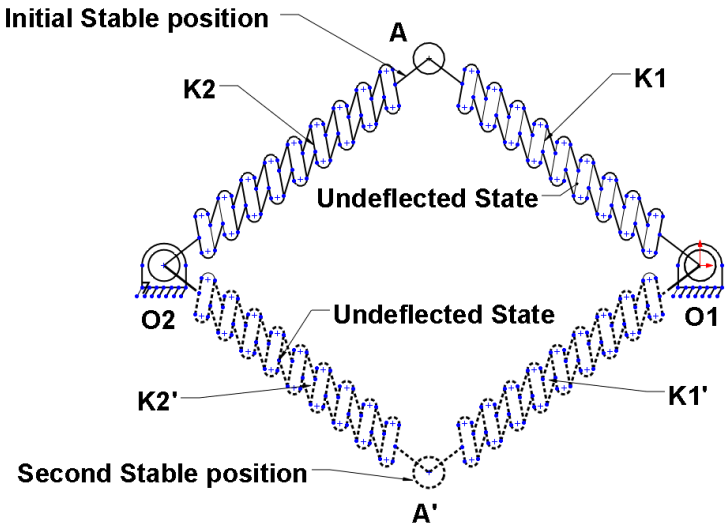

Figure 5.1: A compliant "snap-through" mechanism that is used to illustrate the type of bistable behavior used in the BCCM design.

The mechanism shown in Figure 5.1 is a type of bi-stable mechanism called a *snap-through* mechanism. Snap-through mechanisms exhibit nonlinear potential energy curves and are bistable [95, 96]. The snap-through mechanism in Figure 5.1 consists of two (possibly nonlinear) springs (K_1,K_2) that are connected in series by revolute joints to ground points *O1* and *O2.* In order to deduce the stable configurations of this mechanism, it is sufficient to know the distance between the ground pivots and the equilibrium lengths of the springs. If these three lengths satisfy the triangle inequality (i.e. the sum of any two of the lengths is greater than the length of the third), the mechanism will be bistable regardless of the stiffness characteristics of the springs. If the springs are sufficiently flexible, there will be a (possibly many) deflection path from the first equilibrium configuration to the second equilibrium configuration. The two springs (K_1,K_2) may be complicated functions yet the exact nature of their stiffness and motion does not have to be known to determine the second stable configuration because that configuration is inherent in the symmetry which the second equilibrium configuration shares with the first. The importance of this snap-through mechanism is that it demonstrates that *snap-through* bistability is geometric condition and such mechanisms can be designed without motion, force, or stress analyses. To experimentally verify bistability, it is sufficient to show that a mechanism has two configurations which it will hold while being perturbed (i.e. being shaken, turned upside down, etc.)

Alqasimi and Lusk demonstrate a shape-morphing space frame using a linear Bistable Compliant Crank-Slider Mechanism [24] that is arranged in a specific pattern to produce a shape-changing structure [25]. Bistable shape-shifting surfaces (SSS) can produce morphing structures with line-of-sight integrity, i.e. effectiveness as a physical barrier [26]. Shape-changing structures and surfaces can add value to applications as in collapsible structures and folding geometries [27, 28, 29, 30].

5.1.2 Overview

The rest of the chapter is organized as follows: First, we discuss the two configurations (lamina and frustum) and our strategy for morphing. Then, we discuss the type synthesis of a linkage to coordinate the motion, then the dimension synthesis of the mechanism and how to make it bistable. Finally, we show the prototype and results.

5.2 Collapsible Compliant Mechanism

The frustum shape is decomposed into a number of sub-mechanisms. In order to compress the frustum into its planar position, the straight sides of the frustum are bent into polygonal spirals, which allow these lengths to be effectively placed as shown in Figure 5.2. Here, a polygon spiral is used for the design because its straight segments are compatible with rigid links in a mechanism.

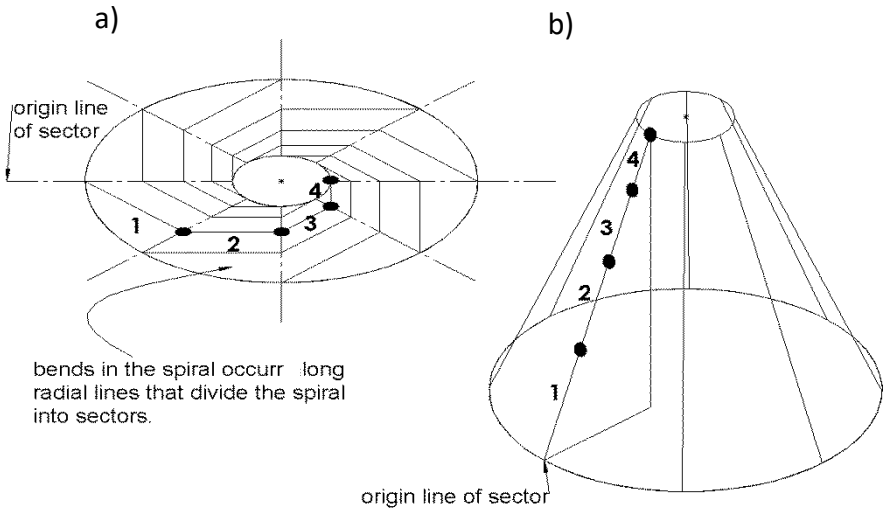

Figure 5.2: The shape change process. a) A polygonal spiral in its planar position. b) A frustum shape after straightening the spiral lines

In this section, we discuss the design of the exterior of the polygonal spiral, in the subsequent section we describe its interior, which is a mechanism for coordinating the bending of straightening in the spiral s shown in Figure 4.3, The polygon spiral is designed in a pattern which can be adjusted and modified with a constant ratio, as:

$$\frac{a_{i+1}}{a_i} = \frac{r_{i+1}}{r_i} = \frac{r_1}{R} = \cos(\frac{2\pi}{n}) \tag{5.1}$$

where R is the radius of the base, r_i is the distance from the center of the circle to the ith spiral corner from the outer radius, n is the number of sectors. The polygonal spiral has k segments.

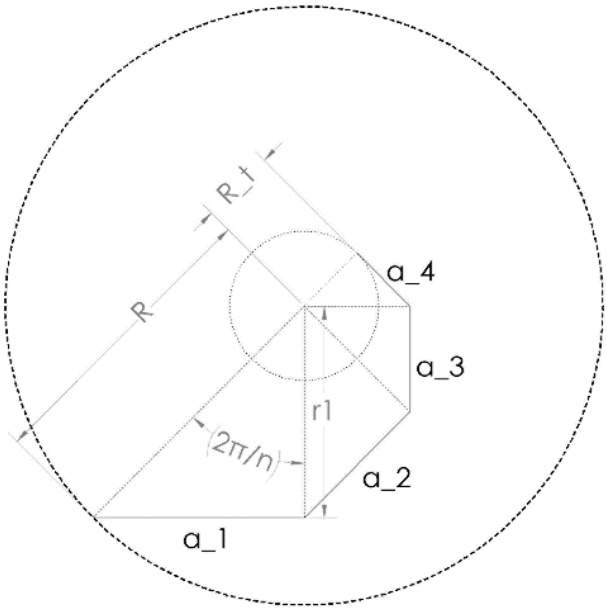

Figure 5.3: Polygon spiral calculation and ratio with *k*=4 segments and *n*= 8 sectors.

The length of the spiral can be calculated as the summation of all side lengths (a_i):

$$L = a_1 + a_2 + \cdots + a_k \tag{5.2}$$

$$L = a_1 * (\sum_{i=0}^{k-1} \cos^i(\frac{2\pi}{n})) \qquad i = 0,1,2,3,\ldots.k \tag{5.3}$$

$$a_1 = R * \sin(\frac{2\pi}{n}) \tag{5.4}$$

We have chosen to have the polygonal spiral terminate 180° from its origin on the outer radius. This means that each spiral passes through half the sectors n, so the number of segments k

equal *n/2.* The length of spiral allows the calculation of the height of the frustum shape using the Pythagorean Theorem as shown in Figure 5.4.

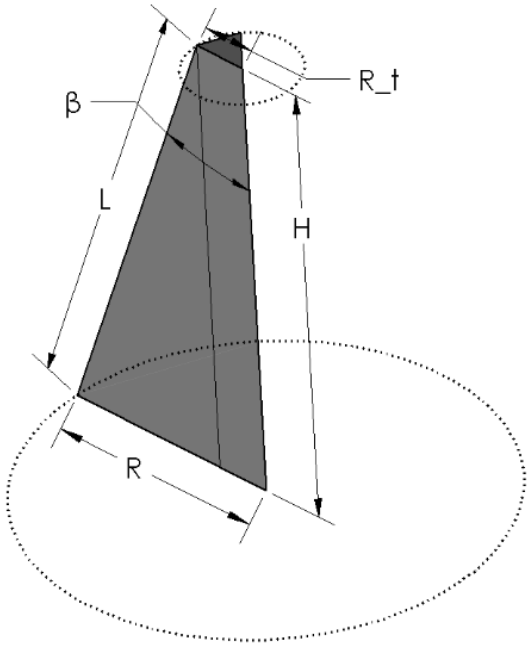

Figure 5.4: A slice of the polygon frustum to measure the height.

$$H^2 = L^2 - (R - R_t)^2 \tag{5.5}$$

where *H* is the height of the frustum, and R_t is the radius of the top frustum surface. The top radius R_t can be calculated by iterating Eq. (5.1) as:

$$\frac{R_t}{R} = \left(\frac{r_1}{R}\right)^{\frac{n}{2}} = \cos^{\frac{n}{2}}\left(\frac{2\pi}{n}\right) \tag{5.6}$$

This ratio shows that the area of the top frustum surface is controlled by *n* where the increase of *n* increases the radius R_t. Solving for *H* in Eq. (5.5) using (5.3), (5.4), and (5.6):

$$H = R * \left\{\left[\sin\left(\frac{2\pi}{n}\right) * \sum_{i=0}^{\frac{n}{2}-1} \cos^i\left(\frac{2\pi}{n}\right)\right]^2 - \left[1 - \cos^{\frac{n}{2}}\left(\frac{2\pi}{n}\right)\right]^2\right\}^{\frac{1}{2}} \tag{5.7}$$

$$\beta = \tan^{-1}\left(\frac{R - R_t}{H}\right) \tag{5.8}$$

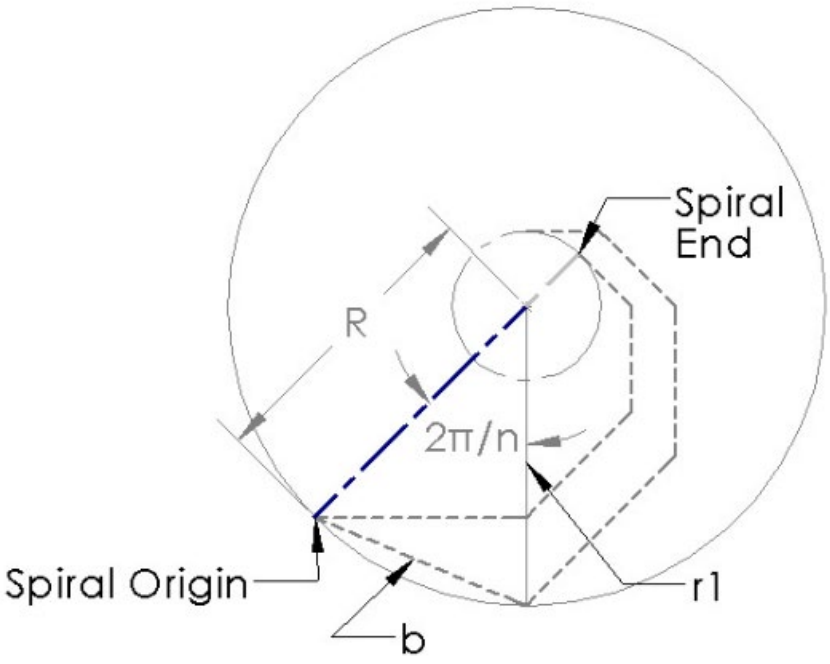

Figure 5.5: Sector calculation for *n*= 8 sectors.

It can be clearly seen that the height equation depends on the number of sectors and the outer radius and the increase of sectors increases the height. However, the increase of sectors tends to increase the number of segments per spiral which requires a more complex interior design. Moreover, there is not a large difference in the height of the frustum shape because the ratio of the spiral Eq. (5.1) is diminished with the increase in the number of sectors.

$$\%Height\ Improvement = \frac{H_{i+1} - H_i}{H_i} * 100 \qquad (5.9)$$

Table 5.1: The improvement of height with the increase of sectors *n*.

n	R	L	b	R_t	H	%
6	1	1.515544	1	0.125	1.29731	

Table 5.1 (Continued)

8	1	1.81066	0.765367	0.25	1.648026	0.27
10	1	2.011057	0.618034	0.346	1.866693	0.13
12	1	2.157592	0.517638	0.421	2.020647	0.08
14	1	2.269888	0.445042	0.481	2.136045	0.05
16	1	2.358878	0.390181	0.530	2.226137	0.04

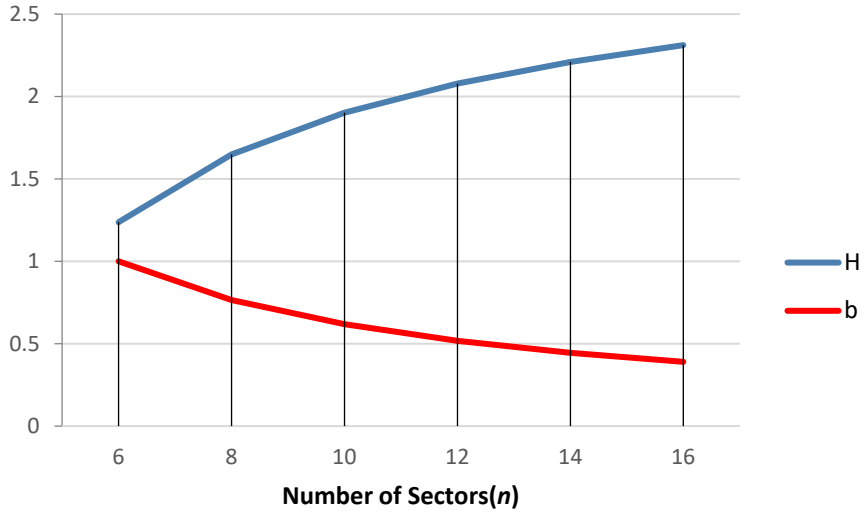

Figure 5.6: The height (*H*) and the sector width (*b*) as a function of the number of sectors *n* for a unit radius *R*.

Table 5.1 shows the parameters needed for the frustum design. It can be seen that the percentage change in height diminishes with increasing sectors. Besides, as sectors increase, the sector width *b,* (see Figure 5.6) reduces:

$$b = 2R * \sin(\frac{\pi}{n}) \qquad (5.10)$$

As the sector width, *b,* becomes smaller, the design of the shape changing interior mechanism becomes more challenging.

5.3 Design Criteria

The interior of the polygonal spiral is desired to be a one degree of freedom compliant mechanism, i.e. its pseudo-rigid-body model (PRBM) is a 1-D.o.F mechanism, and which can fit the two configurations. Every sector is designed as an independent mechanism, then coupled at the inner and outer circles (the top and the bottom of the frustum). Because the design is symmetric, the motion of the left side of each sector must correspond to its right side, i.e. the sides have equal lengths and rotations where adjacent sides in adjacent sectors are connected with hinges. The normal to the sectors are all parallel and vertical in the planar position while in the frustum position, they bend to an angle $\frac{2\pi}{n} * tan\beta$ with respect to the adjacent sector. Our design has of *k=4* segments, without internal links, its minimum design is 10-bar mechanism (see the dotted lines in Figure 5.5). There are 230 possible 10-bar mechanism types [2] with 1-D.o.F, which seemed like a poor place to begin the type synthesis. So, we considered subdividing the sector and coupling the resulting mechanisms.

The polygonal spiral has a glide-translational scaling symmetry (GTS) as shown in Figure 5.7b, where the dart-shaped quadrilateral labeled (1) has (GTS) symmetry with quadrilateral (2), which has the same symmetry with (3) etc. As a result, each quadrilateral of the design (1, 2, 3, 4, etc.) can be designed independently. However, because each such design should have a least one-degree of freedom, having four independently designed quadrilaterals results in a minimum of four degrees of freedom per sector. Fortunately, a similar scaling applies in the frustum position (Figure 5.7a), even though the glide-translation is different. To limit the degrees of freedom in each sector, we chose designs which couple the motion of the quadrilateral as is shown in Figure 5.7. We

looked at 6-bar and 8-bar designs which couple two quadrilaterals with the objective of learning how to couple all four quadrilaterals together.

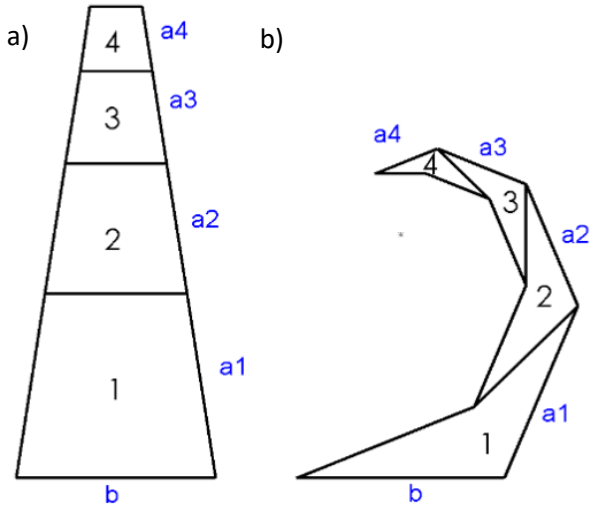

Figure 5.7: A single sector of the design (when *n*= 4) that shows a repeatable quadrilateral element with constant size ratio in the two stable configurations.

Using a 6-bar design as shown in Figure 5.8a, the coupling between sectors subdivisions is too rigid and the distance between the left and right sides does not compress. Figure 5.8a shows that the left and right sides rotate with respect to each other but are forced to maintain a constant radial distance. The 8-bar design shown in Figure 5.8b is a more effective coupling because it allows relative translation and enhanced collapsing of the sector sides. This shows a variety of possible motions of the mechanism and that it can have different radii circle between the bases of the quaternary links.

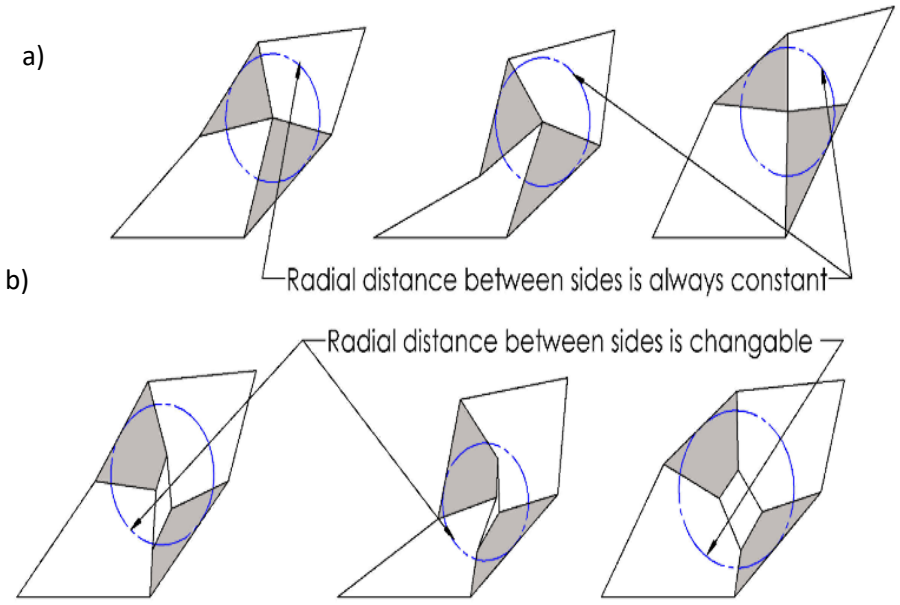

Figure 5.8: a) Limited collapsing motion is possible in 6-bar mechanisms. b) Better collapsing motion is possible in 8-bar mechanisms.

For planar mechanism, Kutzbach's equation (30) is used to compute the mobility [2] [97].

$$M = 3 * (g - 1) - 2J_1 - J_2 \qquad (5.11)$$

where: M is the degree of freedom. g is the number of links. J_1 is the number of lower pairs and J_2 is the number of higher pairs.

Because the kinematic chain is designed for a compliant mechanism, all joints are modeled as revolute joints or lower pairs and there will not be any higher pairs. Substituting M= 1, g = 8, J_2=0 into Eq (5.11) gives J_1 = 10. Based on this calculation, the 8-bar mechanism should have 10 lower pairs for one D.o.F. Many types of links can produce a mechanism but to reduce the complexity only binary (B, order = 2), ternary (T, order = 3), and quaternary (Q, order = 4) links and no multiple joints are considered. The total number of links can be [2]:

$$B + T + Q = g = 8 \qquad (5.12)$$

and the number of joints is found by [2]:

$$\frac{2B + 3T + 4Q}{2} = J_1 = 10 \tag{5.13}$$

Thus, the maximum number of quaternary links will be two [98]. The possible 8-bar mechanisms are presented in three categories for Q= 0, 1 and 2 as shown in Figure 5.9.

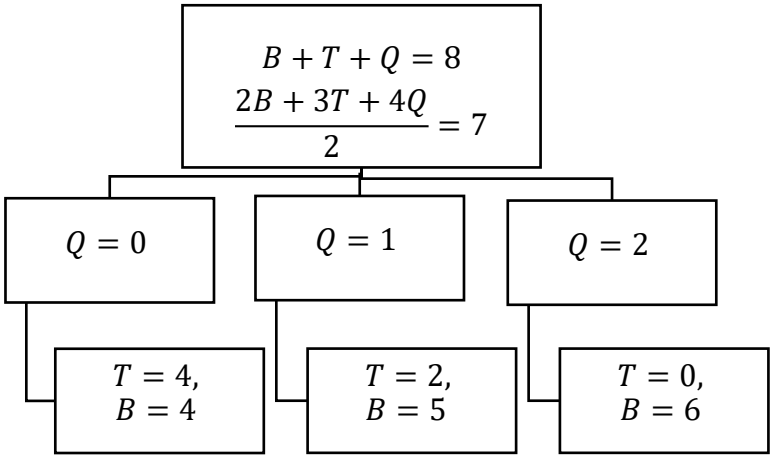

Figure 5.9: Three kinematic categories when Q= 0, 1, and 2. They are obtained from Eq (31), and (32). For category 1, (Q=0) leads to T=4, B=4 and can represent 9 linkage chains. For category 2, (Q=1) leads to T=2, B=5 and can represent 5 linkage chains. For category 3, (Q=2) leads to T=0, B=6 and can represent 2 linkage chains.

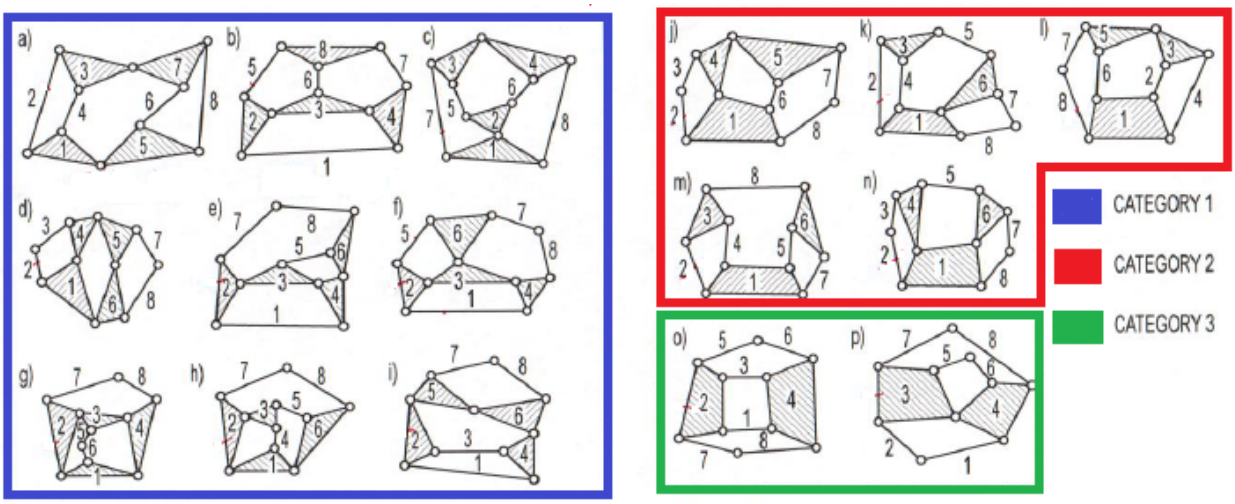

Figure 5.10: All 16 possible 1 D.o.F Sets resulting from Eq. (5.12) and (5.13). [2]. Category 1 represents 9 configurations of Q=0, T=4, and B=4. Category 2 represents 5 configurations of Q=1, T=2, and B=5. Category 3 represents 2 configurations of Q=2, T=0, and B=6.

According to R. L. Norton, there are 16 types one D.o.F. mechanisms, which are categorized as in Figure 5.10 [2]. The kinematic chains in Figure 5.10 are evaluated based on the following criteria:

1. The links in the outer loops should be an even number. This provides parallel links which are necessary for the spiral design (section 5.2). This rules out designs c, g, h, and i.
2. The number of ternary and quaternary links has to be even to ensure the symmetry of the mechanism. Otherwise, it will increase the complexity of the design, which rules out all of category 2, designs j, k, l, m, and n.
3. The mechanism has to have a symmetric outer loop, which rules out designs e, f, and h.
4. The mechanism loops must be collapsible; thus the ternary and quaternary links cannot be connected directly. Otherwise, this design will have a limited range of motion, as described for a six-bar in Figure 5.10. This rule out designs b, d, and p. All sixteen mechanism configurations are evaluated based on these criteria. Only two mechanisms pass, which are shown in Figure 5.11.

5.4 Graph Theory Representation

In this section, we used graph theory to assist in the type synthesis of the interior of the polygonal spiral. The graphs of the two candidate mechanisms in Figure 5.11 are shown in Figure 5.12. In Figure 5.12, links in the mechanism become vertexes in the graph and joints become edges [37, 38].

Graph theory shows a symmetry in the connection between the links which allow us to extend the mechanism as in Figure 5.13a. This extension of the mechanism by adding similar segments is analogous to the process of polymerization in chemistry, in which single units (monomers) are combined to useful longer chains (polymers). Such polymerized mechanisms that

do not change their mobility are useful as deployable mechanisms, such as those used in the aerospace industry. Polymerization provides a mechanism design that can increase the number of segments, and each segment can be scaled with respect to the previous one.

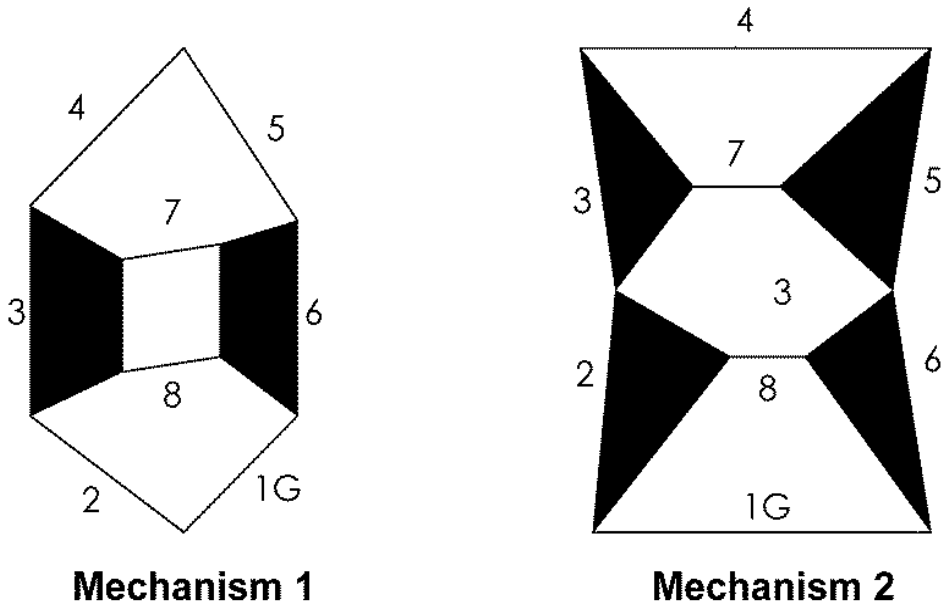

Figure 5.11: Two 1 D.o.F. mechanisms acquired and pass all design criteria. Mechanism 1 is composed of Q=2 and B=4. Mechanism 2 is composed of T=4 and B=4.

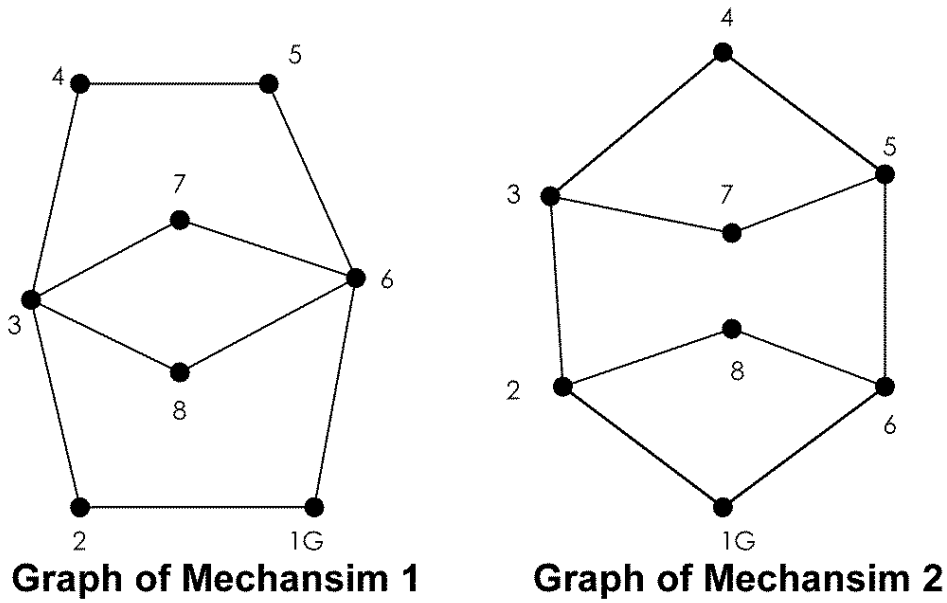

Figure 5.12: Graph representations of the two feasible mechanisms.

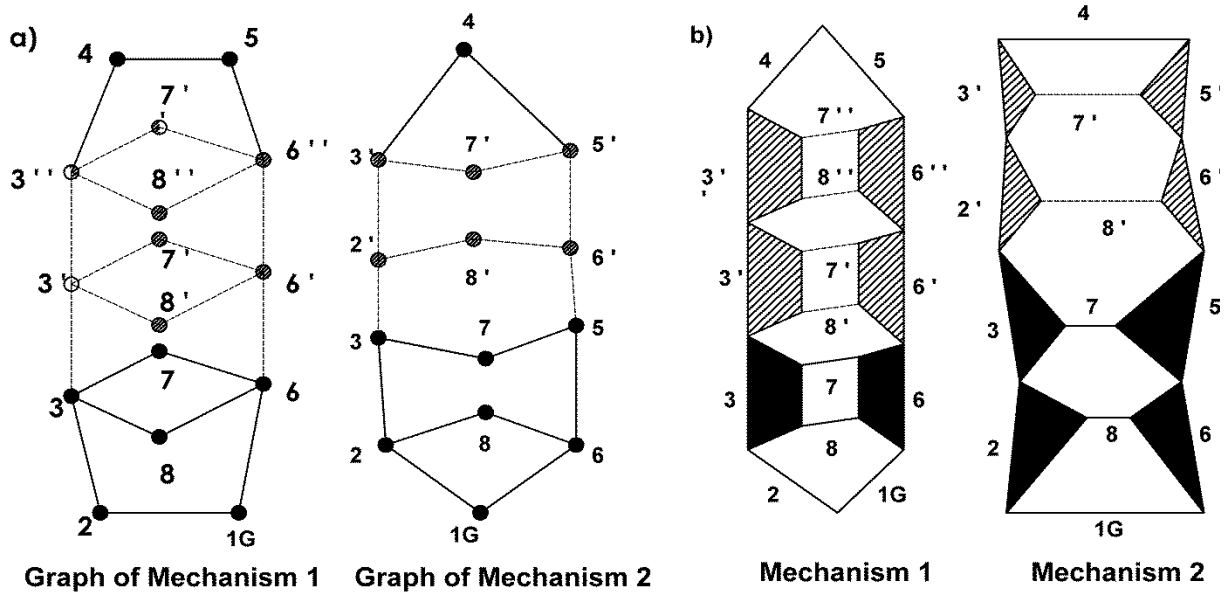

Figure 5.13: Repeating (polymerizing) the structure of the two mechanisms in Figure 5.11. a) Graph representation. b) Mechanism representation.

Still, in Figure 5.13, we see that polymerization of a mechanism may cause an increase in mobility. By transferring the graph back to the mechanism state as in (Figure 5.13b, mechanism 2), the result of Eq (5.11) for (L=14, J_1= 18, J_2=0) gives *M*=3 D.o.F. Thus, it cannot be used as a repeating pattern. On the other hand, mechanism 1 does not increase its mobility and passes all design criteria and is the best design for the collapsible compliant mechanism.

In designing the mechanism, a parametric CAD program is used to achieve the design goal in less time. Parametric CAD can provide clear visualization of the design approach. It allows kinematic chains and structure properties such as displacement, etc. to be straight analyzed and it allows design constraints to be specified, and link lengths are automatically adjusted to meet those specifications. In the current study, the two positions of mechanism 1 are the main constraints of the design. Thus, we identify the initial and the final configurations of the design for synthesis of mechanism 1 using parametric CAD [99].

We used Solidworks for the dimensional synthesis of the polymerized 8-bar in Figure 5.14a by setting the design constraints. The exterior links lengths in both 1st and 2nd positions are equal and have fixed locations. The quaternary links should keep the same shape and dimensions throughout the translation which requires having constant angles between their four sides as in Figure 5.14b. While the constraints were being applied, Solidworks did not automatically keep all interior joints and the internal spacing of quaternary links. Also, it happened that after all the constraints were applied, the interior links protruded outside the designed exterior and result in links that would interfere with adjacent sectors. However, by adjusting one angle of the quaternary links in one position, and linking the corresponding angle in the other position using LINK VALUE option in Solidworks, we had an adjustable parameter for the quaternary links, which was changed until all joints and links fit inside the sector interior in both configurations as shown in Figure5.14c.

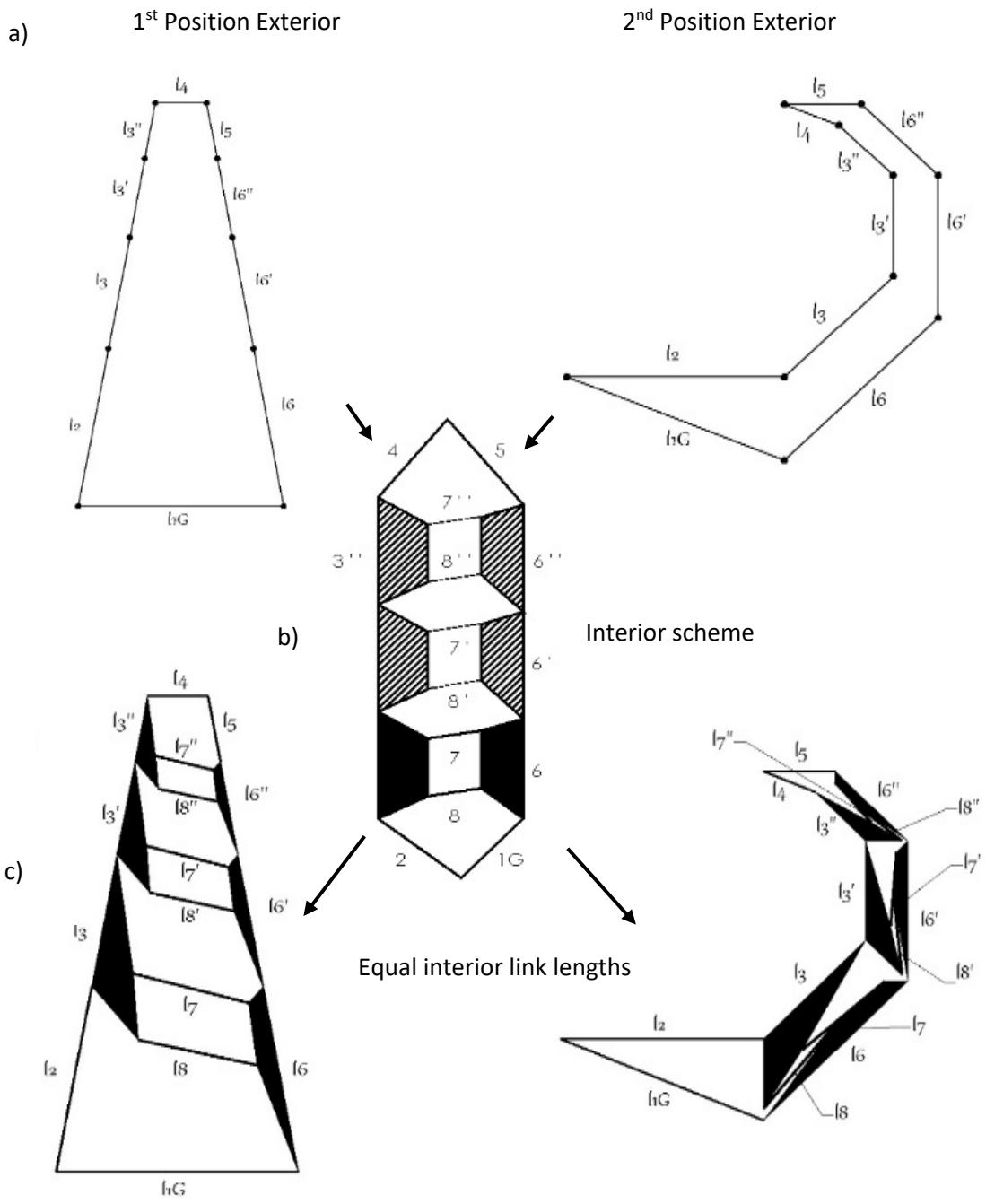

Figure 5.14: The dimensional synthesis process to create the sector mechanism from the selected 8-bar kinematic chain. Parametric CAD was used to apply the exterior constraints as shown in part (a),and to implement the interior scheme of the selected 8-bar kinematic chain (shown in part (b)), which achieves the final two designs shown in part (c) which Solidworks produced after equality constraints were set between equivalent links in the two positions.

5.5 Bistable Mechanism

The snap-through concept is used in the lamina- frustum mechanism to achieve bistability. Figure5.15 shows how the previous concept is applied on the lamina frustum mechanism where the nonlinear springs are the compliant links of the mechanism that accommodate the motion between the two stable configurations though their elastic behavior. Therefore, if a force applied to the mechanism to any intermediate position, the mechanism will snap to one of the stable configurations.

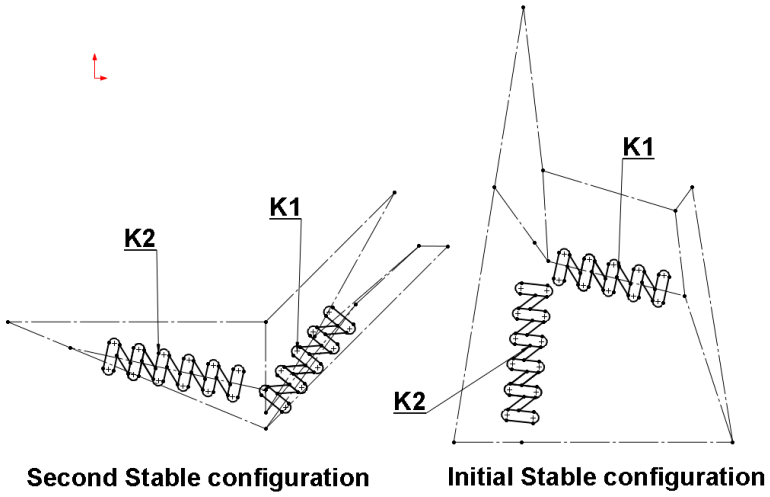

Figure 5.15: BCCM bistable configurations.

In order to apply the snap-though behavior to make the mechanism bistable, we added a link that creates the snap-through geometry. This forces some of the links to bend to accommodate the tension or compression of the added link when moving. As a result, the added link has to gain a potential energy when the mechanism goes toward its unstable equilibrium configuration (presumably when K1 and K2 are parallel) and lose it to go to one of the stable positions. The additional link can only be in one of the two outer loops of the polymerized 8-bar mechanism, so it doesn't interfere with the repeating pattern. The additional link is placed between two nonadjacent links in the two position of the mechanism so that it has the same undeflected length

in both stable positions as shown in Figure 5.16. In nonstable positions, the link is compressed resulting in increased potential energy, and stress in the mechanism. This mechanism is bistable between the 1st and 2nd configurations and forms the BCCM.

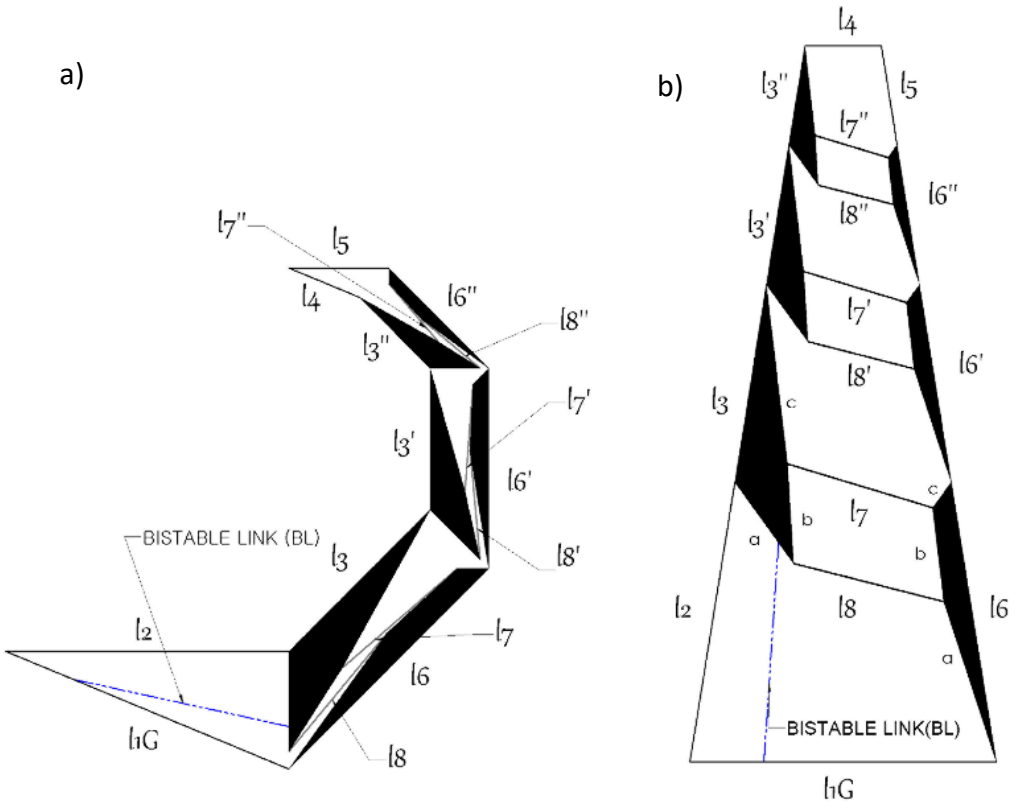

Figure 5.16: a) A stable position forming the lamina polygon spiral shape. The BCCM design: part b) a stable position forming the frustum shape.

5.6 Design Prototype

The design was prototyped using a laser cutting machine, the number of sectors, *n,* was chosen to be *n*=8 due to limitations in cutting small sizes. Our design was chosen to have a base radius, *R*=150 mm. All parameters of the design were derived using the relations given in Section 1 and using parametric CAD, and are shown in Table 5.2. These parameters can be used to represent the 1st and 2nd positions of a sector, and all the primed (‘,”) links lengths are found by multiplying the unprimed values by the spiral ratio, once for the single primes, twice for the double

primes as labeled in Figure 5.16. In Figure 5.16, the 8-bar mechanism from Section 3 is polymerized by a repeating pattern to satisfy the design parameters. Because the n= 8, the number of repeating patterns (P) can be calculated:

$$P = \frac{n}{2} - 1 \tag{5.14}$$

Initial design parameters are found to be as in Table 5.2 as follows:

- Number of sectors (n) = 8.
- Number of repeating patterns (P) = 3.
- Initial cylinder radius (R) = 150 mm.

Table 5.2: Design parameters (mm) for n= 8 and R=150mm.

n	a_i	R	L	b	R_t	H
8	4	150	271.59	114.80	37.5	247.20
L_1 G	L_2	L_7	L_8	L_3	L_3a	L_3b
114.8	106.07	58.88	58.11	75	37.48	37.28
L_3c	L_6	L_6a	L_6b	L_6c	BL	Spiral Ratio
67.67	106.07	68.21	35.3	11.86	82.19	0.707

Each sector creates an independent BCCM, and the assembly of 8 sectors forms the frustum shape. The BCCMs were laser cut from a 1/8 inch thick Polypropylene co-polymer material (Figure 5.17) in the position shown in Figure 5.16b. Each element is attached to the base by a torsion bar and two pins as shown in Figure 5.19. The torsion bars are part of the ground link (l_1G), and act as a hinge in the transition from the planar to the frustum position [3]. The top is designed to connect all sectors at link (l_4). The top has enough flexibility, to accommodate the relative rotation of the sectors as the mechanism moves to the frustum position. These features, the base and the top, do not affect the mechanism's bistability. The top is made of Polypropylene material laser cut from a 1/16 inch thick sheet and the connections to each other are flexible, so that each end can bend and twist independently, as shown in Figure 5.20.

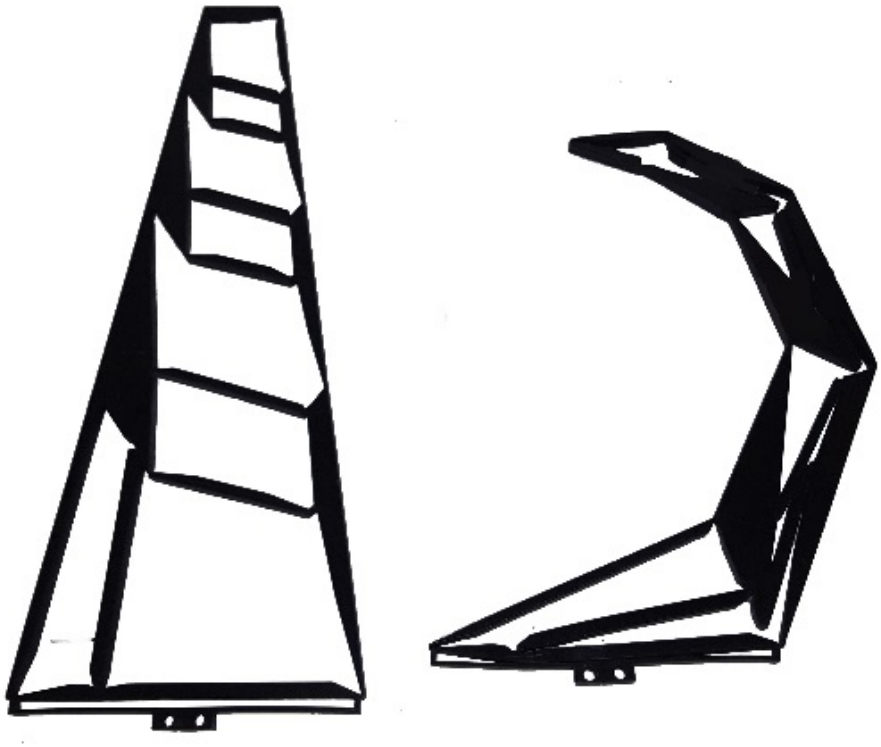

Figure 5.17: BCCM Prototype made of 1/8" thick polypropylene material.

Figure 5.18 shows the Lamina Emergent Frustum in both stable positions. All eight BCCMs were attached to base and to top. A compressive force and 180º rotation were applied in the top to transition to the planar position from the frustum.

Figure 5.18: Lamina Emergent Frustum in both stable positions. The planar position and frustum position (top and side views).

Figure 5.19: The torsion-bar that connects the BCCM to the base. [3].

Figure 5.20: The top is made of a 1/16 inch (mm) thick polypropylene.

5.7 Results and Discussion

This section will compare the results between the mathematical model and the prototype. The mathematical model predicts the height of the frustum, and the prototype height was measured experimentally. The prototyped BCCMs were fastened together to coordinate their out-of-plane movement and prevent the interference of the elements. The prototype loses a little height due to gravity causing the links to sag, additionally the polypropylene flexures tend to creep and exhibit some plastic deformation. Thus, the comparison between the two methods is done using the percentage error of the relative change between the height values as shown in Table 5.3.

Table 5.3: Comparison between the mathematical model and the prototype in height.

	Math. Model(mm)	Prototype(mm)	Error (%)
Height	271.599	260	4.3

In this prototype, we verified bistability experimentally by shaking the mechanism in its two stable positions, but did not optimize for fatigue life. Further, in our design of the mechanism, we tacitly assumed that each sector, which are planes in the stable configurations (see figures 5.16 and 5.17) would remain planes during their transition. This turned out not to be the case, resulting in torsional deformations in the small-length flexural pivots in the mechanism. This may have

consequences for the fatigue life of the mechanism, though repeated experiments to date have not resulted in fatigue failures.

5.8 Closure

This paper has presented a new Bi-stable Collapsible Compliant Mechanism (BCCM). Graph theory and kinematic chain design strategies were described. The collapsible bistable compliant mechanism of frustum-spiral planar shape was modeled geometrically and prototyped as a proof of concept.

CHAPTER 6

CONCLUSION AND FUTURE WORK

6.1 Conclusion

This dissertation presents design concepts for shape-morphing structures. These concepts describe methodologies for transforming a stable shape in planar configuration into spatial stable configurations using compliant mechanisms. Bistable complaint mechanisms are used to achieve stable configurations. The dissertation provides geometrical relationships for the mechanisms that form the primary structure described in step-by-step processes. The novel contributions of the work are in three models.

The first model presents a methodology to induce bistability behavior into an origami reverse fold. Two different mechanical approaches were explained: an origami mechanism (the reverse fold) using two layers of paper, and a four-bar spherical partially compliant mechanism (developed using 3D STL printer). An analogy between the synthesis of planar 4-bar mechanisms and the synthesis of spherical 4-bar mechanisms was introduced, and it was also applied to an origami vertex. An additional linkage can be included in the spherical mechanism and origami vertex which were forced to deform and store strain energy throughout the motion and thus providing bistable behavior. Finally, physical prototypes of both the origami and spherical mechanism were built and studied. The second model deals with the design and development of a bistable triangular-shaped mechanism with motion limits and dwell behavior at the two stable configurations. The mechanism used is based on a 6-bar dwell mechanism which fits in a triangular shape. An example which uses an array of three such mechanisms was designed and the two stable

configurations, flat and cube corner shapes were demonstrated. The model emphasizes the advantage of the mechanism's intrinsic behavior of having dead center motion limits to limit the motion of the mechanism in its two stable configurations. The design process, which involves designing of the dead center motion limits using instant center method and kinematic synthesis of the mechanism, is systematically discussed in a step by step process. Finally, physical prototypes of two examples; a cube corner, and portable box were built and studied. The third model presents a design for a collapsible compliant mechanism used for a lamina-emergent frustum. This model describes the design and prototyping of a compliant mechanism that is bistable in planar and truncated-cone configurations. A single kinematic mechanism is found that meets the geometric requirements. The design process is discussed in detail. The procedure for determining kinematic constraints and a suitable mechanism that deploys from a planar to a cone-type structure goes through a thorough process of selecting the desired mechanism for each segment using parametric CAD and type-synthesis techniques. The rigid link mechanism is converted to a compliant mechanism with the use of living hinges and an additional energy-storage link is added to give the device bistable behavior. In addition, a novel contribution to the bistable compliant mechanism is the ability to extend the mechanism's segments (to accommodate different frustum height) without changing the mobility. Finally, physical prototypes of lamina emerge frustum prototype were built and studied.

6.2 Future Work

The dissertation presents design concepts that allow designers to create shape morphing structures consist of bistable mechanisms. The work of the dissertation provides the necessary theoretical and geometrical analysis for the design which allows for future work to make practical applications of those devices.

In Chapter 3, the future work would involve in adding more elastic members to investigate the possibility of multistable configurations. It would also involve in experimenting various type of joints between panels which may enhance the stability. Tiling the mechanism would be beneficial for creating shape morphing origami and surfaces that have multiple stable configurations. In Chapter 4, the future work would involve in identifying more possible packages shapes that use different angles configurations of the triangle-shaped bistable mechanism. On the experimental side, force and potential energy measurements on the prototype would improve the study's results and verifications. Also improving the actuation scheme for the structures to a single actuation for better and simple deployment. In Chapter 5, the future work would be in the area of fatigue life and stress concentration. It also suggested to expand the use of the bistable elements in different applications such as a robot finger that has single actuation and a stable grip.

REFERENCES

[1] W. Cleghorn, *Mechanics of Machines*, New York: Oxford University Press, 2005.

[2] R. L. Norton, *Design of Machinery,* Worcester: McGraw Hill, 2012.

[3] J. Jacobsen, G. Chen, L. Howell and S. Magleby, "“Lamina Emergent Torsion (LET) Joint," *Mechanism and Machine Theory,* vol. 44, pp. 2098-2109, 2009.

[4] J. Patel and G. Ananthasuresh, "A Kinematic theory for redially foldable planar linkages," *International Journal of Solids and Structures,* vol. 44, pp. 6279-6298, 2007.

[5] A. Hartmann and B. Hoffert, "SPACE-Saving Furniture Projects for the Home," *Library Journal,* vol. 124, no. 8, p. 107, 1999.

[6] M. Frensemeier, D. Schirra, M. Weinmann, O. Weber and E. Kroner, "Shape-Memory Topographies on Nickel–Titanium Alloys Trained by Embossing and Pulse Electrochemical Machining," in *Advanced Engineering Materials*, Wiley-VCH Verlag, 2016, pp. 1388-1395.

[7] T. Chen, J. Mueller and K. Shea, "Integrated Design and Simulation of Tunable, Multi-State Structures Fabricated Monolithically with Multi-Material 3D Printing," *Sci. Rep.,* vol. 7, no. doi: 10.1038/srep45671, p. 45671, 2017.

[8] K. M. Al-Obaidi, M. A. Ismail, H. Hussein and A. M. Abdul Rahman, "Biomimetic building skins: An adaptive approach," *Renewable and Sustainable Energy Reviews,* vol. 79, pp. 1472-1491, 2017.

[9] J. R. Raney and e. al., "Stable propagation of mechanical signals in soft media using stored elastic energy," in *Proceedings of the National Academy of Sciences*, 9722–9727 (2016).

[10] N. Hu and R. Burgueno, "Buckling-induced smart applications: recent advances and trends," *Smart Materials and Structures,* vol. 24, p. 063001, 2015.

[11] T. Islam, Y. Cheng, J. Shengqi and R. Luc, "Dynamic analysis of Scissor Lift mechanism through bond graph modeling," in *IEEE/ASME International Conference on Advanced Intelligent Mechatronics (AIM)*, Besançon, France, 2014.

[12] T. Schioler and S. Pellegrino, "Space Frames with Multiple Stable Configurations," *AIAA Journal,* vol. 45, pp. 1740-1747, 2007.

[13] A. Wingert, M. Lichter, S. Dubowsky and M. Hafez, "Hyper-Redundant Robot Manipulators Actuated by Optimized Binary Dielectric Polymers," in *Proceedings of SPIE*, San Diego, CA, 415–423 (2002).

[14] M. Lichter, V. Sujan and S. Dubowsky, "Computational Issues in the Planning and Kinematics of Binary Robots," in *Proc. of the IEEE International Conf. on Robotics and Automation*, Minneapolis, MN , 1996.

[15] S. Kola, J. Hetrick and R. Osborn, "Design and Application of Compliant Mechanisms for Morphing Aircraft Structures," *Proc. SPIE,* vol. 5054, pp. pp. 24-33, 2003.

[16] K. Zhao, J. P. Schmiedeler and A. P. Murray, "Design of Planar Shape-Changing Rigid-Body Mechanisms for Morphing Aircraft Wings," *ASME J. Mech. Rob,* vol. 19, no. 9, p. p.041007, 2012.

[17] G. Washington and H. Yoon, "An Optimal Method of Shape Control for Deformable Structures With an Application to a Mechanically Reconfigurable Reflector Antenna," *Smart Mater. Struct.,* vol. 19, no. 10, p. P.105004, 2010.

[18] K. J. Lu and S. Kota, "Design of Compliant Mechanisms for Morphing Structureal Shapes," *J. Intell. Mater. Syst. Struct.,* vol. 14, no. 6, pp. pp. 379-391, 2003.

[19] S. Daynes and P. M. Weaver, "A Shape Adaptive Airfoil for a Wind Turbine Blade," *Proc. SIPE,* vol. 7979, p. p. 79790H, 2011.

[20] A. T. Yang and F. Freudenstein, "Application of Dual-Number Quaternion Algebra to the Analysis of Spatial Mechanism," *ASME Journal of Applied Mechanics,* vol. 86, pp. 300-308, 1964.

[21] T. Murphy, J. Kanaber and C. Koehler, "PEZ: Expanding CubeSat Capabilities through Innovative Mechanism Design," in *Proceedings of the AIAA/USU Conference on Small Satellites*, 2011.

[22] O. Shai and I. Polansky, "Finding Dead-Point Positions of Planar Pin-Connected Linkages Through Graph Theoretical Duality Principe," *Journal of Mechanical Design,* vol. 128, pp. 599-609, 2006.

[23] M. M. Stanisic, *Mechanisms and Machines: Kinematics, Dynamics, and Synthesis,* Cengage Learning, 2014.

[24] Alqasimi, A., Lusk, C., Chimento, J., "Design of a Linear Bi-stable Compliant Crank-Slider-Mechanism (LBCCSM)," in *Proceedings of the 2014 Design Engineering Technical Conferences & Computers and Information in Engineering Conference*, Buffalo, 2014.

[25] Alqasimi A., Lusk C., "Shape-Morphing Space Frame (SMSF) Using Linear Bistable Elements," in *Proceedings of the 2015 Design Engineering Technical Conferences & Computers and Information in Engineering Conference*, Boston, 2015.

[26] Lusk, C. and Montalbano, P., "Design Concepts for Shape-Shifting Surfaces," in *Proceedings of the 2011 Design Engineering Technical Conferences & Computers and Information in Engineering Conference*, Washington, DC, 2011.

[27] J. M. Gattas and Z. You, "Geometric assembly of rigid-foldable morphing sandwich structures," *Engineering Structures,* vol. 94, p. 149–159, 2015.

[28] C. M. Wheeler and M. L. Culpepper, "Soft origami : classification, constaint, and actuation of highly compliant origami structures.," *Journal of Mechanisms and Robotics,* vol. 8, no. 5, p. 051012, 2016.

[29] E. Peraza Hernandez, . D. Hartl and D. Lagoudas, "Kinematics of origami structures with smooth folds.," *Journal of Mechanisms and Robotics,* vol. 8, no. 5, p. 0161019, 2016.

[30] J. Solomon, E. Vouga, M. Wardetzky and E. Grinspun, "Flexible developable surfaces.," *In Computer Graphics Forum,* vol. 31, no. 5, pp. 1567-1576, 2012.

[31] W. L. *Cleghorn, Mechanics of Machines*, New York, NY: Oxford University Press, 2005.

[32] L. L. Howell, *Complaint Mechanisms*, New York: John Wiley & Son, Inc., 2001.

[33] J. E. Shigley and C. R. Mischke, *Mechanical Engineering Design*, New York, NY: McGraw-Hill, 1989.

[34] H. W. Stoll, *Product Design Methods and Practices*, New York, NY: Marcel Dekker, 1999.

[35] S. Shuib, M. I. Ridzwan and A. H. Kadarman, "Methodology of Compliant Mechanisms and Its Current Developments in Applications: A Review," *American Journal of Applied Sciences,* vol. 4, no. 3, pp. pp. 160-167, 2007.

[36] J. A. Bondy and U. S. R. Murty, *Graph Theory with Applications*, New York, NY: Elsevier Science , 1976.

[37] T. S. Liu and C. C. Chou, "Type synthesis of vehicle planner suspension mechanism using graph theory," *ASME Journal of Mechanical Design,* vol. 115, no. 3, pp. 652-657, 1993.

[38] L. T. Feng C. M., "A graph-theory approach to designing deployable mechanism of reflector antenna," *Acta Astronautica,* vol. 87, pp. 40-47, 2013.

[39] L.-W. Tsai, *Mechanism Design: Enumeration of Kinematic Structures According to Function*, CRC Press, 1999.

[40] X. L. Xilun Ding, "Design of a type of deployable/retractable mechanism using," *Mechanism and Machine Theory,* vol. 92, pp. 273-288, 2015.

[41] P. A. B. V. T. ,. A. C. &. L. G. Martin A, "Topological Synthesis of Planar Metamorphic Mechanisms for Low-Voltage Circuit Breakers," *Mechanics Based Design of Structures and Machines,* vol. 40, no. 4, pp. 453-468, 2012.

[42] L. Wen-Tzong, The Design Of Adjustable Spherical Mechanisms Using Plane-To-Sphere And Sphere-To-Plane Projections, Newark, NJ: Ph.D Dissertation, New Jersey Institute of Technology, 2004.

[43] I. Her, Methodology for Compliant Mechanisms Design, West Lafayette, IN: Purdue University, 1989.

[44] L. L. Howell, A. Midha and T. W. Norton, "Evaluation of Equivalent Spring Stiffness for Use in a Pseudo-Rigid-Body Model of Large-Deflection Compliant Mechanisms," *ASME Journal of Mechanical Design,* vol. 118, no. 1, pp. 126-131, 1996.

[45] M. D. Murphy, A Generalized Theory for the Type Synthesis and Design of Compliant Mechanisms, Ph.D. Dissertation, Purdue University, 1993.

[46] L. Howell and A. Midha, "A loop-Closure Theory for the Analysis and Synthesis of Compliant Mechanisms," *Journal of Mechanical Design,* vol. 118, no. 1, pp. 121-125, 1996.

[47] H. Su and L. M. McCarthy, "Synthesis of bistable compliant four-bar mechanisms using polynomial homotopy," *Trans. ASME, J. Mechan. Design,* vol. 129, p. 1094–1098, 2007.

[48] M. A. Pucheta and A. Cardona, "Design of bistable compliant mechanisms using precision-position and rigid-body replacement methods," *Mech. Mach. Theory,* vol. 45, p. 304–326, 2010.

[49] J. R. Lang, "Albert Joints the Fold," *New Scientist,* vol. 124, no. 1696/1697, pp. pp. 38-57, 1989.

[50] J. R. Lang, "Origami: Complexity Increasing," *Engineering & Science,* vol. 52, no. 2, pp. pp. 16-23, 1989.

[51] J. Maekawa, "Evoluation of Origami Organisms," *Symmetry: Culture and Science,* vol. 5, no. 2, pp. pp. 167-177, 1994.

[52] S. Zirbel, R. Lang, M. Thomson and et al, "Accommodating thichness in Origami-based Deployable Arrays1," *ASME. J. Mech. Des.,* vol. 135, no. 2, p. doi:10.1115/1.4025372, 2013.

[53] B. Trease, M. Thomson, D. Sigel, P. Walkemeyer, A. Shannon, Zirbel, L. Howell and R. Lang, "Origami-Inspired Folding of Thick, Rigid Panels.," in *NASA Tech Brief*, Pasadena, California , 2014.

[54] S. Zirbel, M. Wilson, S. Magleby and L. Howell, "An Origami-Inspired Self-Deployable Array," in *ASME 2013 Conference on Smart Materials, Adaptive Structures and Intelligent Systems*, Snowbird, Utah, USA, 2013.

[55] A. Shannon, Zirbel, B. Trease, M. Thomson, R. Lang, S. Magleby and L. Howell, "HanaFlex: a large solar array for space applications.," in *Proc. SPIE 9467 Micro-and Nanotechnology Sensors, Systems, and Applications VII*, Baltimore, Maryland, United States, 2015.

[56] S. Zirbel, B. Trease, S. Magleby and L. Howell, "Deployment Methods for an Origami-Inspired Rigid-Foldable Array.," in *Proc. of 42nd Aerospace Mechanism Symposium (AMS).*, Baltimore, MD; United States, 2014.

[57] S. Miyashita, S. Guitron, K. Yoshida, S. Li, D. Damian and D. Rus, "Ingestible, Controllable, and Degradable Origami Robot for Patching Stomach Wounds," in *IEEE International Conference on Robotics and Automation (ICRA)*, Stockholm, Sweden, 2016.

[58] K. Zhao and J. P. Schmiedeler, "Using Rigid-Body Mechanism Topologies to Design Shape-Changing Compliant Mechanisms," *J. of Mechanisms and Robotics,* vol. 8, p. p. 011014, 2016.

[59] L. Kerr-Jia and K. Sridhar, "Design of Compliant Mechanisms for Morphing Structural Shapes," *J. of Intelligent Material Systems and Structures,* vol. 14, pp. pp. 379-391, 2003.

[60] D. S. Lucato SL, J. Wang, P. Maxwell and e. al, "Design and demonstration of a high authority shape morphing structure," *International Journal of Solids and Structures ,* vol. 41, no. 13, pp. 3521-3543, 2004.

[61] A. Milojevic and N. Pavlovic, "Development of a new adaptive shape morphing compliant structure with embedded actuators," *Journal of Intelligent Material Systems and Structures,* vol. 27, no. 10, pp. 1306-1328, 2016.

[62] H. Greenberg and S. Mableby, "Using Lamina Emergent Mechanisms to Address Needs for a Space Environment," in *Utah Space Grant Consortium*, 2011.

[63] K. Kuribayashi, K. Tsuchiya, Z. You, D. Tomus, M. Umemoto, T. Ito and M. Sasaki, "Self-Deployable Origami Stent Grafts as a Biomedical Application of Ni-Rich TiNi Shape Memory Alloy Foil," *Mater. Sci. Eng.: A,* vol. 419, no. 1-2, pp. 131-137, 2006.

[64] C. Lusk and S. Chester, "Modeling and Parameter Study of Bistable Spherical Compliant Mechanisms," University of South Florida, Tampa, 2011.

[65] B. Hanna, J. Lund, R. Lang, S. Magleby and L. Howell, "Waterbomb base: a symmetric single-vertex bistable origami mechanism," *Smart Materials and Structures,* vol. 23, no. 9, 2014.

[66] S. Waitkaitis, R. Menaut, G. Chen and M. Hecke, "Origami Multistability: From Single Vertices to Metasheets," *PHYSICAL REVIEW LETTERS,* vol. 114, 2015.

[67] H. Yasuda, Z. Chen and J. Yang, "Multitransformable Leaf-Out Origami With Bistable Behavior," *Journal of Mechanisms and Robotics ,* vol. 8, 2016.

[68] S. Ishida, H. Uchida, H. Shimosaka and I. Hagiwara, "Design Concepts and Prototypes of Vibration Isolators Using Bi-Stable Foldable Structures," in *ASME 2015 International Design Engineering Technical Conferences and Computers and Information in Engineering Conference*, Boston, 2015.

[69] A. Pagano, B. Leung, B. Chien, T. Yan, A. Wissa and S. Tawifck, "Multi-Stable Origami Structure for Crawling Locomotion," in *ASME 2016 Conference on Smart Materials, Adaptive Structures and Intelligent Systems*, Stowe, 2016.

[70] T. B. S. Hull, "Modelling the folding of paper into three dimensions using affine transformations," *Linear Algebra and its Applications ,* vol. 348 , p. 273–282, 2002.

[71] W. W. leana Streinu, "Single-vertex origami and spherical expansive motions," in *Japan Conf. Discrete and Computational Geometry (JCDCG 2004), Springer Verlag, Tokai University*, Tokyo, 2005.

[72] L. Bowen, W. Baxter, S. Magleby and L. Howell , "A Position Analysis of Coupled Spherical Mechanisms in Action Origami," *Mechanism and Machine Theory,* vol. Vol. 77, pp. 13-24, 2014.

[73] E. R. Leal and J. Dai, "From Origami to a New Class of Centralized 3-DOF Parallel Mechanisms," in *ASME 2007 International Design Engineering Technical Conferences and Computers and Information in Engineering Conference*, 2007.

[74] R. J. Lang, *Origami Design Secrets: Mathematical Methods for an Ancient Art*, CRC Press, 2012.

[75] H. Liu and J. Dai, "Kinematics and mobility analysis of carton folds in packing manipulation based on the mechanism equivalent," in *In Proceedings of the Institution of Mechanical Engineers Part C: Journal of Mechanical Engineering Science*, 2002.

[76] L. A. Bowen, "A Study of Action Origami as Systems of Spherical Mechanisms," Brigham Young University, Provo, 2013.

[77] F. Harary, *Graph Theory,* Addison-Wesley, 1970.

[78] Kells, Kern and Bland, *Plane And Spherical Trigonometry*, McGraw-Hill , 1940.

[79] A. Alqasimi and C. Lusk, "Design of Four-Bar-Mechanism Stability Using Over-Constraint," in *Proceedings of the ASME 2016 International Design Engineering Technical Conferences and Computers and Information in Engineering Conference*, 2016.

[80] J. Chu and J. Sun, "Synthesis of Coupler Curves of Spherical Four-bar Mechanism Through Fast Fourier Transform," in *12th IFToMM World Congress*, Besançon (France), 2007.

[81] C. Chiang, *Kinematics of Spherical Mechanisms*, Cambridge University Press, 1988.

[82] K. Zhao and J. Schmiedeler, "Using rigid-body mechanism topologies to design shape changing compliant mechansims," in *Preceedings of ASME international design engineering technicla conferences and computers and information in engineering conference*, Portland, OR, 2013.

[83] Y. Hong-Sen and W. Long-long, "On the Dead-Center Position of Planar Linkage Mechanisms," *Journal of mechansims, Transmission, and Automation in Design,* vol. 111, pp. 40-46, 1989.

[84] A. H. Soni, *Mechanism Synthesis and Analysis*, New York: MCGraw-Hill, 1974.

[85] R. S. Hartenberg and J. Denavit, *Kinematic Synthesis of linkages*, New York: McGraw-Hill, 1964.

[86] H. Iseri, "Paper Models of Surfaces with Curvature," *Creative Visualization Labs Baltimore Joint Mathmatics Meeting,* 18 January 2003.

[87] H. Iseri, "Impulse Gauss Curvatures," in *SSHE-MA Conference*, Mansfield, 2002.

[88] I. L. Delimont, S. P. Magleby and L. L. Howell, "Evaluating Compliant Hinge Geometries for Origami-Inspired Mechanisms," *Journal of Mechanisms and Robotics,* vol. 7, no. 11, 2015.

[89] J. Qiu, J. H. Lang and A. H. Slocum, "A curved-beam bistable mechanism," *J. Microelectromech. Syst.,* vol. 13, p. 137–146, 2004.

[90] Z. Shouyin and . C. Guimin, "Design of Compliant Bistable Mechanism for Rear Trunk Lid of Cars," in *4th International Conference, ICIRA*, Aachen, Germany, 2011.

[91] D. Manan and S. Dibakar, "Design of double toggle switching mechanisms," *Journal of Mechanism and Machine Theory,* pp. 163-190, 2014.

[92] C. Guimin, Z. Shouyin and L. Geng, "Multistable Behaviors of Compliant Sarrus Mechanisms," *Journal of Mechanisms and Robotics ,* vol. 5, no. 2, 2013.

[93] J. O. Jacobsen, B. G. Winder, S. P. Howell and S. P. Magleby, "Lamina emergent mechanisms and their basic elements," *Journal of Mechanisms and Robotics 2,* pp. 1-9, 2010.

[94] S. E. Wilding, L. L. Howell and S. P. Magleby, "Spherical lamina emergent mechanisms," *Mechanism and Machine Theory,* vol. 49, p. 187–197, 2012.

[95] R. Wiebe, L. Virgin, I. Stanciulescu, S. Spottswood and T. Eason, "Characterizing Dynamic Transitions Associated With Snap-Through: A Discrete System," *Journal of Computational and Nonlinear Dynamics,* vol. 8, pp. 011010-1, 2013.

[96] L. Qun Chen and K. Li, "Equilibriums and their stabilities of the snap-through mechanism," *Archive of Applied Mechanics,* vol. 86, pp. 403-410, 2016.

[97] C. Wen-Tung, Chen-Chou Lin and Long-Iong Wu, "A NOTE ON GRASHOF'S THEOREM," *Journal of Marine Science and Technology,* vol. 13, no. 4, pp. 239-248, 2005.

[98] P. Vladimir and E. Ekaterina, "Number structural synthesis and enumeration process of all possible sets of multiple joints for 1-DOF up to 5-loop 12-link," *Mechanism and Machine Theory,* vol. 90, pp. 108-127, 2015.

[99] E. C. Kinzel, J. P. Schmiedeler and G. R. Pennock, "Kinematic Synthesis for Finitely Separated Positions Using Geometric Constraint Programming," *ASME Mechanism and Machine Theory,* vol. 128, p. 1070, 2006.

[100] J. Sun, Q. Guan, Y. Liu and J. L, "Morphing aircraft based on smart materials and structures: A state-of-the-art review," *Journal of Intelligent Material Systems and strucures,* vol. 27, no. 17, p. 2289–2312, 2016.

[101] D. M. Elzey, A. Y. Sofia and H. N. Wadley, "A bio-inspired, High-authority actuator for shape morphging structure," in *proceedings of SPIE*, San Diego CA, 2003.

[102] A. Y. N. Sofia, D. M. Elzey and H. N. G. Wadley, "Shape morphing hinged truss structures," *Journal of Smart Materials and Structures,* vol. 18, no. 6, 2009.

[103] D. S. and W. PM, "Review of shape-morphing automobile structures: concepts and outlook.," in *Proceeding of the Institution of Mechanical Engineers*, 2013.

APPENDIX A

MATLAB CODE FOR MODELING THE TRIANGLE-SHAPED COMPLIANT MECHANISM

```
clear all
% the mechanism parameters.
t20=45;%44.90388395;
t60=302;%303.4177457;
r2=0.2453;
r3=0.180175;
r4=0.336433;
r5=0.2546845;
r6=0.26147998;
r7=0.1741;
r8=0.207925;
g=25.66;
xi= 31.14;
%-------------------------------------------------------------------
delta1_min= r6-r7+.0106;
omega_min=acosd((r5.^2+r3.^2-delta1_min.^2)./(2.*r5*r3));
psi_max= 180-omega_min;
delta_max= (r2.^2+r3.^2-2*r3*r2*cosd(psi_max)).^(1/2);
%-------------------------------------------------------------------
delta= linspace(.3355,0.4209,10001);
psi=acosd((r3.^2+r2.^2-delta.^2)./(2.*r2.*r3));
omega=180-psi;
delta1=(r5.^2+r3.^2-2*r3*r5*cosd(omega)).^(1/2);
peta=acosd((delta1.^2+r3.^2-r5.^2)./(2.*r3.*delta1));
alpha=acosd((r7.^2+delta1.^2-r6.^2)./(2.*r7.*delta1));
eta=acosd((r3.^2+delta.^2-r2.^2)./(2*r3*delta));
nu=360-xi-eta-peta-alpha;
r1=(delta.^2+r4.^2-2.*r4.*delta.*cosd(nu)).^(1/2);
mu=acosd((delta.^2+r2.^2-r3.^2)./(2.*r2.*delta));
phi=acosd((r1.^2+delta.^2-r4.^2)./(2.*r1.*delta));
t2=phi+mu;
tw=acosd((r6.^2+delta1.^2-r7.^2)./(2.*r6.*delta1));
%-------------------------------------------------------------------
th3=360-(omega -t2);
th4=(t2+psi+eta+nu);
```

```
th6=360+t2-omega-peta+tw;
k6=.61;
%-----------------------------------------------------------------
% theta 3
A1=(r1.^2+r2.^2+r3.^2-r4.^2)/(2.*r3.*r2);
B1=r1/r3;
C1=r1/r2;
q1=A1+C1-(B1+1).*cosd(t2);
p1=2.*sind(t2);
L1=A1-C1-(B1-1).*cosd(t2);
t3= (t2<=45.11).*(360+2.*atand((-p1-((p1.^2)-
(4.*(q1).*(L1))).^(1/2))./(2.*q1)))+(t2>45.11&
t2<=46.95).*(360+2.*atand( (-p1+((p1.^2)-
(4.*(q1).*(L1))).^(1/2))./(2.*q1)))+(t2>46.95).*(2.*atand( (-
p1+((p1.^2)-(4.*(q1).*(L1))).^(1/2))./(2.*q1)));
t3 = 180/pi*(unwrap(pi/180*(real(t3))));
%-----------------------------------------------------------------
%theta 4
A2=(r1.^2+r2.^2+r4.^2-r3.^2)/(2.*r4.*r2);
B2=r1/r4;
C2=r1/r2;
q2=A2+C2-(B2+1).*cosd(t2);
p2=2.*sind(t2);
L2=A2-C2-(B2-1).*cosd(t2);
t4= (t2 >= 45.11).*(360+ 2.*atand( (-p2-((p2.^2)-
(4.*(q2).*(L2))).^(1/2))./(2.*q2)))+(t2< 45.11).*(360+ 2.*atand(
(-p2+((p2.^2)-(4.*(q2).*(L2))).^(1/2))./(2.*q2)));
%-----------------------------------------------------------------
%theta 6
A3=(r3.^2+r5.^2+r6.^2-r7.^2)/(2.*r6.*r5);
B3=r3/r5;
C3=r3/r6;
z= cosd(t2)-B3.*cosd(t3);
s= sind(t2)-B3.*sind(t3);
w= cosd(t3-t2);
q3= A3-z-C3.*w;
p3= 2.*s;
L3= A3+z-C3.*w;
t6 = 360+2.*atand( (-p3+((p3.^2)-
4.*(q3).*(L3)).^(1/2))./(2.*(q3)));
%-----------------------------------------------------------------
%theta 7
t7= (t2 <= 46.72).*(xi+t4-360)+(t2 > 46.72).*(t4+xi);
%theta 8
t8= (t2 <= 46.72).*(t7+360-xi-g)+(t2 > 46.72).*(t7-xi-g);
%-----------------------------------------------------------------
% Kinematic Coefficients
```

```
h42=(r5.*sind(t2-t3)-(r2+r5).*(tand(t6).*cosd(t3)-
sind(t3)).*sind(t2))./(r8.*(tand(t6).*cosd(t3)-
sind(t3)).*cosd(t8)+r7.*sind(t7-t3));
h62=(-(r2+r5).*cosd(t2)-r8.*h42.*cosd(t8))./(r6.*cosd(t6));
h32=-(r2.*cosd(t2)+r4.*h42.*cosd(t4))./(r3.*cosd(t3));
h12=-r2.*sind(t2)-r3.*h32.*sind(t3)-r4.*h42.*sind(t4);
h23=1./h32;
h24=1./h42;
h21=1./h12;
h26=1./h62;
%-----------------------------------------------------------------------
% Force and Potential Energy analysis
force=(-k6.*(degtorad(t2-t20)-degtorad(t6-
t60).*h62))./(r2.*cosd(t2)-r3.*cosd(t3).*h32);

figure;
plot(t2,t6);
hold on
plot(t2,th6);
figure;
plot(t2,force);
title('The Force-Input Angle');
xlabel('\theta_2');
ylabel('Force(N)');
axis([44 61 -1.5 .5]);
grid on

figure;
PE = cumtrapz(r1,force)+0.08;
plot(t2,PE)
title('Potential Enregy Curve')
xlabel('\theta_2');
ylabel('PE(J) ')
grid
axis([44 61 0 .1]);

figure;
subplot(3,1,2);
 plot(r1,t2);
 ylabel('\theta_2 ');
  title('First Configuration region')
 grid on
axis([0.63 0.68 44 46]);
number_of_ticks=0
xt=xlim
set(gca,'xtick',linspace(xt(1),xt(2),number_of_ticks))
subplot(3,1,1);
```

```
 plot(r1,t2);
 ylabel('\theta_2 ');
 title('Vertex Angle t2 with Input r1')
 grid on
 number_of_ticks=0
xt=xlim
set(gca,'xtick',linspace(xt(1),xt(2),number_of_ticks))
subplot(3,1,3);
 plot(r1,t2);
 ylabel('\theta_2 ');
  title('Second Configuration region')
 grid on
axis([0.25 0.35 59 61]);

number_of_ticks=0
xt=xlim
set(gca,'xtick',linspace(xt(1),xt(2),number_of_ticks))

figure;

grid on
subplot(3,1,2);
 plot(t3,t2);
 ylabel('\theta_2 ');
  title('First Configuration region')
 grid on
axis([310 350 44 46]);
number_of_ticks=0
xt=xlim
set(gca,'xtick',linspace(xt(1),xt(2),number_of_ticks))
subplot(3,1,1);
 plot(t3,t2);
 ylabel('\theta_2 ');
 title('Vertex Angle t2 with Input t3')
 grid on
 number_of_ticks=0
xt=xlim
set(gca,'xtick',linspace(xt(1),xt(2),number_of_ticks))
subplot(3,1,3);
 plot(t3,t2);
 ylabel('\theta_2');
 title('Second Configuration region')
 grid on
axis([400 410 59 61]);
number_of_ticks=0
xt=xlim
set(gca,'xtick',linspace(xt(1),xt(2),number_of_ticks))
```

```
figure;
subplot(3,1,1);
 plot(delta,t2);
 ylabel('\theta_2');
 title('Vertex Angle t2 with Input delta')
  grid on
  number_of_ticks=0
xt=xlim
set(gca,'xtick',linspace(xt(1),xt(2),number_of_ticks))
subplot(3,1,2);
 plot(delta,t2);
 ylabel('\theta_2 ');
 grid on
 title('First Configuration region')
axis([.34 .37 44 46]);
number_of_ticks=0
xt=xlim
set(gca,'xtick',linspace(xt(1),xt(2),number_of_ticks))
subplot(3,1,3);
 plot(delta,t2);
 ylabel('\theta_2 ');
 title('Second Configuration region')
 grid on
 axis([.42 .4211 59 61]);
 number_of_ticks=0
xt=xlim
set(gca,'xtick',linspace(xt(1),xt(2),number_of_ticks))
W=0:0.1:0.2;
W1=0.8:0.1:1;
whos
```

APPENDIX B

THE FORCE ANALYSIS FOR THE TRIANGLE-SHAPED COMPLIANT MECHANISM

The generalized coordinate is chosen to be θ_2 (input). The applied force is vertical on the joint between link 3 and link4.

$$\vec{F} = F_{in}\hat{J} \tag{B.1}$$

The vector from the origin to placement to the applied force is:

$$\vec{Z} = r_2 \sin(\theta_2) - r_3 \sin(\theta_3)\ \hat{j} \tag{B.2}$$

The virtual displacement is measured be differentiation the position vector as:

$$\delta\vec{Z} = \frac{d\vec{Z}}{d\theta_2}\delta\theta_2 = (r_2 \cos(\theta_2) - r_3 \cos(\theta_3) * h_{32})\ \hat{j} \tag{B.3}$$

The virtual work due the force is taken by:

$$\delta W = \vec{F} \cdot \delta\vec{Z}$$
$$\delta W = -F_{in}(r_2 \cos(\theta_2) - r_3 \cos(\theta_3)h_{32})\ \delta\theta_2 \tag{B.4}$$

The virtual work due the potential energy of the torsional spring in link 6 is taken by:

$$\delta W = -k_6\left[(\theta_2 - \theta_{2_0}) - (\theta_6 - \theta_{6_0})h_{62}\right]\delta\theta_2 \tag{B.5}$$

By summing the virtual work terms and apply the principle of virtual work ($\delta W = 0$).

$$F = \frac{-k_6\left[(\theta_2 - \theta_{2_0}) - (\theta_6 - \theta_{6_0})\right]h_{62}}{r_2 \cos(\theta_2) - r_3 \cos(\theta_3)\, h_{32}} \tag{B.6}$$

APPENDIX C

THE POSITION ANALYSIS FOR THE TRIANGLE-SHAPED COMPLIANT MECHANISM

The position analysis for the triangle-shaped mechanism was carried out using closed-form equations. The input was the virtual distance δ. The law of cosines was used to calculate the internal angles form Figure C.1.

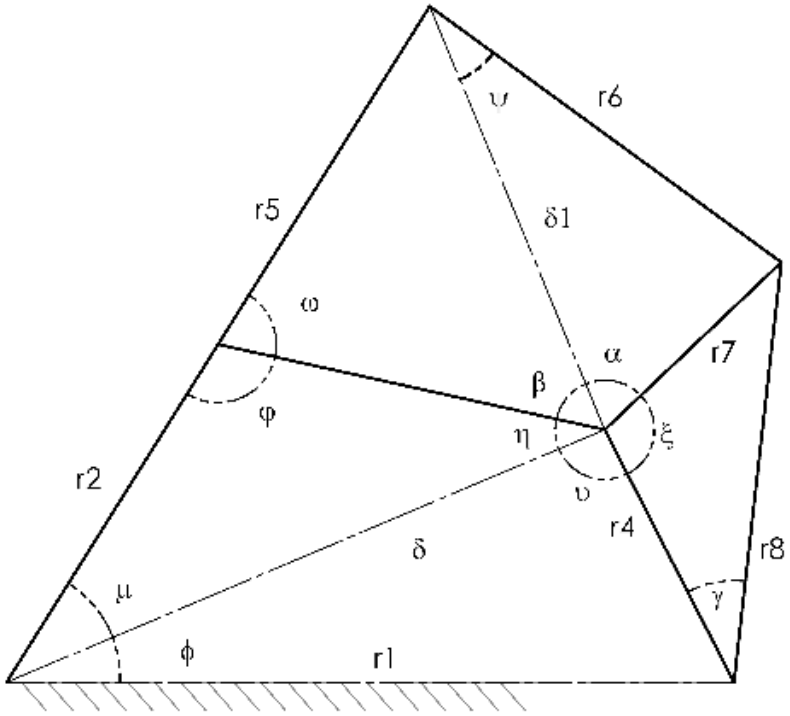

Figure C.1: Position analysis for the triangle-shaped mechanism.

$$\varphi = \cos^{-1}\left(\frac{r_3^2 + r_2^2 - \delta^2}{2r_2 r_3}\right) \tag{C.1}$$

$$\omega = \pi - \varphi \tag{C.2}$$

$$\theta_2 = \mu + \emptyset \tag{C.3}$$

$$\delta_1 = (r_5^2 + r_3^2 - 2r_3 r_5 \cos\omega)^{\frac{1}{2}} \tag{C.4}$$

$$\beta = \cos^{-1}\left(\frac{\delta_1^2 + r_3^2 - r_5^2}{2\delta_1 r_3}\right) \tag{C.5}$$

$$\alpha = \cos^{-1}\left(\frac{r_7^2 + \delta_1^2 - r_6^2}{2r_7\delta_1}\right) \tag{C.6}$$

$$\eta = \cos^{-1}\left(\frac{r_3^2 + \delta^2 - r_2^2}{2r_3\delta^2}\right) \tag{C.7}$$

$$\vartheta = 2\pi - \xi - \eta - \beta - \alpha \tag{C.8}$$

$$\mu = \cos^{-1}\left(\frac{r_2^2 + \delta^2 - r_3^2}{2r_2\delta}\right) \tag{C.9}$$

$$r_1 = (\delta^2 + r_4^2 - 2\delta r_4 \cos\vartheta)^{\frac{1}{2}} \tag{C.10}$$

$$\emptyset = \cos^{-1}\left(\frac{r_1^2 + \delta^2 - r_4^2}{2r_1\delta}\right) \tag{C.11}$$

$$\Psi = \cos^{-1}\left(\frac{r_6^2 + \delta_1^2 - r_7^2}{2r_6\delta_1}\right) \tag{C.12}$$

$$\theta_2 = \mu + \emptyset \tag{C.13}$$

$$\theta_3 = 2\pi + \theta_2 - \omega \tag{C.14}$$

$$\theta_4 = \theta_2 + \varphi + \vartheta + \eta \tag{C.15}$$

$$\theta_6 = 2\pi + \theta_2 - \omega - \beta + \Psi \tag{C.16}$$

APPENDIX D

THE KINEMATICS COEFFICIENTS OF THE TRIANGLE-SHAPED COMPLIANT MECHANISM

The kinematic coefficients are calculated from the vector loops in Figure 7. The complex number method may be used for the kinematic analysis as:

$$\overrightarrow{R_2} + \overrightarrow{R_3} + \overrightarrow{R_4} = \overrightarrow{R_1}$$
$$r_2 e^{i\theta_2} + r_3 e^{i\theta_3} + r_4 e^{i\theta_4} = r_1 e^{i\theta_1} \quad \text{(D.1)}$$

$$\overrightarrow{R_4} + \overrightarrow{R_5} + \overrightarrow{R_6} + \overrightarrow{R_8} = \overrightarrow{R_1}$$
$$r_4 e^{i\theta_4} + r_5 e^{i\theta_2} + r_6 e^{i\theta_6} + r_8 e^{i\theta_8} = r_1 e^{i\theta_1} \quad \text{(D.2)}$$

By taking the derivative of each equation with respect to $\theta_2 \frac{d\theta_o}{d\theta_i} = h_{oi}$, each equation will have real and complex forms.

$$ir_2 e^{i\theta_2} + ir_3 e^{i\theta_3} h_{32} + ir_4 e^{i\theta_4} h_{42} = ir_1 e^{i\theta_1} h_{12} \quad \text{(D.3)}$$

$$-r_2 \sin\theta_2 - r_3 \sin\theta_3 \, h_{32} - r_4 \sin\theta_4 \, h_{42} = h_{12} \quad \text{(D.4)}$$

$$r_2 \cos\theta_2 + r_3 \cos\theta_3 \, h_{32} + r_4 \cos\theta_4 \, h_{42} = 0 \quad \text{(D.5)}$$

$$ir_4 e^{i\theta_4} h_{42} + ir_5 e^{i\theta_2} + ir_6 e^{i\theta_6} h_{62} + ir_8 e^{i\theta_8} h_{82} = ir_1 e^{i\theta_1} h_{12} \quad \text{(D.6)}$$

$$-r_2 \sin\theta_2 - r_5 \sin\theta_2 - r_6 \sin\theta_6 \, h_{62} - r_8 \sin\theta_8 \, h_{82} = h_{12} \quad \text{(D.7)}$$

$$r_2 \cos\theta_2 + r_5 \cos\theta_2 + r_6 \cos\theta_6 \, h_{62} + r_8 \cos\theta_8 \, h_{82} = 0 \quad \text{(D.8)}$$

Note $h_{82} = h_{42}$

By solving for h_{42} the kinematic coefficients can be found as:

$$h_{42} = \frac{r_5 \sin(\theta_2 - \theta_3) - (r_5 + r_2)(\tan\theta_6 * \cos\theta_3 - \sin\theta_3)\sin\theta_2}{r_7 \sin(\theta_7 - \theta_3) + r_8 (\tan\theta_6 \cos\theta_3 - \sin\theta_3)\cos\theta_8} \quad \text{(D.9)}$$

$$h_{32} = -\frac{r_2 \cos\theta_2 + r_4 h_{42} \cos\theta_2}{r_3 \cos(\theta_2)} \quad \text{(D.10)}$$

$$h_{62} = \frac{(r_2 + r_5)\cos(\theta_2) - r_8 h_{42} \cos(\theta_8)}{r_6 \cos(\theta_6)} \quad \text{(D.11)}$$

$$h_{12} = -r_2 \sin(\theta_2) - r_3 h_{32} \sin(\theta_3) - r_4 h_{42} * \sin(\theta_4) \quad \text{(D.12)}$$

APPENDIX E

COPYRIGHT PERMISSIONS

E.1 Copyright Permission for Material Used in Chapter 3 and Chapter 5

Conference Publication Permission Request

Beth Darchi <DarchiB@asme.org> Wed, Sep 19, 2018 at 4:01 PM
To: Rami Alfattani <rami1@mail.usf.edu>

Dear Prof. Alfattani,
It is our pleasure to grant you permission to use **all or any part of** the following ASME papers:

- A Lamina-Emergent Frustum Using a Bistable Collapsible Compliant Mechanism (BCCM), by Rami Alfattani and Craig Lusk, Paper No. DETC2016-59590
- Design of a Bistable Origami Reverse-Fold Using Spherical Kinematics, by Rami Alfattani and Craig Lusk, Paper No. DETC2017-67867

cited in your letter for inclusion in a Dissertation entitled Design of Shape-morphing structures consisting of

bistable mechanisms to be published by University of South Florida.

Permission is granted for the specific use as stated herein and does not permit further use of the materials without proper authorization. Proper attribution must be made to the author(s) of the materials. **Please note:** if any or all of the figures and/or Tables are of another source, permission should be granted from that outside source or include the reference of the original source. ASME does not grant permission for outside source material that may be referenced in the ASME works.

As is customary, we request that you ensure full acknowledgment of this material, the author(s), source and ASME as original publisher. Acknowledgment must be retained on all pages where figure is printed and distributed.

E.2 Copyright Permission for Material Used in Chapter 5

Journal Publication Permission Request

Beth Darchi <DarchiB@asme.org> Mon, Oct 1, 2018 at 2:02 PM
To: Rami Alfattani <rami1@mail.usf.edu>

Dear Prof. Alfattani,
It is our pleasure to grant you permission to use **all or any part of** the ASME paper "A Lamina-Emergent Frustum Using a Bistable Collapsible Compliant Mechanism," by Rami Alfattani and Craig Lusk, J. Mech. Des 140(12), 2018, cited in your letter for inclusion in a Dissertation entitled Design of Shape-morphing structures consisting of bistable mechanisms to be published by University of South Florida.

Permission is granted for the specific use as stated herein and does not permit further use of the materials without proper authorization. Proper attribution must be made to the author(s) of the materials. **Please note:** if any or all of the figures and/or Tables are of another source, permission should be granted from that outside source or include the reference of the original source. ASME does not grant permission for outside source material that may be referenced in the ASME works.

As is customary, we request that you ensure full acknowledgment of this material, the author(s), source and ASME as original publisher. Acknowledgment must be retained on all pages where figure is printed and distributed.

Many thanks for your interest in ASME publications.

Sincerely,

Beth Darchi

Publishing Administrator

ASME

2 Park Avenue

New York, NY 10016-5990

E.3 Copyright Permission for Material Used in Chapter 4

Rami Alfattani <rami1@mail.usf.edu>

Conference Publication Permission Request

Beth Darchi <DarchiB@asme.org> Thu, Nov 8, 2018 at 2:26 PM
To: Rami Alfattani <rami1@mail.usf.edu>

Dear Mr. Alfattani,

It is our pleasure to grant you permission to use **all or any part of** the ASME paper "Shape-Morphing Using Bistable Triangles With Dwell-Enhanced Stability," by Rami Alfattani and Craig Lusk, Paper No. DETC2018-86235, cited in your letter for inclusion in a dissertation entitled Design Shape-morphing structures consisting of bistable mechanisms to be published by University of South Florida.

Permission is granted for the specific use as stated herein and does not permit further use of the materials without proper authorization. Proper attribution must be made to the author(s) of the materials. **Please note:** if any or all of the figures and/or Tables are of another source, permission should be granted from that outside source or include the reference of the original source. ASME does not grant permission for outside source material that may be referenced in the ASME works.

As is customary, we request that you ensure full acknowledgment of this material, the author(s), source and ASME as original publisher. Acknowledgment must be retained on all pages where figure is printed and distributed.

Many thanks for your interest in ASME publications.

Sincerely,

Beth Darchi

Publishing Administrator

ASME

2 Park Avenue

New York, NY 10016-5990

Tel 1.212.591.7700

darchib@asme.org

E.4 Copyright Permission for Figure Used in 5.10

PERMISSION LICENSE: PHOTOCOPY DUPLICATION USE

Request ID/Invoice Number: RAM15524

Date: December 28, 2015

To: Rami Abdulaziz Alfattani
University of South Florida
4202 E. Fowler Avenue
Tampa, FL 33620
United States
"Licensee"

McGraw-Hill Education Material

Author: Norton, Robert
Title: Design of Machinery
ISBN: 9780073529356
Edition: 5
Description of material: Figure 2-11 Part 2 on page 50 (Total 1 figure) ONLY

Fee: $0.00

Purpose of Reproduction

Course: Proceedings of the ASME 2016 International Design Engineering Technical Conferences & Computers and Information in Engineering Conference IDETC/CIE 2016
School: University of South Florida
Professor: Dr. Craig Lusk
Format: Print
Number of Copies/Print Run: 1
Semester: August, 2016
Distribution: One-time educational use in above-referenced course only.

Permission for the use described above is granted under the following terms and conditions:

1. The permission fee of $0.00 must be received by McGraw-Hill Education, and MUST BE ACCOMPANIED BY A SIGNED COPY OF THIS AGREEMENT. A check

should be made payable McGraw-Hill Global Education Holdings, LLC, Attn: Permissions Department, Wells Fargo Bank, Lockbox #6167, PO Box 8500, Philadelphia, Pa. 19178-6167.

2. No adaptations, deletions, or changes will be made in the material without the prior written consent of McGraw-Hill Education.

3. This permission is non-exclusive, non-transferable, and limited to the use specified herein. McGraw-Hill Education expressly reserves all rights in this material.

4. A credit line must be printed on the first page on which the material appears. This credit must include the author, title, copyright date, and publisher, and indicate that the material is reproduced with permission of McGraw-Hill Education.

5. This permission applies to print only and does not extend to any other media unless otherwise specified.

6. This permission does not allow the use of any material, including but not limited to photographs, charts, and other illustrations, which appears in a McGraw-Hill Education work copyrighted in or credited to the name of any person or entity other than McGraw-Hill Education. Should you desire permission to use such material, you must seek permission directly from the owner of that material and if you use such material, you agree to indemnify McGraw-Hill Education against any claim from the owners of that material.

Please sign and return one copy to the address as outlined above in Clause 1 of this agreement.

For McGraw-Hill Education:

Name Nandini Acharya
Permissions Department
McGraw-Hill Education

For Licensee:

Name

Title Rami A Alfattani

APPENDIX F

POLYPROPYLENE COPOLYMER PROPERTIES

CORTEC CHEMICAL & CORROSION RESISTANT MATERIALS

Typical Physical Properties:

PROTEC® COPOLYMER POLYPROPYLENE

Property	Nominal Value	Units	ASTM Test Method
Melt Index	0.5	g/10 min	D 1238
Density	0.9	g/cm^3	D 1505
Tensile Strength @ Yield	3,500	psi	D 638
Elongation @ Break	10	%	D 638
Coefficient of Linear Thermal Expansion	$6.5x10^{-5}$	In./In.°C	D 696
Flexural Modulus	145,000	psi	D 790
Notched Izod Impact	17	fl-lb/in	D 256
Low Temperature Brittleness F_{50}			
Heat Deflection Temperature @ 66 psi	86	^0C	D 648
Maximum Service Temperature, Air	180		Long Term
Vicat Softening Point	298	^0F	D 1525
Hardness, Shore D	72		D 2240
Absorption	Max.0.01%		D 5709(2)
Flammability Rating	UL94 HB		
Compliances	FDA, USDA, NSF(natural only)		

VYCOM OLEFIN AND PVC SOLUTIONS

801 E. Corey Street, Scranton PA 18505
Phone: (800) 235-8320
Fax: (800) 858-9266
www.vycomplastics.com

Physical properties of plastic sheeting are represented as "Typical". Information contained herein is considered accurate to the best of our knowledge. It is offered for your consideration and investigation, and is not to be construed as a representation or warranty expressed or implied. Our warranties are limited to those expressly stated in formal contracts or in conditions of sale on our invoices and order acceptances. Conditions and methods of use may vary and are beyond the control of Vycom; therefore, Vycom disclaims any liability incurred as a result of the use of this product in accordance with the data contained in our physical property charts. No information herein shall be construed as an offer of indemnity for infringement or as a recommendation to use the products in such a manner as to infringe any patent, domestic or foreign.

The "Typical" properties of our plastic sheet cannot be automatically used when engineering finished components; and the fabricator or end user is responsible for insuring the suitability of our products for their specific application or end use!

January 1st, 2012